AD-A034 876 AIR FORCE INST OF TECH WRIGHT-PATTERSON AFB OHIO SCH--ETC F/G 20/4

AN ANALYTICAL STUDY OF THE EFFECTS OF MASS TRANSFER ON A COMPRE--ETC(U)

DEC 76 A J BEAUREGARD

UNCLASSIFIED GA/MC/76D-3 NL

1 OF 2

AD A034876

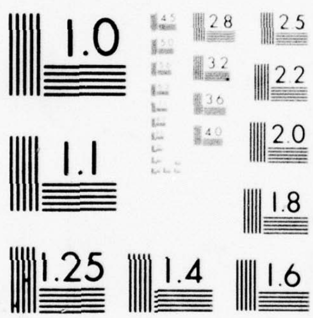

MICROCOPY RESOLUTION TEST CHART
NATIONAL BUREAU OF STANDARDS-1963

GA/MC/76D-3

GA/MC/

Approved

GA/MC/76D-3

1

AN ANALYTICAL STUDY OF THE EFFECTS OF MASS TRANSFER ON A COMPRESSIBLE TURBULENT BOUNDARY LAYER

THESIS

GA/MC/76D-3

A. J. Beauregard
Capt USAF

Approved for public release; distribution unlimited

14 GA/MC/76D-3

6

AN ANALYTICAL STUDY OF THE EFFECTS OF MASS TRANSFER ON A COMPRESSIBLE TURBULENT BOUNDARY LAYER.

THESIS

9 Master's thesis,

Presented to the Faculty of the School of Engineering
of the Air Force Institute of Technology

Air University

in Partial Fulfillment of the
Requirements for the Degree of
Master of Science

by

10 A. J. Beauregard
Capt USAF

Graduate Astronautics

11 December 1976

12 32p.

16 2307 17 04

1473
012225
LB

Preface

The material reported herein is based on the author's thesis submitted in partial fulfillment of the requirements for the Master of Science degree at the Air Force Institute of Technology, Wright Patterson Air Force Base, Ohio.

I would like to thank all those who have helped me complete this study. I am most grateful to Maj Carl Stolberg for his guidance in my search for a topic. I also appreciate the help given to me by Mr Dick Newman, Mr Frank Jones, Dr Charles Kyriss, Dr John Jones, Dr Will Hankey, Dr Andrew Shine, Dr David Lee, Maj John Kitowski, and Capt Steve Millett.

For their assistance in my literature search, I am indebted to Mrs Mary Browning, Mr Stan Boyd, and Mrs Molly Bustard.

For his patience, guidance, and continued interest I sincerely thank my advisor, Lt John Shea. For his sponsorship, I am forever grateful to my teacher and friend, Dr Joe Shang. Finally, a special thanks to Louise Beauregard, my mother, and Miss Nalda Blair for their efforts in the preparation of this manuscript.

Contents

Contents

List of Figures

List of Tables

Nomenclature

a	Speed of sound
c_f	Local coefficient of friction
c_p	Specific heat at constant pressure
F	Velocity ratio, $\frac{u}{u_e}$
H,h	Enthalpies, defined in the expression $H = h + \frac{u^2}{2}$
K_ℓ	Thermal conductivity
K_T	Eddy conductivity
L	Characteristic problem dimension, length of the model in question
ℓ	Defined in Eq (19-1)
M	Mach number
Pr	Prandtl number
p	Pressure
$\dot{q}$	Heat flux or heat flow per unit area
R	Gas constant, 1716 ft^2/sec^2R for air
Re	Reynolds number
$r(r_o)$	Radial coordinate (body radius) for the case of the axi-symmetric cone, measured perpendicularly from the longitudinal centerline, fig 3
S	Viscosity constant of Sutherland (198.6 R)
s	Nondimensional position, x/L
St	Stanton number, $\frac{\dot{q}}{\rho_e u_e (H_e - h_w)}$
T	Temperature
t	Transverse curvature term equal to $\frac{r}{r_o}$
$u(v)$	Velocity component along (perpendicular to) the streamwise direction
V	Transformed velocity expression defined in Eq (18-3)
X	Defined in Eq (27)

x,y Body surface oriented coordinate system in which x runs parallel to the stream direction, pointing downstream, and y is perpendicular to x and is directed into the external flow

Greek Symbols

α	Defined in Eq (19-2)
β	Defined in Eq (19-3)
Γ	Streamwise intermittency distribution or probability factor
γ	The gas constant, ratio of specific heats
γ'	The intermittency factor of Klebanoff
Δ	Change in variable quantity
δ	Boundary layer thickness
δ^*	Displacement thickness
ϵ	Eddy viscosity
$\bar{\epsilon}$	Eddy viscosity function defined following Eq (22)
$\hat{\epsilon}$	Eddy viscosity function defined following Eq (22)
λ	A nondimensional mass transfer rate, $\frac{(\rho v)_w}{(\rho u)_{\infty \text{ or } e}}$
η	Transformed perpendicular boundary layer coordinate and non-dimensional distance along this coordinate
$\underline{\theta}$	Static temperature ratio, $\frac{T}{T_e}$
θ	Momentum thickness
μ	Molecular viscosity
ν	Kinematic viscosity, $\frac{\mu}{\rho}$
ξ	Transformed streamwise boundary layer coordinate and nondimensional length along this coordinate
ρ	Density
τ	Shear Stress
ω	Exponent of the viscosity law of Sutherland

Subscripts and Superscripts

e	Condition at the edge of the boundary layer, also indicative of the input or environmental conditions for Itract in the cone study
∞	Free stream or unperturbed condition
j	Flow index, j = 1 for conical flow, j = 0 for flow over a flat surface
$\delta^*(\theta)$	When used with Re, denotes Reynolds number based on displacement thickness (momentum thickness)
o	Total or stagnation condition except for r_o
$\overline{'}$	Primed quantities indicate instantaneous departures from a mean state or condition in the turbulence model. The accompanying bars over the primed symbols denote a time averaged quantity.
ref	Reference
t	Turbulent condition
w	Condition at the surface of the plate or cone
x	Denotes a particular real x station along the surface of the model

Abstract

This study followed the work of Dr J. Shang, Flight Dynamics Laboratory, Wright Patterson Air Force Base, Ohio. Given a Fortran code written by Dr Shang that solved for the characteristics of a Laminar, transitional, and turbulent boundary layer, the problem was to modify the existing program to predict the boundary layer over a flat plate and sharp nosed axisymmetric cone with mass transfer as a boundary condition at the surface of the model. The surface of the model was maintained at a constant temperature, and only the cases in which air was the transferred gas were studied.

To solve this problem the boundary layer was described by the standard boundary layer equations for continuity, momentum, and energy. Incorporating mass transfer as a boundary condition, the governing equations underwent the transformation of Probstein-Elliott and Levy-Lees. The resulting equations and boundary conditions were solved by finite differencing techniques for nondimensionalized velocity components and temperature at a finite number of nodes in the boundary layer field of flow.

To verify the modified code, three studies were performed. First, the code was verified using analytical and some experimental data from Schlichting for laminar, subsonic flow over a flat surface with constant suction. Second, the code was verified for turbulent, subsonic flow over a flat surface with constant suction to the asymptotic suction limit and for small rates of blowing, using experimental results from Moffat and Kays. Finally, the code was verified with mixed success for hypersonic laminar, transitional, and turbulent flow over an axisymmetric cone for small rates of blowing using the experimental results of Martellucci, Laganelli, and Hahn.

UNCLASSIFIED

SECURITY CLASSIFICATION OF THIS PAGE (When Data Entered)

REPORT DOCUMENTATION PAGE		READ INSTRUCTIONS BEFORE COMPLETING FORM
1. REPORT NUMBER GA/MC-76D-3	2. GOVT ACCESSION NO.	3. RECIPIENT'S CATALOG NUMBER
4. TITLE (and Subtitle) AN ANALYTICAL STUDY OF THE EFFECTS OF MASS TRANSFER ON A COMPRESSIBLE TURBULENT BOUNDARY LAYER		5. TYPE OF REPORT & PERIOD COVERED MS Thesis 6. PERFORMING ORG. REPORT NUMBER
7. AUTHOR(s) A. J. Beauregard Capt, USAF		8. CONTRACT OR GRANT NUMBER(s) 61102F
9. PERFORMING ORGANIZATION NAME AND ADDRESS Air Force Institute of Technology (AFIT-EN) Wright Patterson Air Force Base, Ohio 45433		10. PROGRAM ELEMENT, PROJECT, TASK AREA & WORK UNIT NUMBERS Project 2307-04-18
11. CONTROLLING OFFICE NAME AND ADDRESS Flight Dynamics Laboratory (AFFDL) Wright Patterson Air Force Base, Ohio 45433		12. REPORT DATE December, 1976 13. NUMBER OF PAGES
14. MONITORING AGENCY NAME & ADDRESS(if different from Controlling Office)		15. SECURITY CLASS. (of this report) Unclassified 15a. DECLASSIFICATION/DOWNGRADING SCHEDULE

16. DISTRIBUTION STATEMENT (of this Report)

Approved for public release; distribution unlimited

17. DISTRIBUTION STATEMENT (of the abstract entered in Block 20, if different from Report)

18. SUPPLEMENTARY NOTES

Approved for public release; IAW AFR 190-17

Jerral F. Guess, Captain, USAF
Director of Information

19. KEY WORDS (Continue on reverse side if necessary and identify by block number)

Mass Transfer	Turbulent
Blowing	Boundary Layer
Suction	Flat Plate
Compressible	Sharp nosed Cone

20. ABSTRACT (Continue on reverse side if necessary and identify by block number)

This study followed the work of Dr J. Shang, Flight Dynamics Laboratory, Wright Patterson Air Force Base, Ohio. Given a Fortran code written by Dr Shang, that solved for the characteristics of a laminar, transitional, and turbulent boundary layer, the problem was to modify the existing program to predict the boundary layer over a flat plate and sharp nosed axisymmetric cone with mass transfer as a boundary condition at the surface of the model. → next page

DD FORM 1473 1 JAN 73 EDITION OF 1 NOV 65 IS OBSOLETE

UNCLASSIFIED

SECURITY CLASSIFICATION OF THIS PAGE (When Data Entered)

The surface of the model was maintained at a constant temperature, and only the cases in which air was the transferred gas were studied.

To solve this problem the boundary layer was described by the standard boundary layer equations for continuity, momentum, and energy. Incorporating mass transfer as a boundary condition, the governing equations underwent the transformation of Probstein-Elliott and Levy-Lees. The resulting equations and boundary conditions were solved by finite differencing techniques for nondimensionalized velocity components and temperature at a finite number of nodes in the boundary layer field of flow.

To verify the modified code, three studies were performed. First, the code was verified using analytical and some experimental data from Schlichting for laminar, subsonic flow over a flat surface with constant suction. Second, the code was verified for turbulent, subsonic flow over a flat surface with constant suction to the asymptotic suction limit and for small rates of blowing, using experimental results from Moffat and Kays. Finally, the code was verified with mixed success for hypersonic laminar, transitional, and turbulent flow over an axisymmetric cone for small rates of blowing using the experimental results of Martellucci, Laganelli, and Hahn.

AN ANALYTICAL STUDY OF THE EFFECTS OF MASS TRANSFER ON A COMPRESSIBLE TURBULENT BOUNDARY LAYER

I. Introduction, a Problem Analysis

Calculating the effects on boundary layer flows subjected to mass transfer perpendicular to the surface has provided engineers a relatively inexpensive model to study ablative effects. This model has provided a means by which to study the heating effects at the surface, skin friction, and the effects on the boundary layer profiles. The purpose of this paper was to investigate the effects of this mass transfer at the solid boundary by means of a numerical code.

Definition of the Problem and Purpose of the Study

The Flight Dynamics Laboratory (FDL) possessed a digital computer code, called Itract, which computed the characteristics of laminar and turbulent boundary layers over flat plates and axisymmetric, conical bodies for the case with no mass transfer at the surface. To initiate this computation the following quantities were specified as inputs: gamma, the gas constant; the Prandtl numbers, both laminar and turbulent; free stream mach number, static temperature, and density; the exponent of the viscosity law of Sutherland; a temperature ratio, wall temperature to free stream stagnation temperature; a point of transition from laminar to turbulent flow along the surface; and a flagged quantity which specified eddy model zero or eddy model one for computation of the eddy viscosity. With these inputs, Itract provided a description of boundary layer features. Some of the output of interest in this

study included the following: the local mach number for any point in the field, boundary layer thickness, displacement thickness, momentum thickness, the coefficient of friction, eddy viscosity, a Stanton number descriptive of heat transfer at the surface, and boundary layer profiles for velocity, static temperature, and density.

Starting with the original code of FDL this study was divided into three sequential steps. The first step was to learn as much about the computer code as possible. This step included a study of the key equations of motion, energy, and continuity needed for boundary layer solution. The second step was to incorporate the needed changes into the code that would include the new boundary condition of mass transfer at the surface of the body exposed to an environment of fluid flow. The last step was to verify the change by comparing key output predictions of the computer code with the results of analytical expressions presented in Schlichting and laboratory experiments for studies of flow over a flat plate and flow over a slender, axisymmetric cone. Completing these three steps, the purpose of this study was to extend the usefulness of a turbulent boundary layer code by incorporating a change that would allow consideration of mass transfer as a boundary condition, and thereby, study its effect on boundary layer characteristics.

Scope and Assumptions

In defining the area of study the topic was limited and the following assumptions were made. First, boundary layer computations and comparisons were performed on flat surfaces and axisymmetric cones with sharp leading edges or tips. For both models there were negligible effects due to the stagnation region at the leading edges, and in the

case of the plate, the shocking phenomena was neglected. Shapiro alluded to the validity of this assumption of free stream conditions existing some distance downstream of the leading edge of a plate in fig 28-21(c) and subsequent text (Ref 1:1149-1150). Eckert discussed this idea further as mach numbers reached supersonic and higher (Ref 2: 10-11). Thus, free stream conditions were assumed to exist downstream of the shock wave. Further, the angle of incidence of the models was assumed to be zero with respect to the flow in the free stream. Second, consideration was given only to the cases of air, at surface temperature, being blown through the surface into the boundary layer, or the boundary layer of air flow being sucked through the porous surface into the model. Thus, this study did not include the effects of chemical reactions that might occur by mixing nonsimilar gases in the boundary layer. Taking the transferred gas to be at the temperature of the wall, which was assumed constant, helped to limit and simplify the problem and the transfer model. This was a realistic limit as many experiments in wind tunnels were performed under these constant temperature conditions. Third, only small rates of injection or suction were compared with experimental results, although the limiting transfer rates of the code were investigated. It was assumed that mass transfer effects were confined to the boundary layer (Ref 3:1,5-6). The solution of this problem was based partially on the boundary layer equation of motion of Prandtl. To have considered massive transfer rates would have violated the proposition of Prandtl that δ was much less than the characteristic length of the model. Thus, a fourth stipulation was that δ would be much less than L. Further, the pressure change across this boundary layer thickness was neglibible, and considered zero in the analytical

solution. Fifth, the problem was limited to experimental cases where pressure change along the stream was also negligible. This was consistent with the two models studied. Numerically, dp/dx was considered zero. Finally, in the studies of both the flat plate and the conical flow, the mass transfer rate was considered constant over the region of transfer unless indicated otherwise in the experiment. Also, the flow was considered fully turbulent throughout the length of the model unless another transition point was clearly indicated in the experimental results. This list of items provided the limits and scope of this study. The following chapter presents a background of information relevant to this study.

II. A Background of Information

Interest in boundary layers perturbed by mass transfer at the surface has been evident from numerous laboratory experiments in which a model equipped with a surface blowing apparatus was exposed to the free stream environment of a wind tunnel. More recently, computer codes have been designed to compute the same fluid characteristics as measured in the experimental efforts. In both these studies those features of the boundary layer that were of greatest interest included the following:

a) Boundary layer velocity profile shape,

b) Energy (temperature) profile shape,

c) Thicknesses - boundary layer, displacement, and momentum,

d) Skin friction reduction for the blowing case, and

e) Heat transfer blockage for the blowing case.

In the experimental study these features have been obtained by measuring a restricted number of quantities.

The devices used to measure these quantities in experiments on boundary layers have included heat transfer gages, pressure sensors, temperature probes, and mass injection concentration probes (Ref 4: 1-10, 32-35, 46-51). The same quantities measured by these devices have been computed by analytical methods. Such a method or computer code was written for the Flight Dynamics Laboratory, Wright Patterson Air Force Base, Ohio.

This code was written to obtain numerical solutions of the governing turbulent boundary layer equations. Because of limited understanding of turbulent processes, completely general solutions to these equations have not been possible. By use of an empirical eddy

viscosity model of these processes, however, the system of governing equations was solved directly. The basic eddy model used in this study was that of Cebeci, Smith, and Mosinskis. The model assumed an inner and an outer viscous layer within the boundary layer. The expression for e in the inner region was based on the mixing length theory of Prandtl as follows:

$$e_i = \ell^2 \left|\frac{\partial u}{\partial y}\right| \tag{1}$$

where ℓ was equal to $K_1 y$. To account for the region close to the wall, Van Driest offered a modification to the mixing length of Prandtl. The new expression for ℓ was

$$\ell = K_1 y \left(1 - \exp(-y/A)\right) \tag{2}$$

where A was equal to $26\nu\ (\tau_w/\rho_w)^{-1/2}$. The shear stress close to the wall was written

$$\tau = \tau_w + \left(\frac{dp}{dx}\right) y \tag{3}$$

If A were redefined to $26\nu\ (\tau/\rho)^{-1/2}$, then expanded

$$A = 26\nu \left\{\frac{\tau_w}{\rho} + \frac{dp}{dx}\frac{y}{\rho}\right\}^{-1/2} \tag{4}$$

Finally then,

$$e_{inner} = K_1^2 y^2 \left\{1 - \exp\left[-\frac{y}{26\nu}\left(\frac{\tau_w}{\rho} + \frac{dp}{dx}\frac{y}{\rho}\right)^{1/2}\right]\right\}^2 \left|\frac{\partial u}{\partial y}\right| \tag{5}$$

The expression for e in the outer region was

$$e_{outer} = K_2 \int_0^\infty (u_e - u)\,dy \tag{6}$$

This became eddy model zero in the code and differed from eddy model one which was formed by multiplying ϵ_{outer} or eddy model zero by the intermittency factor of Klebanoff,

$$\gamma' = \left[1 + 5.5 \left(\frac{y}{\delta}\right)^{6}\right]^{-1} \tag{7}$$

For δ defined as the distance from the surface to a point in the field at which u was equal to $.995u_\infty$, studies have shown that the value for K_1 was .4 and the value for K_2 was .0168 (Ref 5:1975-1976). Having selected the model of Cebeci to describe turbulent activity within the boundary layer, there remained the problem of solving the system of governing equations for laminar, transitional, and turbulent compressible boundary layers (Ref 6).

Finite differencing techniques were incorporated to obtain solutions of the governing system for both flat plate and axisymmetric conical flows. The numerical technique involved a simultaneous solution of the equations of momentum, energy, and continuity by a tridiagonal matrix inversion routine. Through an iterative procedure, the solutions of all three were brought into convergent harmony yielding results which, otherwise, would have been gained only through laboratory experiments. Some of the mathematical modeling incorporated with these three governing equations included a two-layer concept within the turbulent boundary layer with appropriate eddy viscosity models used for the inner and outer regions. These models were considered in addition to the molecular viscosity term applicable in laminar flow. Further, a specified turbulent Prandtl number related turbulent heat flux to the Reynolds stress. Finally, mean properties within the transition region between laminar and turbulent flow were computed by multiplying the eddy

viscosity by an intermittency factor that characterized the growth rate or production of turbulence within a flow whose origin was laminar (Ref 7; Ref 8:1-4). With these models incorporated, the solution followed.

The Equations to be Solved

The flow of compressible, viscous, heat conducting fluid was described by the equations of continuity, Navier-Stokes, and energy, together with a supporting equation of state, a heat conductivity law, and the viscosity law of Sutherland. To arrive at such a description was to accept the propositions of Prandtl. Osborne Reynolds was the first to study turbulent flow in 1883. He said that the instantaneous fluid velocity satisfied the Navier-Stokes equations, and that this velocity was comprised of a mean velocity and a fluctuating component. He modified the Navier-Stokes expressions with these fluctuating components, called Reynolds Stresses, and by making boundary layer approximations he presented the governing equations as follows (Ref 8: 11-12):

Continuity

$$\frac{\partial}{\partial x}(r^j \rho u) + \frac{\partial}{\partial y}\left[r^j \rho\left(v + \frac{\overline{\rho' v'}}{\rho}\right)\right] = 0 \tag{8}$$

Momentum

$$\rho\left[u\frac{\partial u}{\partial x} + \left(v + \frac{\overline{\rho' v'}}{\rho}\right)\frac{\partial u}{\partial y}\right] = -\frac{dp}{dx} + \frac{1}{r^j}\frac{\partial}{\partial y}\left[r^j\left(\mu\frac{\partial u}{\partial y} + \rho\overline{u'v'}\right)\right] \tag{9}$$

Energy

$$\rho\left[u\frac{\partial}{\partial x}(c_p T) + \left(v + \frac{\overline{\rho' v'}}{\rho}\right)\frac{\partial}{\partial y}(c_p T)\right] = u\frac{dp}{dx} + \frac{1}{r^j}\frac{\partial}{\partial y}\left[r^j\frac{K_\ell}{c_p}\frac{\partial}{\partial y}(c_p T)\right]$$

$$+\mu\left(\frac{\partial u}{\partial y}\right)^2 + \frac{1}{r^j}\frac{\partial}{\partial y}\left[r^j\left(-c_p\,\rho\overline{v'T'}\right)\right] - \rho\overline{u'v'}\frac{\partial u}{\partial y} \tag{10}$$

Appendix A was included for further clarification of the above system (Ref 9:145-150).

Eqs (8), (9), and (10), valid descriptions for laminar and turbulent flow, were the laminar governing equations with the addition of turbulent fluctuating quantities which represented the apparent turbulent mass, shear, and heat flux terms. These turbulent additions were incorporated, again, through mathematical modeling. The apparent mass flux, $\overline{\rho' v'}$, was incorporated by the new variable, $\tilde{v}$; the apparent shear stress, $\rho\overline{u'v'}$, became part of the eddy model; and the apparent heat flux, $c_p\rho\overline{v'T'}$, was modeled through an eddy conductivity term, K_T. These relationships were defined by the following equations:

$$\tilde{v} = v + \frac{\overline{\rho' v'}}{\rho}$$

$$e = -\rho \frac{\overline{u'v'}}{\partial u/\partial y} \tag{11}$$

$$K_T = -c_p \rho \frac{\overline{v'T'}}{\partial T/\partial y}$$

With these quantities incorporated, the perfect gas law and the viscosity relation of Sutherland were also added:

Perfect gas law

$$p = c_p \left(\frac{\gamma-1}{\gamma}\right)\rho T \tag{12}$$

Viscosity law

$$\frac{\mu}{\mu_e} = \left(\frac{T}{T_e}\right)^{\frac{3}{2}} \frac{T_e + S}{T + S} \text{ (air only)} \tag{13}$$

Thus, the system of governing equations to be solved consisted of three nonlinear partial differential equations and two algebraic expressions.

But in the present form this system had a singularity at x equal to zero, the leading edge. To alleviate this singularity, and to reduce the growth of the boundary layer as the solution proceeded downstream for numerical efficiency, a variable transformation was made (Ref 8:13-15).

The Transformed Plane

The transformation of Probstein-Elliott and Levy-Lees was used in this analytic study. The transformation was written as follows:

$$\xi(x) = \int_0^x \rho_e u_e \mu_e r_o^{2j} dx \tag{14}$$

$$\eta(x,y) = \frac{\rho_e u_e r_o^{\,j}}{\sqrt{2\xi}} \int_0^y t^j \frac{\rho}{\rho_e} dy \tag{15}$$

Next, the relation between derivatives in the real (x,y) plane and the transformed plane (ξ,η) followed:

$$\left(\frac{\partial}{\partial x}\right)_y = \rho_e u_e \mu_e r_o^{2j} \left(\frac{\partial}{\partial \xi}\right)_\eta + \left(\frac{\partial \eta}{\partial x}\right)\left(\frac{\partial}{\partial \eta}\right)_\xi \tag{16}$$

$$\left(\frac{\partial}{\partial y}\right)_x = \frac{\rho_e u_e r_o^{\,j} t^j}{\sqrt{2\xi}} \left(\frac{\rho}{\rho_e}\right)\left(\frac{\partial}{\partial \eta}\right)_\xi \tag{17}$$

Then, the three parameters, F, $\underline{\theta}$, and V were defined as follows:

$$F = \frac{u}{u_e}$$

$$\underline{\theta} = \frac{T}{T_e}$$

$$V = \frac{2\xi}{\rho_e u_e \mu_e r_o^{2j}} \left(F \frac{\partial \eta}{\partial x} + \frac{\rho \tilde{v} r_o^{\,j} t^j}{\sqrt{2\xi}}\right) \tag{18}$$

With this, the final working form of the governing system, prior to linearization, was reached. Further definitions included

$$\ell = \frac{\rho\mu}{\rho_e\mu_e}$$

$$\alpha = \frac{u_e^{\,2}}{c_p T_e} \tag{19}$$

$$\beta = \frac{2\xi}{u_e}\frac{du_e}{d\xi}$$

Finally, the solvable form of the governing system was obtained as follows:

Continuity

$$\frac{\partial V}{\partial \eta} + 2\xi\frac{\partial F}{\partial \xi} + F = 0 \tag{20}$$

Momentum

$$2\xi F\frac{\partial F}{\partial \xi} + V\frac{\partial F}{\partial \eta} - \frac{\partial}{\partial \eta}\left(t^{2j}\ell\bar{\epsilon}\frac{\partial F}{\partial \eta}\right) + \beta(F^2 - \underline{\theta}) = 0 \tag{21}$$

Energy

$$2\xi F\frac{\partial \underline{\theta}}{\partial \xi} + V\frac{\partial \underline{\theta}}{\partial \eta} - \frac{\partial}{\partial \eta}\left(t^{2j}\frac{\ell}{Pr}\hat{\epsilon}\frac{\partial \underline{\theta}}{\partial \eta}\right) - \alpha\ell t^{2j}\bar{\epsilon}\left(\frac{\partial F}{\partial \eta}\right)^2 = 0 \tag{22}$$

where $\bar{\epsilon} = 1 + \frac{\epsilon}{\mu}\Gamma$ and $\hat{\epsilon} = 1 + \frac{\epsilon}{\mu}\frac{Pr}{Pr_t}\Gamma$.

Casting Eqs (20), (21), and (22) into a finite difference form, this system represented a means by which a boundary layer could be studied numerically. With the inclusion of boundary conditions, this system was solvable. For purposes of this study the boundary conditions were as follows:

$$F(\xi,0) = 0$$

$$V(\xi,0) = V_w(\xi)$$

$$\underline{\theta}(\xi,0) = \underline{\theta}_w,\ \text{a constant} \tag{23}$$

$$F(\xi,\eta_e) = 1$$

$$\underline{\theta}(\xi,\eta_e) = 1 \quad \text{(Ref 8:13-18; Ref 10)}$$

This chapter has introduced the boundary layer problem, and methods by which this problem has been studied and solved. The methods presented, experimental and analytical, represented the techniques employed by those in the engineering community who have studied boundary layer flow extensively. The numerical solution ultimately depended on the boundary conditions imposed on the differential equations. Further, the boundary condition, Eq (23-2), was to become the primary area of study for this thesis. This quantity, $V_w(\xi)$, would ultimately provide Itract with the capability to investigate the effects of mass transfer on a boundary layer. The original FDL code solved the boundary layer problem for no mass transfer, or $V_w(\xi)$ equal to zero. With a $V_w(\xi)$ model incorporated to simulate the mass transfer of air, the code would solve the boundary layer problem such as that investigated by the experimental study mentioned at the beginning of this chapter. To better understand this numerical solution it was necessary to include a program description, Chapter III.

III. A Program Description

The computer code, Itract, solved the system of nonlinear parabolic partial differential equations, Eqs (20), (21), and (22), by casting this system into a series of linear finite difference expressions. Coincidentally, the transformation from the real (x,y) plane to the (ξ,η) plane cast the boundary layer into a rectangular grid of nodes with the surface of the model located at the level $j = 1$, as shown in fig 1.

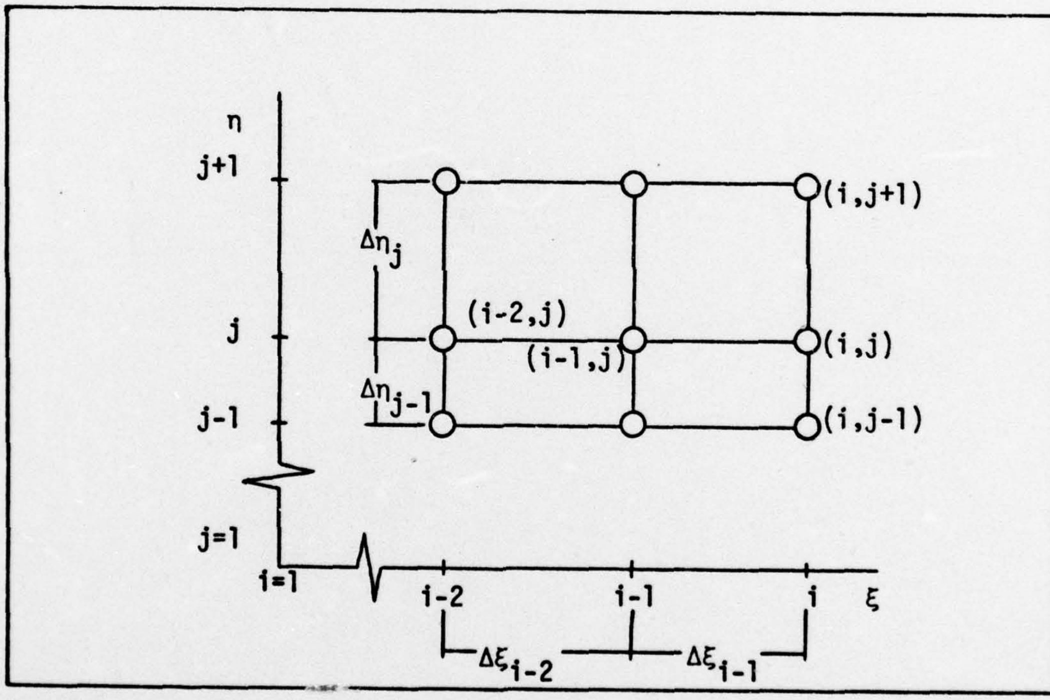

Fig. 1. Finite Difference Grid for Boundary Layer (From Ref 8:33)

The solution of this system of finite difference equations was approximated by computing values of F, $\underline{\theta}$, and V at each of the nodes within the grid. With values for these variables at stations i-2 and i-1 the values of F, $\underline{\theta}$, and V were solved at station i from the surface to the edge of the boundary layer using a three-point differencing scheme and

a tridiagonal matrix inversion routine. With the boundary layer solution completed at station i the problem was stepped in the streamwise direction, ξ, to station i+1 and the node by node computation was performed again from the surface to the edge of the boundary layer. The entire program was, therefore, a sequential solution of a series of columns of nodes from the leading edge to the trailing edge of the surface or model. For the particular problem considered in this study, the program followed the step-by-step procedure depicted in fig 2, with a program listing included in Appendix B.

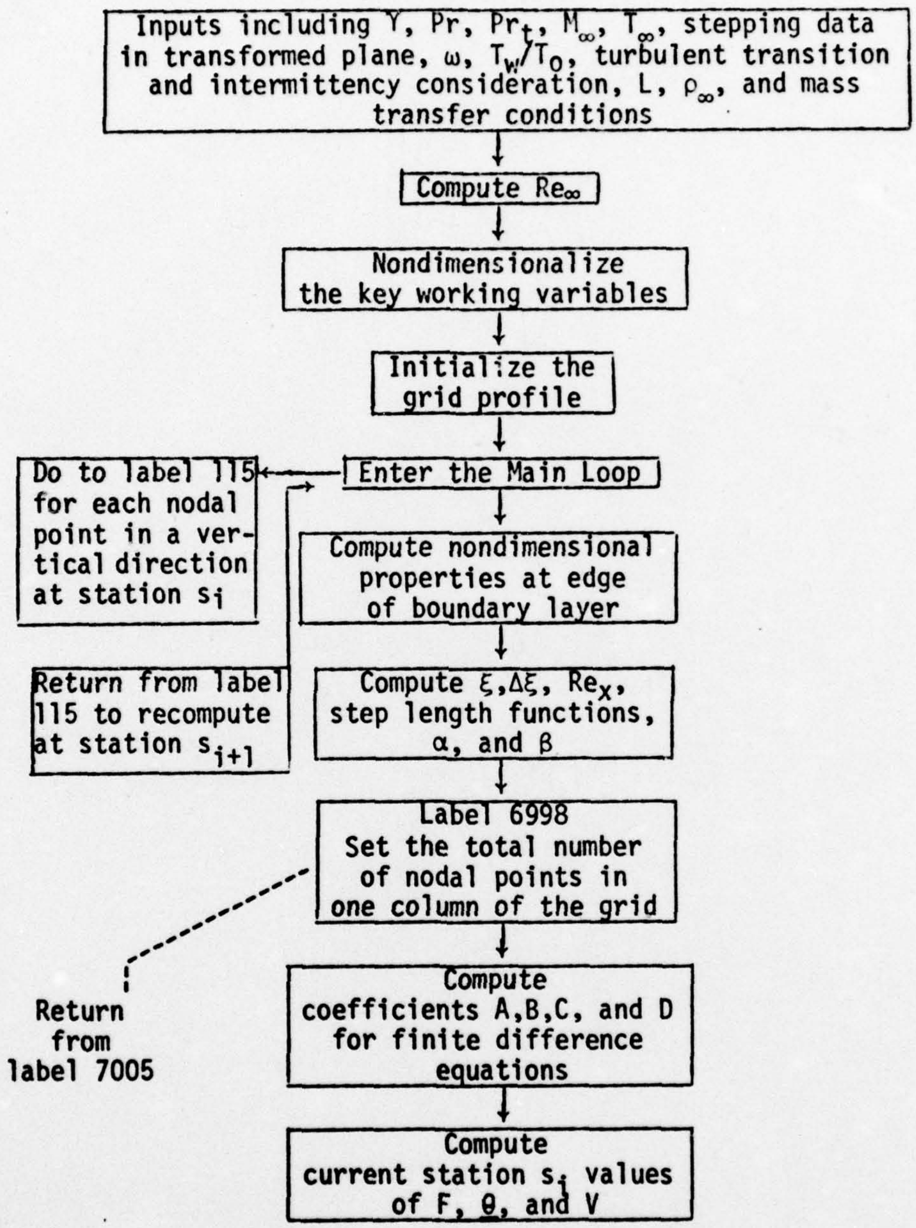

Continued on following page

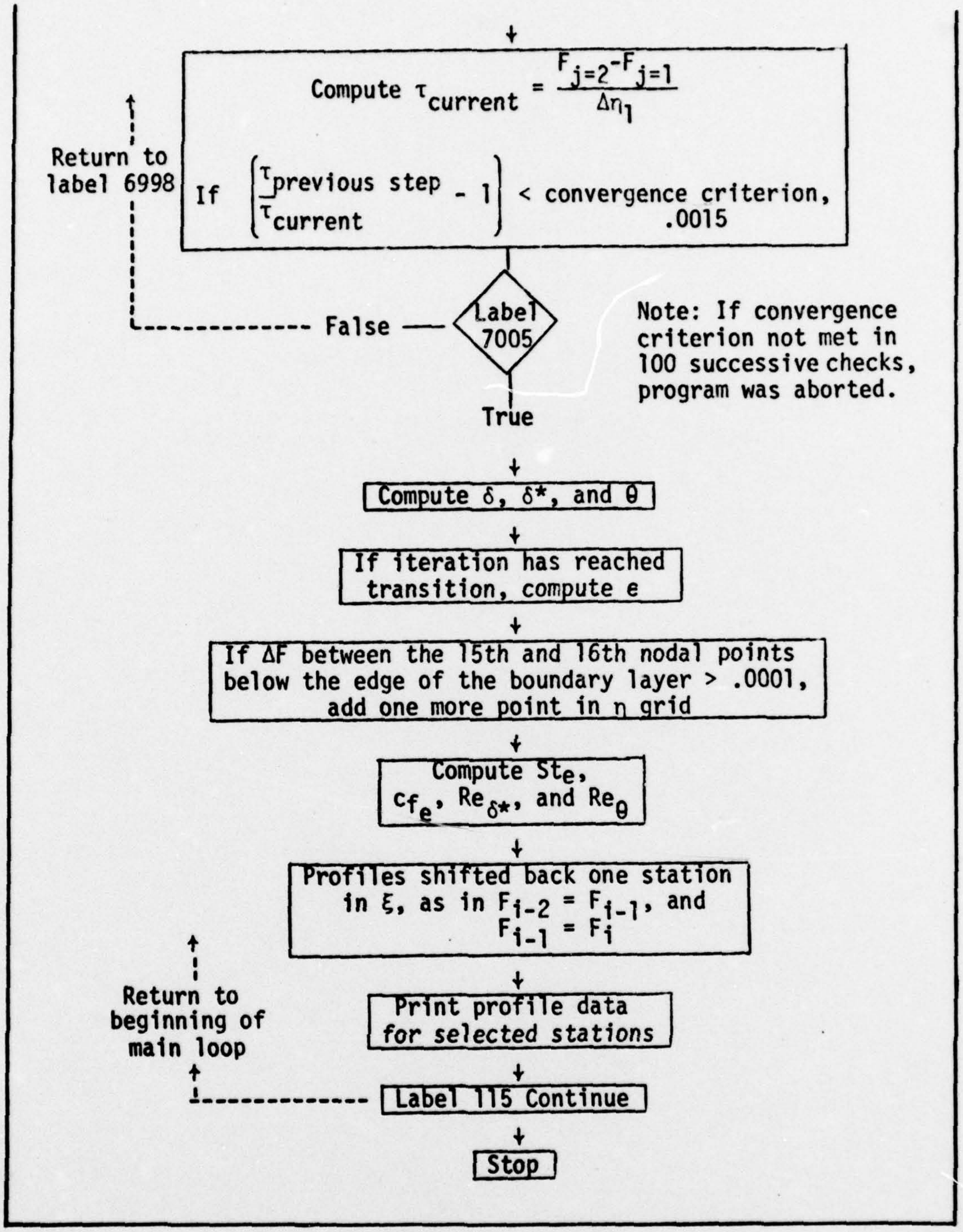

Fig. 2. Flow Diagram of the Logical Steps to Solution within Itract

Key portions of the foregoing logic required further explanation. Therefore, Appendix C was included to discuss four important subsystems of the original code. These subsystems included nondimensionalization of the working variables and initialization of the grid, generation of the finite difference system, the computation of e, and the compution of St_e and c_{f_e}. A Fortran computer code key was also included in Appendix D. With an understanding of these features of the code, the boundary condition of mass transfer was considered. Including this boundary condition represented the major modification to the original code, and the remainder of this chapter was devoted to an explanation of this addition.

Mass Transfer

Mass transfer at the surface was defined by the expression $(\rho v)_w$. Consistent with the nondimensionalized variables used in this problem a mass transfer factor, $\frac{(\rho v)_w}{(\rho u)_{\infty \text{ or } e}}$, was defined and used to express the amounts of mass transfer being considered in any particular problem. This transfer model was incorporated through the variable transformation

$$V = \frac{2\xi}{\rho_e u_e \mu_e r_o^{2j}} \left[F \frac{\partial \eta}{\partial x} + \frac{\rho \tilde{v} r_o{}^j t^j}{\sqrt{2\xi}} \right] \qquad (18\text{-}3)$$

and expressed in the equation of continuity

$$\frac{\partial V}{\partial \eta} + 2\xi \frac{\partial F}{\partial \xi} + F = 0 \qquad (20)$$

where, V appeared explicitly in the finite difference expression for continuity.

Considering Eq (18-3) in detail, the following points were noted: First, at the surface F or u/u_e was zero. Second, t^j, where t was the ratio r/r_o, was set equal to one. This assumption was made following

the proposition that δ was much less than the radius of the cone. Figure 3, though the boundary layer was shown out of proportion, depicted the pictorial justification for this assumption.

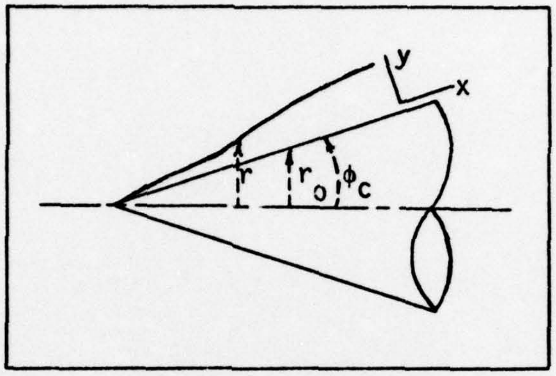

Fig. 3. Radial Measurements on a Cone

Third, from an earlier definition restated, $\tilde{v}$ was equal to $v + \frac{\overline{\rho'v'}}{\rho}$. It was noted that $\tilde{v}_w$ was equal to v_w at the wall or surface as the apparent mass flux, $\overline{\rho'v'}$, was zero. With these three propositions Eq (18-3) was expressed for the wall condition as follows:

$$V_w = \frac{(\rho v)_w \sqrt{2\xi}}{\rho_e u_e \mu_e r_o^{\,j}} = V(\xi,0) \text{ or } V(i,1) \text{ in the grid notation} \tag{24}$$

Returning to the entire equation of continuity, integration yielded an expression for V at any grid point at station s_i:

$$V(i,j) = V(i,1) - \int_0^{\eta_j} \left(2\xi \frac{\partial F}{\partial \xi} + F\right)_i d\eta \tag{25}$$

where V(i,1) was the boundary condition of mass transfer. To include V_w or V(i,1), further substitution within Eq (24) was performed. From fig 3, r_o was equal to x sin ϕ_c, and it could be shown that

$$\xi = \rho_\infty u_\infty \mu_\infty L^{2j+1} \left(\frac{\mu_{ref}}{\mu_\infty}\right) \sin^{2j}(\phi_c) \int_0^x \frac{\rho_e}{\rho_\infty} \frac{u_e}{u_\infty} \frac{\mu_e}{\mu_{ref}} \left(\frac{x}{L}\right)^{2j} d\left(\frac{x}{L}\right) \tag{26}$$

Letting

$$X = \int_0^x \frac{\rho_e}{\rho_\infty} \frac{u_e}{u_\infty} \frac{\mu_e}{\mu_{ref}} s^{2j}\, ds \tag{27}$$

and with one additional intermediate step it was shown that

$$\sqrt{2\xi} = \left[\rho_\infty u_\infty \mu_\infty L \frac{\mu_{ref}}{\mu_\infty}\right]^{1/2} L^j (\sin\phi_c)^j (2X)^{1/2} \tag{28}$$

and, finally,

$$V_w = \left[\left(\frac{\rho_\infty u_\infty L}{\mu_\infty}\right)^{1/2} \Big/ \left(\frac{\mu_{ref}}{\mu_\infty}\right)^{1/2}\right] \frac{1}{s^j} \left(\frac{(2X)^{1/2}}{\frac{\rho_e}{\rho_\infty} \frac{u_e}{u_\infty} \frac{\mu_e}{\mu_{ref}}}\right) \left(\frac{\rho_w v_w}{\rho_\infty u_\infty}\right) \tag{29}$$

Now in terms of quantities immediately available in the program, this expression was cast into an equivalent form using nondimensional program variables (Ref 8:18,35; Ref 10). With Eq (29) including the effects of mass transfer, the equation of continuity was considered next.

Cast into a form of finite differences, continuity was expressed as follows:

$$C3(1,3)V(i,j+1) + C3(1,2)V(i,j) + C3(1,1)V(i,j-1) + A3(1,2)F(i,j) = D3(1) \tag{30}$$

At the surface this expression simplified to

$$C3(1,1)V(i,j-1) = D3(1) \tag{31}$$

Setting C3(1,1) equal to one and D3(1) equal to the right side of Eq (29) the mass transfer boundary condition had been set and was included with the other boundary conditions in solving the system of finite difference equations.

In order to set an appropriate boundary condition at each station along ξ during the computation, two subroutines were added to the program. For the case in which a constant mass transfer rate was specified in a real sense along the surface from some initial longitudinal station to a second station where mass transfer was terminated, subroutine Conblw provided an appropriate transformed value for the transfer at each station computed. A second subroutine, Genblw, provided the same information, but for a generally varying mass transfer rate. Using a linear interpolation between stations of known mass transferring strength, the boundary condition was computed for each streamwise station within the specified region of mass transfer. Finally, although not incorporated into the code, an approximation using a cubic spline description between known or specified points of transfer rate was devised during this study. It was thought that this technique would have provided a better description of a generally varying mass transfer rate, and the theory of the proposed modification was included in Appendix E (Ref 11). However, with the other modifications completed, numerical solutions with mass transfer were compared with analytical and actual experimental results, and the results of those comparisons were included in Chapter IV.

IV. Results and Discussion of the Study, Flat Plate and Cone

The modified program was compared with theory and data from three primary sources. First, using mostly analytical expressions and some experimental data presented in Schlichting (Ref 12) a study was made of laminar, subsonic flow over a flat plate for the cases of no mass transfer and a constant rate of suction throughout the length of the model. Second, from the results of an experiment performed by Moffat and Kays (Ref 13) a comparison was made for fully turbulent, subsonic flow over a flat plate. The comparison was made for the cases of no mass transfer, constant blowing, and constant suction over a specified region of the model. Finally, from an experiment performed for flow over a sharp nosed, axisymmetric cone by Martellucci, Laganelli, and Hahn (Ref 14; Ref 15), data was obtained to test the computer code for the case of hypersonic flow. For this case of hypersonic, conical flow, the numerical results were compared in laminar, transitional, and turbulent environments for the cases of no mass transfer and positive mass transfer or blowing.

In these studies a number of important assumptions were made, some of which were mentioned earlier in introductory comments. The boundary layer thickness, δ, was minutely small compared to the characteristic length, L. The velocity gradient, $\frac{\partial u}{\partial y}$, was large in this region, and the shear stress, $\mu\frac{\partial u}{\partial y}$, assumed large values. Beyond the boundary layer no large velocity gradients existed and viscosity was negligible. The flow was considered inviscid and potential beyond the edge of the boundary layer. Finally, the Navier-Stokes equations were simplified to the boundary layer equations to describe flow characteristics for y less than δ(Ref 12:117-121).

Schlichting, Primarily an Analytical Verification for Laminar Flow Over a Flat Plate

For purposes of this study, a hypothetical model and some flow conditions were needed to make the comparison between analytic results and the predictions of the code. A comparison for the case of no mass transfer was followed by a study with a constant rate of suction over a flat plate.

Beginning with the case of laminar subsonic flow with no mass transfer at the surface, working variables were assigned the following values. Re_∞ was adjusted to about $1.(10)^6$ in keeping with the laminar propositions of Blasius. Further, T_w was selected equal to T_∞ to be consistent with the environment for which Eq (33) would be valid. It was also consistent with the results of Eq (32);

$$T_w - T_\infty \gtrless \sqrt{Pr}\,\frac{u_\infty^2}{2\,c_p} : \text{Heat wall} \rightleftarrows \text{gas} \tag{32}$$

The right side of this inequality for the test under investigation produced an extremely small difference between T_w and T_∞, and hence, there was zero heat transfer or the adiabatic case. Finally, a length of three ft was chosen for the hypothetical model of the flat plate in order to specify Re_∞. The remaining inputs for this first test for program verification included an M_∞ equal to .01, a T_∞ of 533.1 R, and a ρ_∞ equal to $1.12(10)^{-2}\,\frac{lb_f sec^2}{ft^4}$. For verification in at least this case of steady laminar flow over a flat plate without mass transfer, the resulting computations at station s equal to .155 and station s equal to .750 were chosen for comparison with the calculations of the exact expressions listed in Schlichting. The quantities chosen for comparison were δ^*, τ_w, c_f, and δ^*/θ. Also included was a comparison of velocity

and temperature profiles with data presented in Schlichting from the work of Hantzsche and Wendt (Ref 12:323). From Schlichting, the following expressions of Blasius were used for computation:

$$1.721 = \delta^* \left(\frac{u_\infty}{\nu x}\right)^{1/2}$$

$$.332 = \frac{\tau_w}{\mu u_\infty}\left(\frac{\nu x}{u_\infty}\right)^{1/2}$$

$$\frac{c_f}{2} = \frac{\tau_w(x)}{\rho u_\infty^2} = .332\left(\frac{\nu}{u_\infty x}\right)^{1/2} = \frac{.332}{(Re_x)^{1/2}} \qquad (33)$$

$$2.59 = \delta^*/\theta$$

The results of a comparison between computations performed by the use of the above expressions and by calculations performed by the computer code, Itract, were summarized in Table I.

Table I

A Comparison of Methods for Boundary Layer Calculations

Quantity for Comparison	Station s = .155		Station s = .750	
	Schlichting	Itract	Schlichting	Itract
δ^*(ft)	$2.03\ (10)^{-3}$	$2.00\ (10)^{-3}$	$4.47\ (10)^{-3}$	$4.40\ (10)^{-3}$
$\tau_w(lb_f/ft^2)$	$1.21\ (10)^{-3}$	$1.21\ (10)^{-3}$	$5.52\ (10)^{-4}$	$5.52\ (10)^{-4}$
c_f	$1.68\ (10)^{-3}$	$1.70\ (10)^{-3}$	$7.66\ (10)^{-4}$	$7.71\ (10)^{-4}$
δ^*/θ	2.59	2.61	2.59	2.62

To quantify the difference noted between the predictions of Itract and the analytical or experimental data, an error was defined as the quotient of the absolute difference between the quantities compared and the larger

of the two quantities. Thus, the results of Table I demonstrated a closeness to within the following percentage errors. At station s equal to .155 the calculations of δ^* were within 1.5 percent, τ_w results were nearly identical, the calculations of c_f were within 1.1 percent, and the computations of δ^*/θ were within .8 percent of one another. A similar trend was noted at station s equal to .750. The calculations of δ^* were within 1.5 percent, τ_w results were again equivalent, the calculations of c_f were within .6 percent, and the computations for δ^*/θ were within 1.1 percent of one another.

Further tests for verification of the program in this first case study were accomplished by comparing velocity and temperature profiles calculated by Hantzsche and Wendt with the predictions of Itract (Ref 12:323, fig 13-11). It was noted that $5(y/\delta)$ in the code was equivalent to the η of Blasius. Further, the $\frac{u}{u_\infty}$ of Blasius was equivalent to $.995 \frac{u}{u_e}$ in Itract. With these relationships plus the computational equivalence of T_e in Itract to T_∞ in Schlichting, the results of the comparison were listed in Table II with a graphical presentation of the velocity profiles presented in fig 4. Concerning the velocity profile, the data of station s equal to .731 was used for comparison, but with similarity of solution for this particular investigation and the non-dimensionalized nature of the data, another station would have been equally valid for comparison.

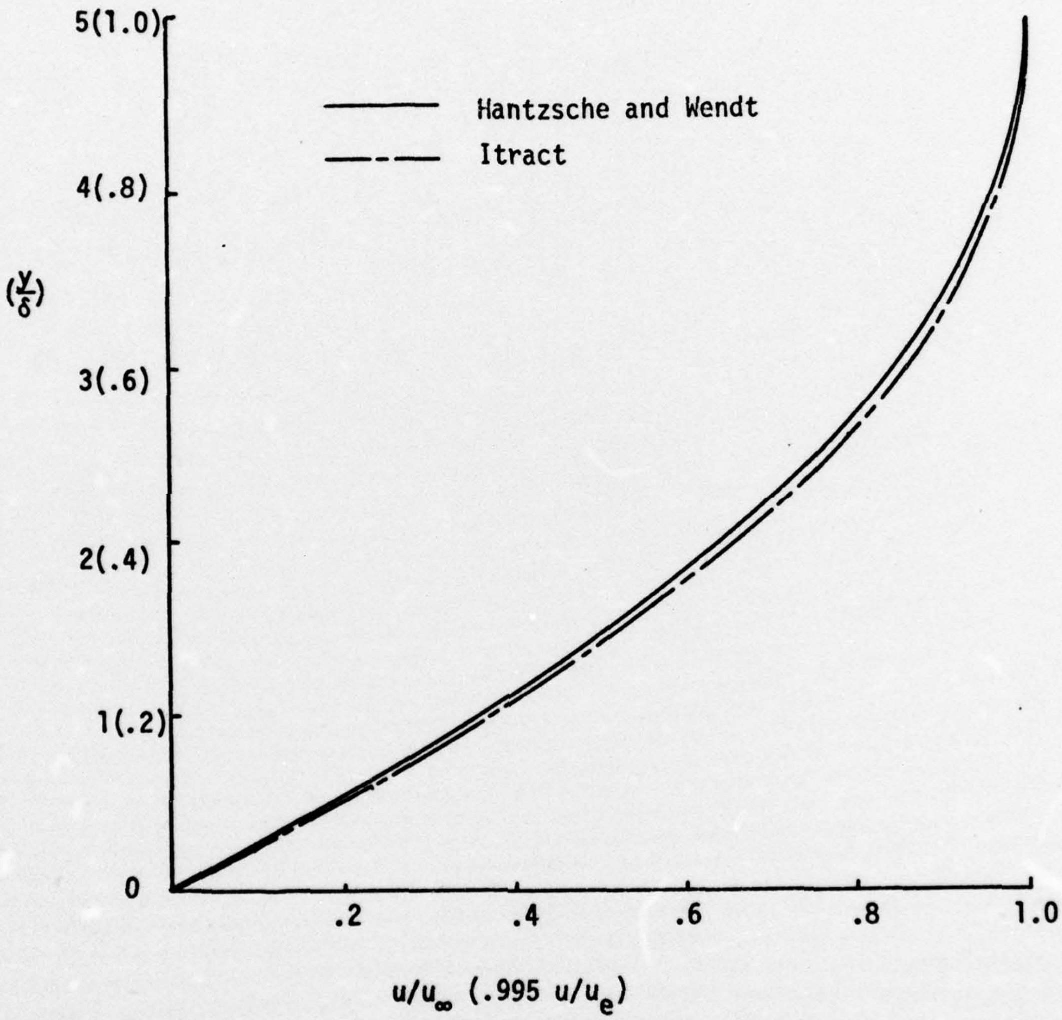

Fig. 4. A Comparison of the Predictions of Hantzsche and Wendt Versus Itract (Ref 12)

Table II

A Comparison of Velocity and Temperature Profiles

Blasius η	Itract y/δ	H and W u/u_∞	Itract .995 u/u_e	H and W T/T_∞	Itract T/T_e
1	.2	.35	.36	1.0	1.0
2	.4	.64	.65	1.0	1.0
3	.6	.84	.85	1.0	1.0
4	.8	.95	.96	1.0	1.0
5	1.0	.99+	.99+	1.0	1.0

The greatest error in this comparison was less than 2.8 percent within the velocity profile study. With these profile comparisons the investigation for the first case was completed. Case two added mass transfer to the problem.

Initial testing of the actual modification to the program began with the addition of a small mass transfer condition, constant suction. Kays also presented the method of Rubesin for analytically studying large mass transfer rates (Ref 16:324-325). To complete the study for small constant suction the experimental and analytical work of Head and Iglisch, as published in Schlichting, was used to verify the results of Itract (Ref 12:373, Fig 14.11.1). T_w remained equal to T_∞ for this second test. ρ_w was then shown to be equal to ρ_∞ by the equation of state, and from fig 14.11.1, therefore, $\frac{(\rho v)_w}{(\rho u)_\infty}$ was equal to $-1.6(10)^{-4}$ in Itract. Data was collected at the nondimensional streamwise position

$$s = \frac{.077\left[\frac{u_\infty}{-v_w}\right]^2}{Re_\infty} \tag{34}$$

This implied that the profile data of Head was recorded along the flat surface at a station where Re_x was approximately $3.00(10)^6$. For this comparison, then, the hypothetical length of the model was extended from 3 ft to 30 ft, where Reynolds numbers of this size would be encountered. Laminar conditions were still assumed to exist. Assuming in fig 14.11.1 of Schlichting that δ was approximately 1.8 mm, a graphical comparison for this test was presented in fig 5.

To show the effect on the shape of the velocity profile by the addition of suction, fig 6 portrayed the results of Itract for the boundary layer flows with and without suction. These results agreed with the results presented in Schlichting (Ref 12:369, fig 14.6).

Now, as with the first case study, there existed an exact solution for flow over a flat plate with continuous, constant suction. The following equation represented an exact solution of the complete Navier-Stokes equations:

$$u(y) = u_\infty \left[1 - \exp\left(\frac{v_w y}{\nu}\right)\right] \tag{35}$$

$$\text{for } v(x,y) = v_w < 0$$

From this expression came the following equations:

$$\delta^* = \frac{\nu}{-v_w}$$

$$\theta = \frac{\nu}{-2v_w}$$

$$\tau_w = \rho(-v_w)u_\infty, \text{ and hence,} \tag{36}$$

$$c_f = \frac{\tau_w}{1/2\rho u_\infty^2} = \frac{-2v_w}{u_\infty}$$

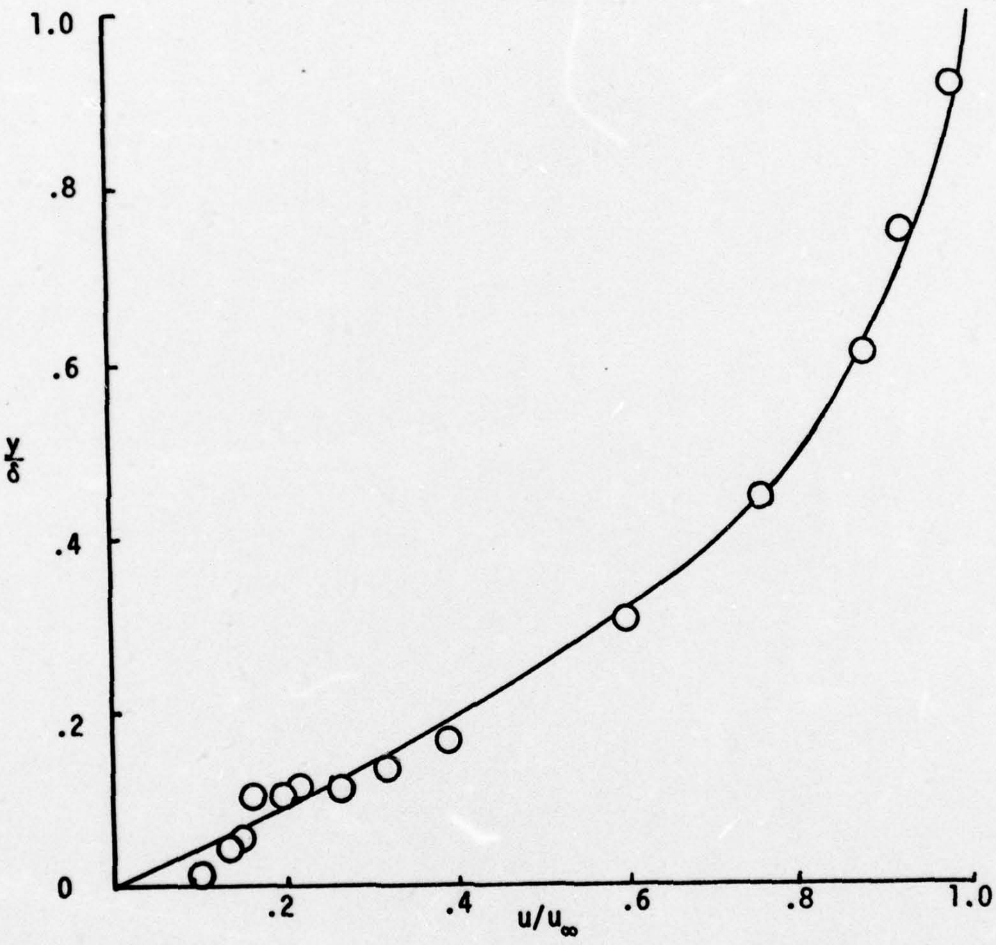

Fig. 5. Experimental Data with Suction Compared to the Prediction of Itract (Ref 12)

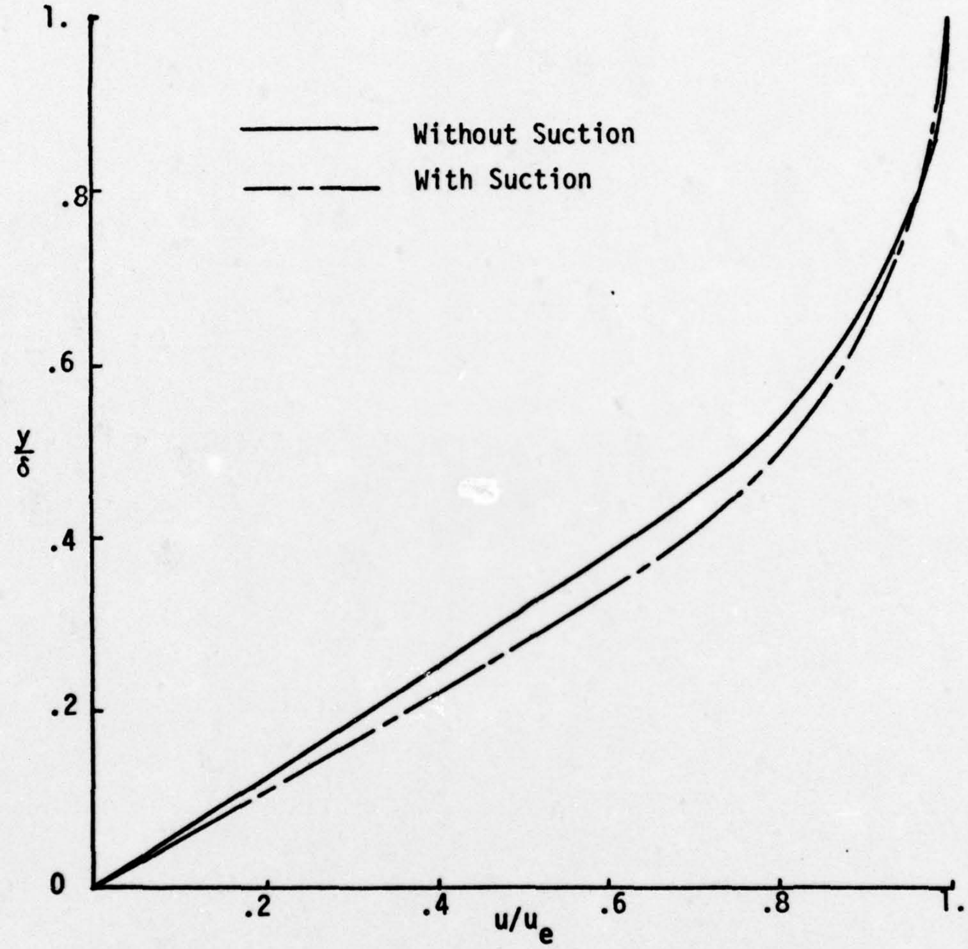

Fig. 6. Matching the Profiles Presented in Schlichting, Fig 14.6 (Ref 12)

It was noted that in each case, δ^*, θ, and c_f were constant. This solution was realized only at some distance from the leading edge. The boundary layer grew from zero at the leading edge and continued downstream asymptotically to the values predicted by Eq (36). These values were reached at what was termed the asymptotic suction layer limit. Iglisch has shown that the asymptotic state was reached after a length of about

$$x = \frac{4\nu}{u_\infty}\left(\frac{u_\infty}{-v_w}\right)^2 \tag{37}$$

To simulate this asymptotic solution the length of the hypothetical model was extended still further to 3000 ft, and the remaining input conditions were held constant. Iglisch then predicted an asymptotic solution by station s equal to .156. Itract had come within 2.3 percent of the final asymptote by s equal to .155. Table III summarized the results from the equations of the exact solution above, and compared those calculations with the corresponding predictions of Itract at an s of .347, the point of closest approach to the analytical asymptotic values.

Table III

A Laminar Flat Plate Study with Suction

Quantity	Exact Solution	Itract	Percent Error
δ^*/L	$6.25(10)^{-6}$	$6.04(10)^{-6}$	3.3
θ/L	$3.12(10)^{-6}$	$2.97(10)^{-6}$	4.9
c_f	$3.20(10)^{-4}$	$3.24(10)^{-4}$	1.2

Finally, all testing thus far that included mass transfer had been accomplished using the routine that incorporated constant mass transfer rates at the surface. Before investigating other experiments with flat plates, the variable mass transfer routine was verified. First, using the three ft model, Itract computed a boundary layer perturbed by a constant rate of suction from a point one ft from the leading edge to a point two ft from the leading edge. The computation was repeated with the same inputs with the exception that the variable mass transfer routine was called to compute the boundary condition in lieu of the constant mass transfer routine. Identical results were noted for the two tests.

With this final check the verification process departed from the laminar flow study and considered turbulent flow over a flat surface. For this study the results of experiments performed by Moffat and Kays were used.

Moffat and Kays, A Verification for Turbulent Flow Over a Flat Plate Using Experimental Results

R. J. Moffat and W. M. Kays of Stanford University performed an experiment in which they were primarily concerned with heat transfer through a turbulent boundary layer over a flat plate which was perturbed by both positive and negative mass transfer at the solid boundary. The results of their wind tunnel study provided a criterion for evaluating the heat transfer model of Itract under turbulent conditions. Heat transfer in the experiment was quantified in the form of a Stanton number, St. The accuracy of the apparatus used allowed determination of the Stanton numbers to within 10^{-4} units over most of the range of mass transfer. The experiment was performed on a transfer range from the

asymptotic suction layer limit discussed earlier to the apparent blow off or separation of the boundary layer. Presented in this section are results of testing and a discussion of a parameter study performed to minimize the effects of higher order terms not included and, hopefully, match this numerical model with the experimental environment for the no transfer case. With accurate predictions for this case, the results for small amounts of blowing and suction were given next. Finally, the range of accurate prediction of the computer code was tested, with these results included last.

To begin, a wind tunnel run was chosen with the following conditions: u_∞ was equal to 44.5 ft/sec, T_∞ was 524.0 R, and T_w was 556.6 R. The experimental data collected was listed in Table V. The length of the model was given as 8 ft. It was assumed that the last value of Re_x was taken from the end of the plate, and could be considered a close approximation to Re_∞. Further, it was assumed that the flow was turbulent over the entire length of the wind tunnel model. A parameter study was then begun to find the best combination of those variables which described the grid to minimize error caused by the truncation of higher order terms, and pick two parameters which helped describe the characteristics of the flow. These two classes of variables included the following: XXK, the constant ratio of any two successive $\Delta\eta$ spaces; PRT, the turbulent Prandtl number taken to be 1. or .9 in the literature; XINTER set to 1. or 0. depending on whether eddy model one or eddy model zero was to be used; DYW, the size chosen for $\Delta\eta_1$; and IEDGE, the total number of divisions in η to be used in the computation of the grid. The objective was to closely predict the Stanton number for a corresponding Re_x that ranged from $4.55(10)^4$, where measurements of heat transfer began, to the end of the plate at an Re_x of

$2.14(10)^6$. Table IV of Appendix F summarized the combinations of variables with Table V of that same appendix actually presenting the results of those variable combinations. The figures of column 4 produced the best match with the experimental results. Excluding the readings at an Re_x of $4.55(10)^4$ the greatest error was recorded at an Re_x of $2.27(10)^5$ with an error of 5.7 percent. Column 3 had produced nearly identical results, but had incorporated inefficiently small stepping increments into the numerical scheme. A graphical presentation of the experimental results with the analytical predictions of column 4 and column 1 was included in fig 7. In a final note, with the exception of readings at Re_x values of $4.55(10)^4$, $2.27(10)^5$, and $3.18(10)^5$, the remaining errors were less than or equal to 3.9 percent.

With the case for zero mass transfer recorded, two more experimental runs were investigated. First, an experiment which included a blowing rate, $\frac{(\rho v)_w}{(\rho u)_\infty}$, of $1.(10)^{-3}$ was run under the following conditions: u_∞ was equal to 44.1 ft/sec, T_∞ was 525.7 R, and T_w was 557.7 R. In a simulation by Itract the results were presented in Table VI of Appendix F with a graphical presentation included in fig 8. From Table VI it was noted that in setting XINTER equal to 0., and thereby using eddy model zero in the calculation of ϵ, more accurate Stanton numbers resulted. Next, an experiment which included a rate of suction, $\frac{(\rho v)_w}{(\rho u)_\infty}$, equal to $-1.15(10)^{-3}$ was run under the following conditions: u_∞ was equal to 42.5 ft/sec, T_∞ was 524.3 R, and T_w was 549.7 R. Again, the results of a simulation by Itract were presented in Table VII of Appendix F with the graphical equivalent included in fig 8. Unlike the case with blowing the tabular results for this case with suction showed that the more accurate predictions of Stanton numbers came by setting XINTER equal to 1., and

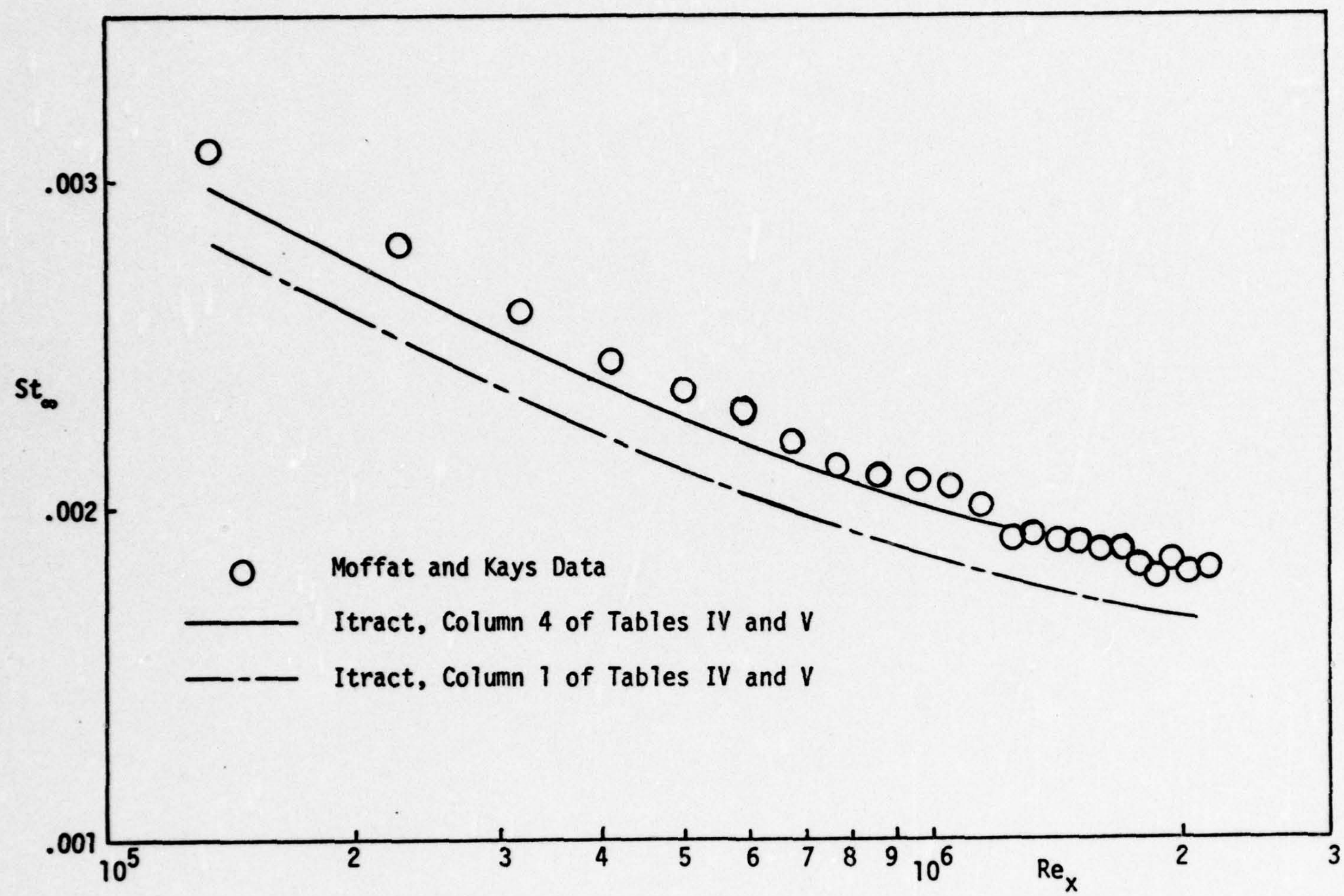

Fig. 7. Matching Itract with Moffat and Kays for the Case of Zero Mass Transfer (Ref 13)

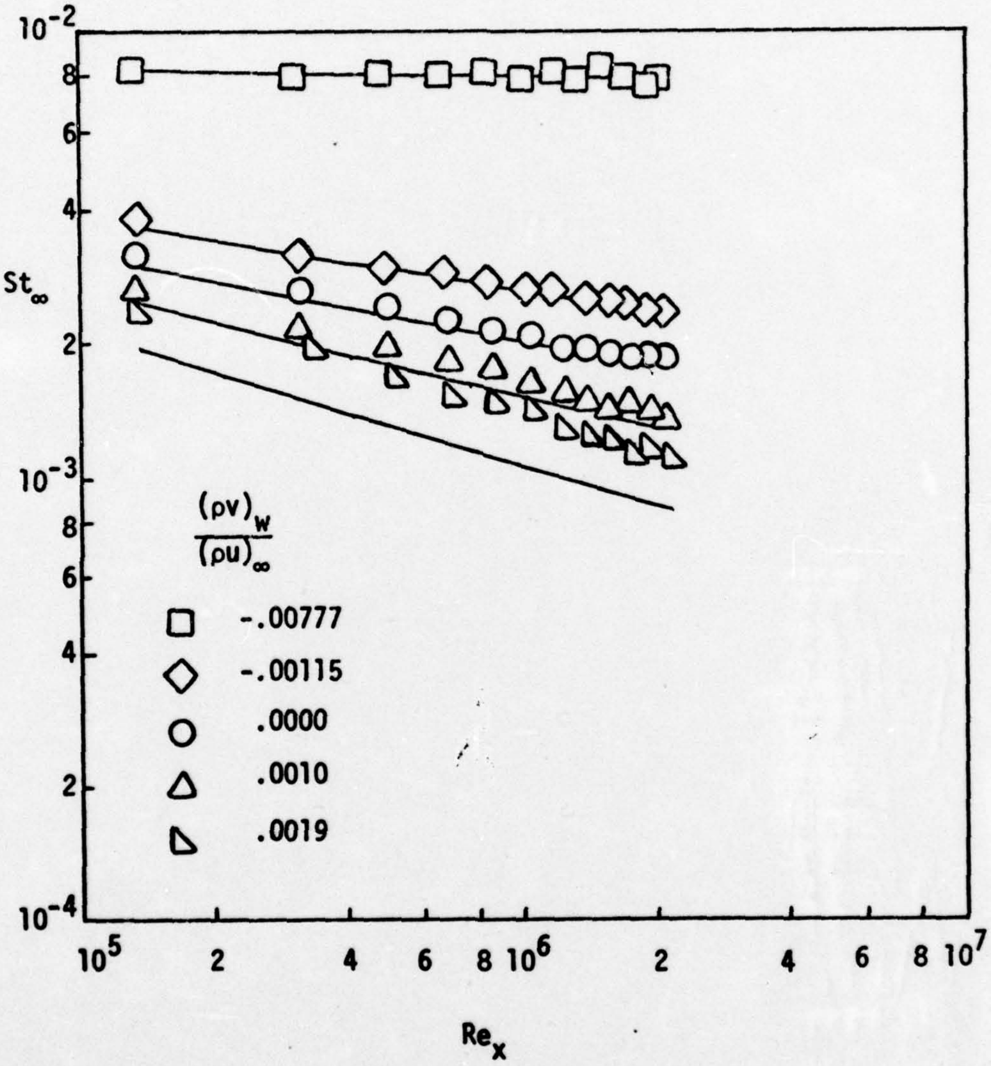

Fig. 8. A Comparison of Itract and Moffat and Kays for the Cases of Blowing and Suction (Ref 13)

thereby using eddy model one. Finally, with simulations performed for both the small positive and negative mass transfer cases, it was then appropriate to find the limits of accurate simulation by Itract.

In this final phase of flat plate testing Itract was simulated at the extreme limits of the Moffat and Kays experiment. In the limiting case for suction, termed the asymptotic suction layer limit, Itract was able to predict Stanton numbers to within 5.3 percent, excluding one reading taken at a station where Re_x was equal to $4.3(10)^4$. The wind tunnel conditions for this test included the following: u_∞ was equal to 41.8 ft/sec, T_∞ was 523.8 R, and T_w was 552. R. The rate of suction was $\frac{(\rho v)_w}{(\rho u)_\infty}$ equal to $-7.77(10)^{-3}$. The tabular results of this test were included in Table VIII with the graphical summary included in fig 8. Again, as with lower suction rates, more accurate results were noted when eddy model one was used. However, unlike the case for suction, in the testing of positive mass transfer or blowing, Itract was unable to predict heat transfer to the limiting point of blow off or boundary layer separation, which occurred experimentally near $\frac{(\rho v)_w}{(\rho u)_\infty}$ equal to $9.6(10)^{-3}$. The results of the predictions of Itract for rates of blowing equal to $1.(10)^{-3}$ have already been presented. For the code, the limiting transfer rate for which there existed experimental data was $1.91(10)^{-3}$. At this transfer rate the numerical scheme could compute the boundary layer problem without an error finish. The results of this test were included in Table IX with a graphical summary included in fig 8. It was noted that with the finer mesh of nodal points Itract was able to predict consistently the Stanton numbers for various Re_x up to a point where the numerical scheme failed. While the scheme was able to compute, Itract consistently predicted Stanton numbers $3.(10)^{-4}$ less than the experimental

results from an Re_x of $2.28(10)^5$ to $1.23(10)^6$ where the program experienced an error finish. With a coarser mesh of nodal points Itract was able to complete the numerical computation, but with predictions of Stanton number that were not as close as previous tests. Rather than a nearly constant difference of prediction as previously seen, the results of this test showed Itract to predict Stanton numbers lower than experimental by about 22.8 percent. From an Re_x of $2.28(10)^5$ through the end of the computation the greatest deviation from this figure was to 25.7 percent. Finally, in a test case for a mass transfer of $3.8(10)^{-3}$, using a coarse grid of $\frac{\Delta\eta_{j+1}}{\Delta\eta_j}$ equal to 1.15, $\Delta\eta_1$ at $5.(10)^{-4}$, and 100 divisions in the η grid, Itract was able to successfully compute the boundary layer without error finish. However, experimental values of Stanton number ranged from $2.36(10)^{-3}$ to $6.2(10)^{-4}$, and with Itract predicting values consistingly greater than $5.(10)^{-4}$ below the experiment, the results were not included.

The results for blowing equal to $1.(10)^{-3}$ displayed the limit of positive mass transfer rate with which Itract could compute accurately. Beyond a transfer rate of $3.8(10)^{-3}$ Itract was neither able to predict Stanton numbers nor successfully complete the computations without an error finish. This completed the comparison with the experiment by Moffat and Kays.

Martellucci, Laganelli, and Hahn, A Study of Turbulent Flow Over an Axisymmetric Cone with Experimental Results

A. Martellucci, A. L. Laganelli, and J. Hahn of the General Electric Reentry and Environmental Systems Division performed an experiment over a two year period in which they were concerned with heat transfer

behavior and boundary layer profile characteristics for hypersonic flow over a sharp nosed, slender, axisymmetric cone. Their experimental results of heat transfer and profile data provided numerous quantities by which to evaluate the modified code.

In the experiment, data was collected for nominal, positive mass transfer rates as follows: 0., $5.(10)^{-4}$, $1.(10)^{-3}$, and $1.5(10)^{-3}$. All four transfer rates were investigated in this study, with comparisons between data and numerical predictions made for the heat transfer at the surface, the velocity profile, and the static temperature profile. In making this comparison there was a problem in describing the flow environment downstream of the leading oblique shock wave.

Unlike the study of flow over a flat plate, the oblique shocking effect on the cone was great enough to significantly change the fluid state downstream of the shock wave. Therefore, for purposes of computation, the actual free stream conditions were not of direct use to the computer code. Rather, the environment downstream of the shock wave was the needed condition for input into Itract. Computing these conditions for input would have been a time consuming problem in itself, and the needed additions to the existing code to perform this computation were not pursued. In order to provide the conditions at the edge of the boundary layer, graphs of characteristics of flow over a cone, such as those found in NACA 1135, were considered. Not only did the resolution of the graphical information seem inadequate for the range of mach number being considered, but the data presented was for an inviscid, compressible solution. Tabulated data such as that included in reference 17 was considered, and though accurate, it still posed data for an inviscid solution. Investigations were made using the data of the

inviscid solution in reference 17 as inputs to Itract. It was judged that this method did not yield results close enough to the physical situation at hand to be considered a valid approximation. To obtain viscous inputs for Itract, the decision was made to use data presented with the results of the experiment performed at General Electric.

A review of the experimental technique was appropriate. As stated previously, the data collected in the experiment was of two categories. These two categories of data were collected in separate runs of the wind tunnel. Initially, the model of the cone was exposed to flow at an M_∞ equal to eight for a few seconds. The heat transfer data was collected and flow within the tunnel was stopped. After the surface data had been taken, flow, again at an M_∞ equal to eight, was started. The interaction of the flow over the model of the cone was allowed to reach an equilibrium state, and the second category of data profile information was collected (Ref 4:11). Within this profile data, the following measurements or computations were taken for various stations along the cone: M_e, T_e, u_e, ρ_e, $(\rho v)_w$, $(\rho u)_e$, and T_w/T_o. The above quantities, mostly representative of conditions at the edge of the boundary layer, became the new conditions at infinity to be used as inputs to Itract. These inputs were used by Itract to predict surface as well as the field data of the boundary layer. With this assumption, the following approximations were made for computational purposes: First, where data from multiple stations, both longitudinal and azimuthal, along the model was catalogued for the same wind tunnel environment, an arithmetic average of quantities such as M_e, T_e, and ρ_e at these stations was used to compute a new, constant M_∞, T_∞, and ρ_∞ for Itract. Further it was approximated that T_w/T_o was a constant ratio equal to an arithmetic average of

the readings taken along the surface in a streamwise direction. In fact, wall temperature did vary in the experiment and the temperature ratio was seen to vary plus or minus three or four percent from the figure used in computation. It was noted that one term in the denominator of the expression used to compute Stanton numbers was $(1 - T_w/T_o)$, and values for T_w/T_o of .5 to .8 were common (Ref 14; Ref 15). Also, since the definition of the Stanton number of Martellucci was actually an St_∞, it was necessary to multiply the Itract figure by the factor $\frac{\rho_e u_e}{\rho_\infty u_\infty}$ prior to comparison with the experimental data. Finally, there were three descriptions for mass transfer rate: First, a nominal figure for blowing was presented such as $5.(10)^{-4}$, $1.(10)^{-3}$, and $1.5(10)^{-3}$. Second, an actual measurement of this blowing rate would be found by performing the division $(\rho v)_w/(\rho u)_\infty$. This was designated as λ_∞. In like manner, $(\rho v)_w/(\rho u)_e$ was computed and defined as λ_e. All three had different actual values, and all three figures were tested in the modified code. Though all were describing the same mass transfer activity, λ_e was finally selected as the appropriate boundary condition for this code.

Using the assumptions and approximations listed above, the cases tested and presented were of four categories: First, a study of the case for no mass transfer was considered. After this, three investigations followed with nominal mass transfer rates of $1.5(10)^{-3}$, $1.(10)^{-3}$, and $5.(10)^{-4}$. These four cases comprised the entire study of flow over the sharp nosed, axisymmetric cone.

Beginning the study of flow over a cone with a nonblowing case, an experimental test case, data group 132, was chosen from the results of Martellucci, Laganelli, and Hahn. This was a data group depicting heat transfer at the surface of the cone in the form of St_∞ for numerous

longitudinal positions along the surface. Connected with this heat transfer data group were data groups 74 through 79 that presented profile or field data and were the product of the same free stream conditions as data group 132. The free stream conditions included an M_∞ equal to 7.87, T_∞ equal to about 92.9 R, and a ρ_∞ of 2.59 $(10)^{-5}$ $\frac{lb_f sec^2}{ft^4}$. Using data groups 74 through 79, the actual input conditions to Itract were an M_e equal to 6.84, a T_e equal to 121. R, and a ρ_e equal to 3.66$(10)^{-5}$ $\frac{lb_f sec^2}{ft^4}$. The length of the model was five ft, the point of transition was approximated from the experimental Stanton number curve to be about 1.33 ft from the tip of the cone, and an average T_w/T_o was found to be approximately .68. Using this information a tabulated comparison of the heat transfer results was listed in Table X of Appendix G with a graphical depiction included in fig 9. This graph not only showed the results of Itract in comparison with the experimental data but provided theoretical boundaries for heat transfer as predicted by Bell Aircraft Corporation (Ref 18). The lower Bell curve predicted heat transfer assuming the flow was laminar throughout the length of the model. The upper Bell curve predicted the heat transfer assuming fully turbulent flow for the entire length of the model. Concerning the prediction of Itract, it was noted that the curve continually overpredicted the experimental heat transfer, followed similar heat transfer trends as the flow proceeded along the surface, and settled to within 2.3 to 8.4 percent of the data for the last 1.5 ft of the cone. It was further found that, unlike the flat plate study with blowing, eddy model one yielded the better results in predicting heat transfer for the cone. Some of the disparity of heat transfer prediction in the region of transition was due to an approximated turbulent transition point. The first departure

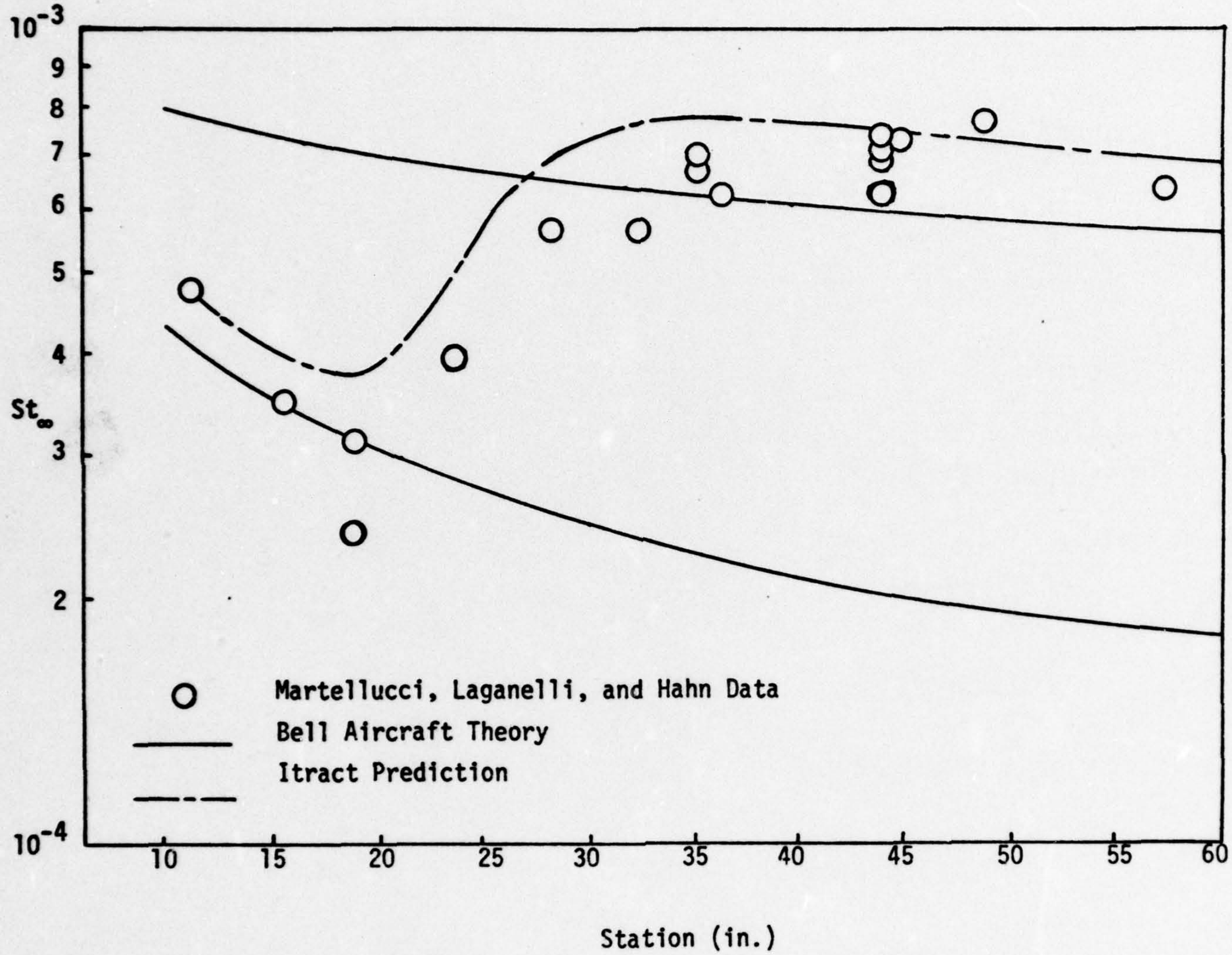

Fig. 9. Matching Itract with Martellucci, Laganelli, and Hahn for the Case of Zero Mass Transfer, Heat Transfer Group 132 (Ref 14)

from a linear trend in the Stanton number data plotted on a logarithmic scale was used as the point of transition (Ref 10). To further investigate this case for no mass transfer two more cases were considered.

It was thought at General Electric that the results of two particular cases offered excellent references or test cases by which to compare the predictions of Itract (Ref 19). The first case was termed a hot wall experiment, a nearly adiabatic wall, and was similar to each of the succeeding cases with mass transfer that would be studied. The free stream conditions for this test, data group 150, included an M_∞ of 8.0, a T_∞ of 97.6 R, and a ρ_∞ of $7.53(10)^{-5}\ \frac{lb_f sec^2}{ft^4}$. For actual inputs to Itract the edge conditions of data groups 148, 149, 207, and 208 were used to simulate conditions downstream of the shock wave of group 150. This led to an M_e of approximately 7.1, a T_e of 123.1 R, and a ρ_e of $1.17(10)^{-4}\ \frac{lb_f sec^2}{ft^4}$. The results of Itract were included with those of General Electric in fig 10 with tabulated results in Table XI of Appendix G. Again, the results showed Itract passing through the field of laminar data points and settling high in the fully turbulent region. In the fully laminar region Itract was within 2.6 percent of the data, and with the exception of one point, Itract settled within 9.3 percent of the data in the fully turbulent region for the last 1.5 ft of the cone. For the second test a cold wall experiment was considered, data group 1. The same free stream and edge conditions existed, and only the T_w was changed. The wall was cooled from 1060 R to 580 R and the experiment was repeated. The results of this comparison were included in fig 11 with a tabular summary in Table XII of Appendix G. Near identical results were noted among the three theoretical codes: Itract, Nsbl, and Vizaad. Nsbl and Vizaad were codes used by General Electric to check

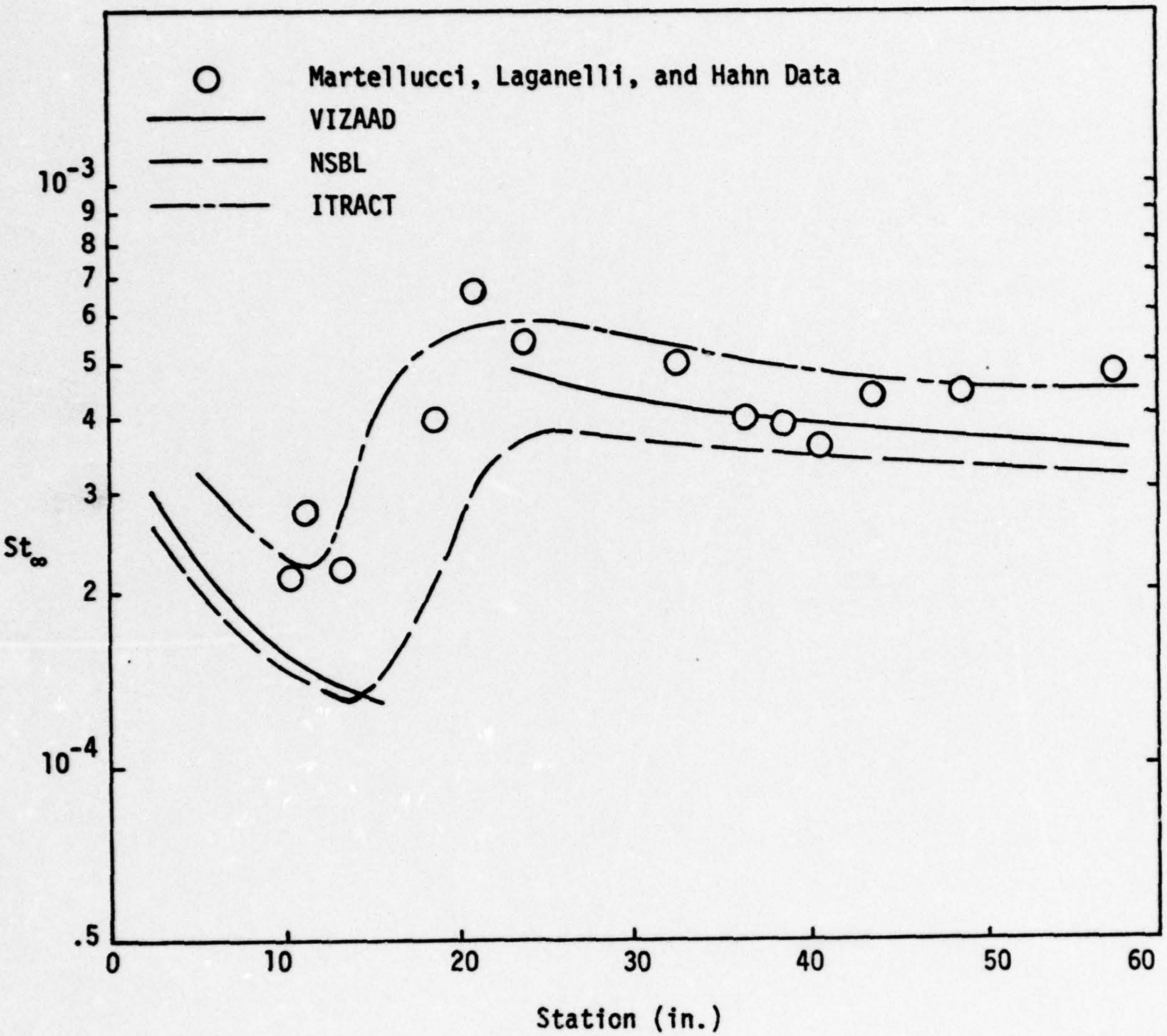

Fig. 10. Comparison with a Hot Wall Reference Test Case, Heat Transfer Group 150 (Ref 15)

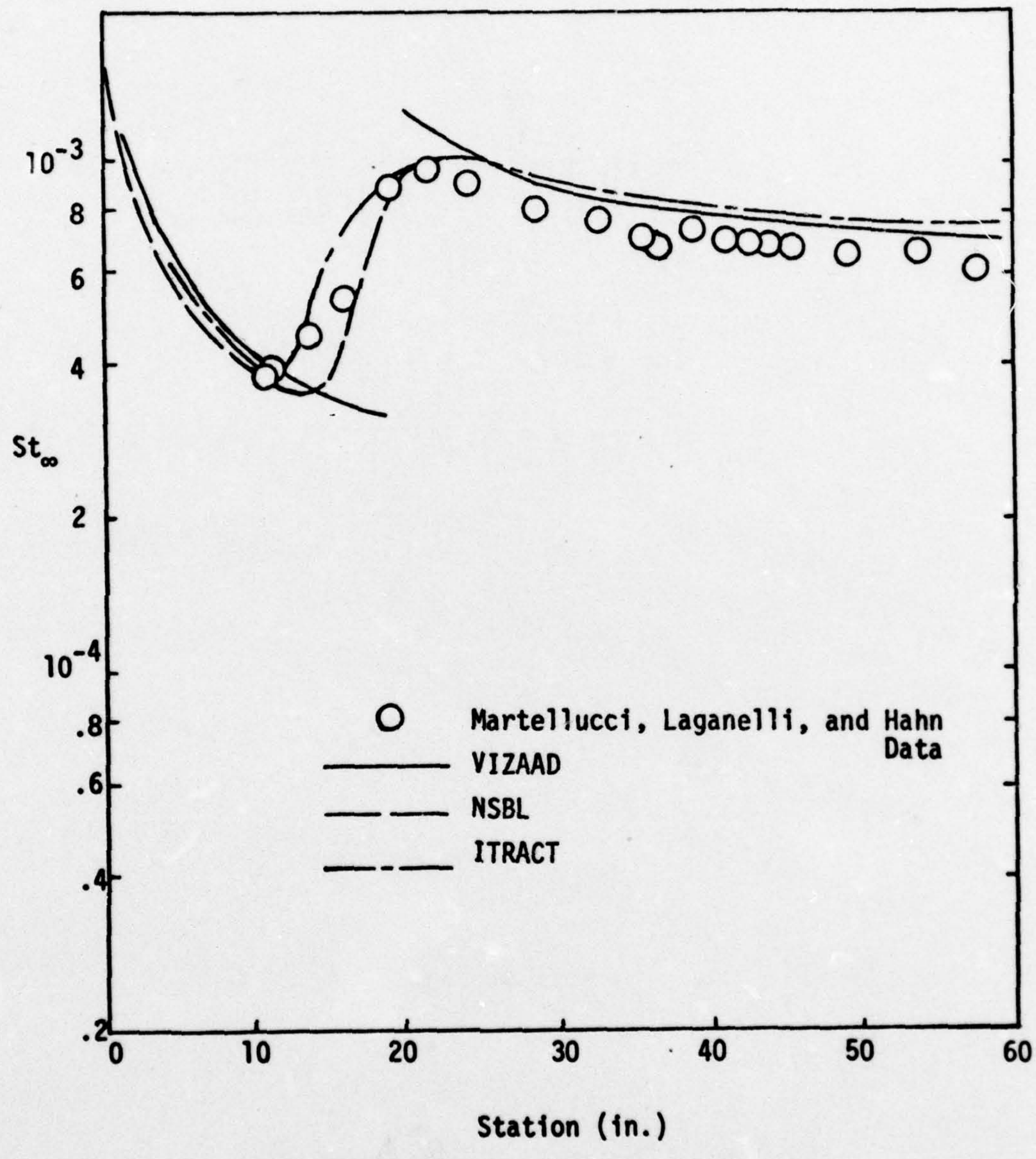

Fig. 11. Comparison with a Cold Wall Reference Test Case, Heat Transfer Group 1 (Ref 15)

their experimental results. In this test Itract was within 8.9 percent of the data over the laminar region and maintained a consistent 13 to 15 percent high prediction over the entire turbulent region. Consistent with the results of data 132, these last two test cases were predicted best using eddy model one. Having noted the consistent trend set in these three heat transfer cases, attention was directed back to profile data groups 74 through 79.

Having used the output of these groups for the investigation of data group 132, the profile data group 74 was again used by Itract to predict the profile shape of velocity and temperature versus $\frac{y}{\delta}$ for station s equal to .466. The results were included in fig 12. Due to the questionable data points for $\frac{y}{\delta}$ less than .4 no percentage error was included.

These results represented the best predictions for heat transfer obtained during the study of the cases for no mass transfer. As with the flat plate study, numerous combinations of grid size, Pr_t, and eddy models were attempted in order to minimize the error in neglecting higher order finite differencing terms and best describe the flow behavior. Having completed the cases with no mass transfer, study began in those cases with transfer.

Beginning with the greatest blowing rate of $1.5(10)^{-3}$, data groups 66, 68, and 73 were chosen for consideration. It was found that Itract was neither able to predict the heat transfer of data group 66 nor the nondimensional profiles of data groups 68 and 73. Various grid sizes were attempted, which in the extreme cases included a $\Delta\eta_1$ equal to $1.25(10)^{-4}$, 250 divisions in the grid along the streamwise direction, and 150 divisions in the grid along the η direction. The ratio, $\frac{\Delta\eta_{j+1}}{\Delta\eta_j}$, was

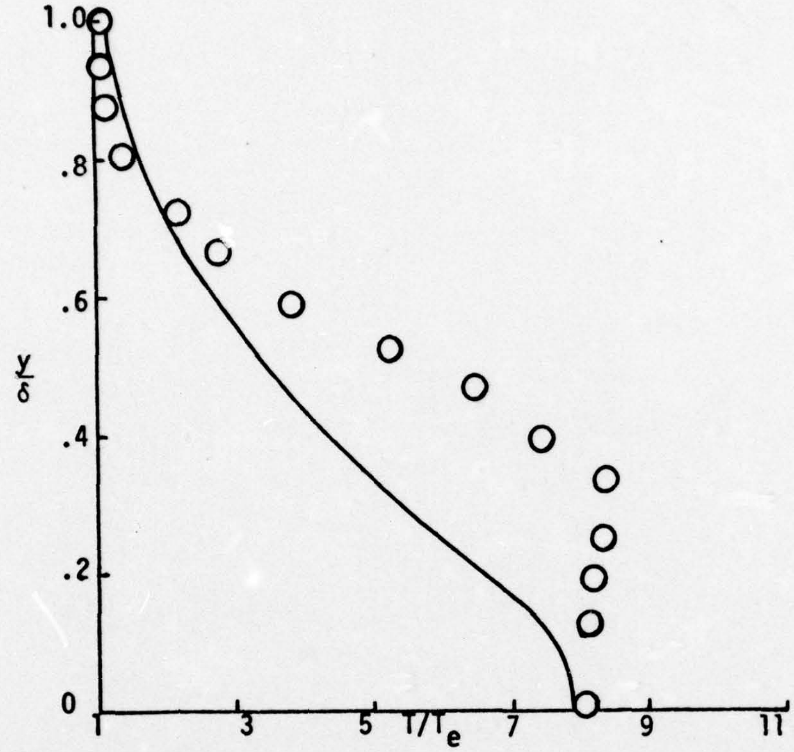

Fig. 12a. A Profile Comparison for Data Group 74 (Ref 14)

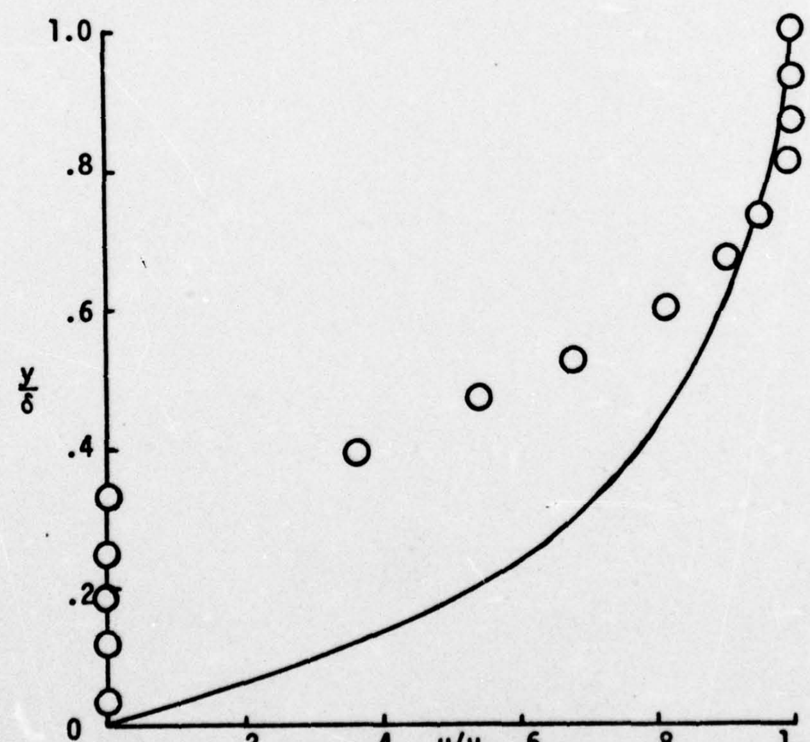

Fig. 12b. A Profile Comparison for Data Group 74 (Ref 14)

decreased to a value of 1.05. Even with the finer mesh size the temperature change at the first two stations at which mass transfer was occurring was so great that the numerical scheme failed due to attempting undefined arithmetic operations related to these temperature differences. One step prior to failure, the coefficient of skin friction and heat transfer were seen to be decreasing rapidly. This was indicative of a numerical separation of the boundary layer and the imminent failure of the computer code. A smaller transfer rate of $1.(10)^{-3}$ nominally was attempted next.

Data group 60, depicting heat transfer, and data group 59, depicting profile data, were chosen as test cases for investigating a mass transfer rate of $1.(10)^{-3}$. This was the first case involving mass transfer in which Itract was able to complete the calculation of the boundary layer without terminating in an error finish. This did not imply the accuracy of the predictions, only that the finite differencing scheme was able to proceed through a complete computation of the grid of nodal points.

As the profile data group 59 was the only field data associated with data group 60 for heat transfer, the information from group 59 alone was used to determine the inputs to Itract. For computation purposes Itract was provided the following pseudo-infinity conditions: M_e was approximately equal to 6.7, T_e was 112.4 R, and ρ_e was $1.26(10)^{-5}$ $\frac{lb_f sec^2}{ft^4}$. From the graphical presentation of St_∞ versus station along the surface of the cone an initial transition point was chosen to be over two ft from the tip of the cone. Also, from tabular and graphical presentations, the ratio, T_w/T_o, was approximately .57. Related to the blowing rate, the supposed actual rates of transfer, λ_∞, were $8.3(10)^{-4}$ from 9.5 in. to 22. in., $8.(10)^{-4}$ from 22. in. to 34.5 in., $9.6(10)^{-4}$ from 34.5 in. to 47. in., and $9.(10)^{-4}$ from 47. in. to the end of the model. This

disagreed expectedly with the figure for $\frac{(\rho v)_w}{(\rho u)_e}$ from data group 59 which was $6.3(10)^{-4}$. Initially, the blowing rates for λ_∞ were chosen for testing.

Initial testing with the aforementioned inputs led to a series of error finishes. Itract was able to compute for the first 3.5 ft of the cone at which point the coefficient of friction and Stanton numbers had decreased rapidly to values of 10^{-5} or 10^{-6}. At this point Itract simulated boundary layer separation with an error finish. Again, many combinations of grid spacing were attempted. The transfer rate seemed clearly too great. With the lack of clarity of a transition point, an attempt was made to run the program assuming turbulent conditions from the tip of the cone. With this one change, Itract was then able to successfully solve the boundary layer problem, but with two conditions at input still in question. First, further scrutiny of the heat transfer curve showed justification for choosing a transition at 1.5 ft from the tip of the cone. Then, to be consistent with the newly defined pseudo-infinity conditions downstream of the shock wave, the proper mass transfer rate was thought to be $\frac{(\rho v)_w}{(\rho u)_e}$ in lieu of $\frac{(\rho v)_w}{(\rho u)_\infty}$. From the transfer reading of data group 59 a scaling factor was used to adjust the blowing rates from $8.3(10)^{-4}$, $8.(10)^{-4}$, $9.6(10)^{-4}$, and $9.(10)^{-4}$ to $5.4(10)^{-4}$, $5.3(10)^{-4}$, $6.3(10)^{-4}$, and $5.9(10)^{-4}$ for the four sections of the cone previously mentioned. With these adjustments, Itract was again run for the final test of data groups 59 and 60. The results of the heat transfer study were included in Table XIII of Appendix G with a graphical depiction in fig 13. In the turbulent region Itract overpredicted the experimental heat transfer data by about 70 percent with a 30 percent average in the laminar region. In the profile results of

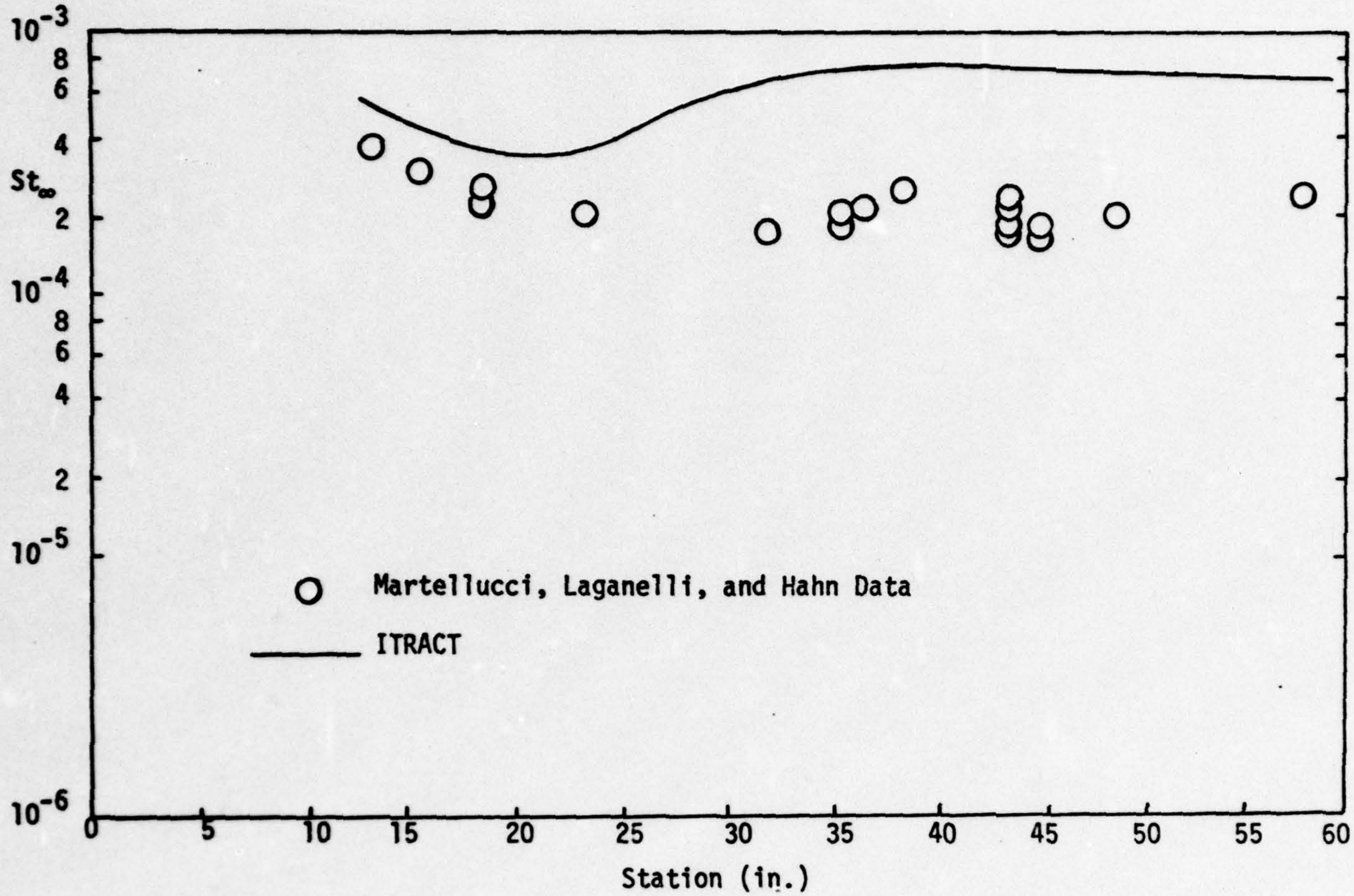

Fig. 13. A Heat Transfer Comparison for Data Group 60 (Ref 14)

fig 14 there were identical temperature predictions near the wall with a disparity greater than 46 percent near the center depth of the boundary layer. Concerning the velocity profile, the General Electric data depicted a near separated condition at station s equal to .658, and the disparity between Itract and the data was again greatest near the middle of the boundary layer thickness with a 58 percent error. Observing the near separated condition, it was consistent to also observe low heat transfer data results. This concluded the final investigation of data groups 59 and 60. One final case with a nominal mass transfer of $5.(10)^{-4}$ was then selected.

From experimental results, data group 203 was chosen to study heat transfer, and data groups 200, 201, and 202 were chosen to study the profile characteristics of the boundary layer for this lowest mass transfer case. Free stream conditions included an M_∞ equal to 8.0, a T_∞ equal to 98.1 R, and a ρ_∞ of $7.48(10)^{-5}\ \frac{lb_f sec^2}{ft^4}$. From groups 200, 201, and 202, the inputs to Itract for the study of group 203 and the heat transfer consisted of an M_e equal to approximately 7.1, a T_e equal to 120.6 R, and a ρ_∞ of $1.18(10)^{-4}\ \frac{lb_f sec^2}{ft^4}$. T_w/T_o was .78 and a constant $\frac{(\rho v)_w}{(\rho u)_e}$ equal to $3.1(10)^{-4}$ was used as the transfer rates computed at the three profile data stations were nearly equal. The results of the comparison between Itract and the experimental data of group 203 were summarized in Table XIV with a graphical presentation in fig 15. There were no laminar data points with which to compare, but in the turbulent zone Itract underpredicted the heat transfer by a 30 to 50 percent margin. Noting the sensitivity of the code to even small changes in mass transfer rates, data group 203 was retested for possible actual mass transfer rates of $1.(10)^{-4}$ and $2.(10)^{-4}$. The numerical predictions

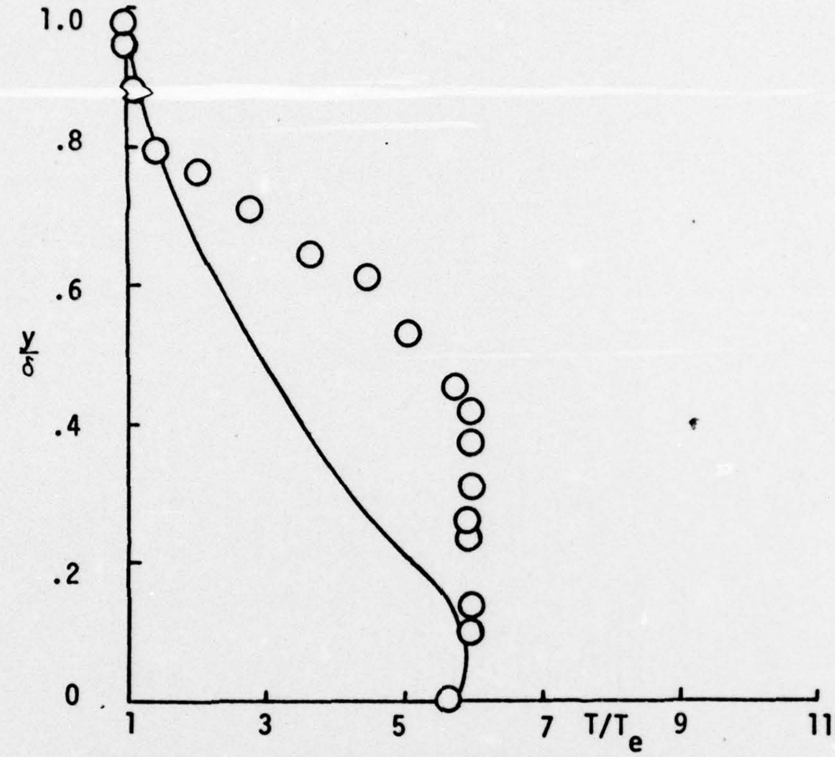

Fig. 14a. A Profile Comparison for Data Group 59 (Ref 14)

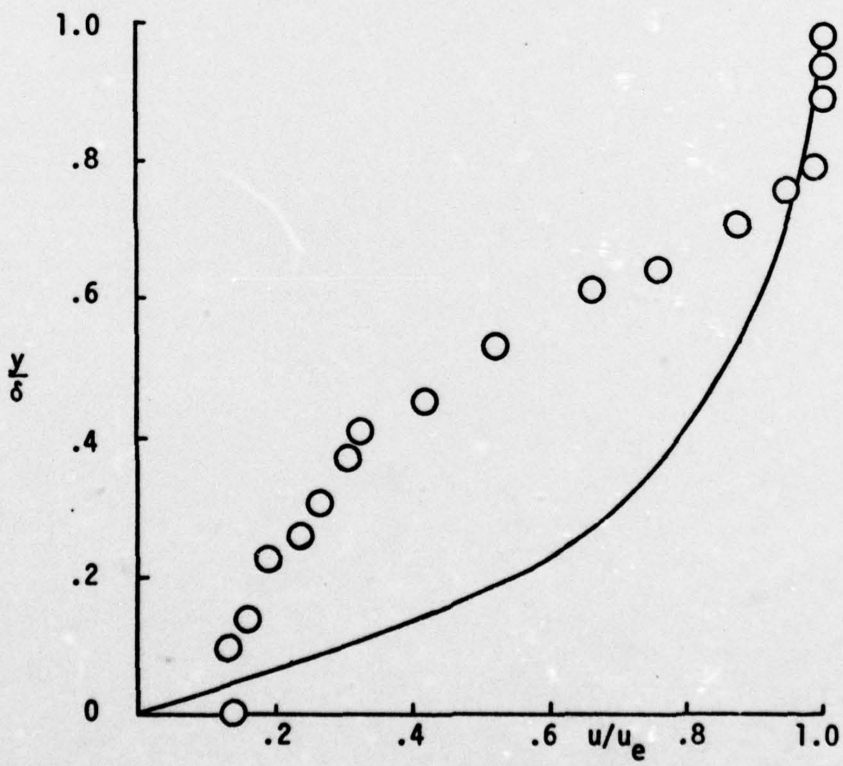

Fig. 14b. A Profile Comparison for Data Group 59 (Ref 14)

were shown to pass through the region of turbulent data points, also shown in fig 15. The study of data group 203 provided the closest results of Itract for the investigations that included mass transfer, and the corresponding profile results of data group 201 were, likewise, the best. A comparison of Itract with the profile data of station s equal to .646, data group 201, was included in fig 16. Near a $\frac{y}{\delta}$ of .1 the temperature profile was 33 percent in error with a 20 percent error in the velocity profile for a similar boundary layer depth. Both error figures represented the extremes in error between the numerical results and the experimental data.

With this test, the investigation of the cone, both with and without mass transfer had been completed. A summation of the investigations of the cone, as well as the plate, followed.

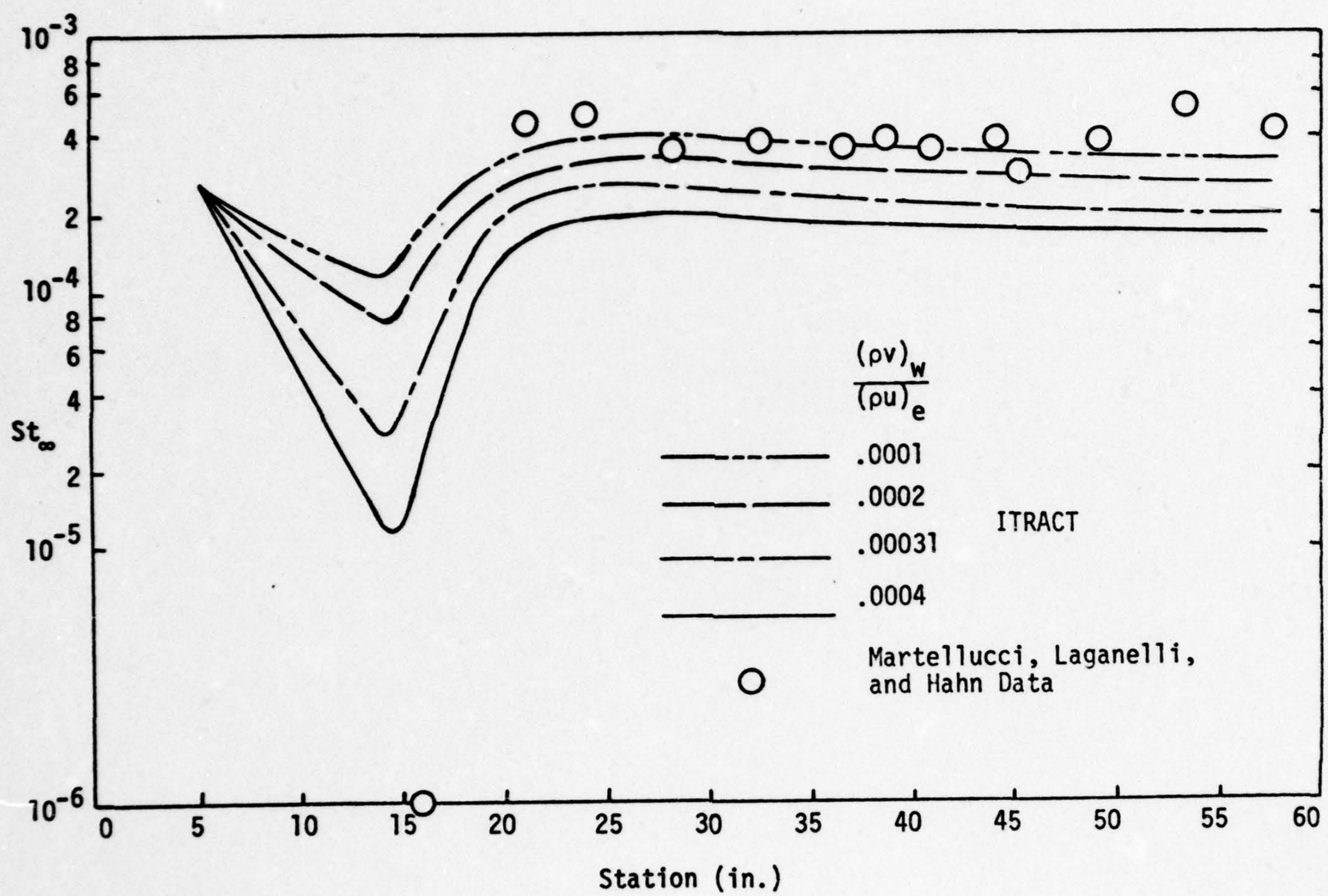

Fig. 15. A Heat Transfer Comparison for Data Group 203 (Ref 15)

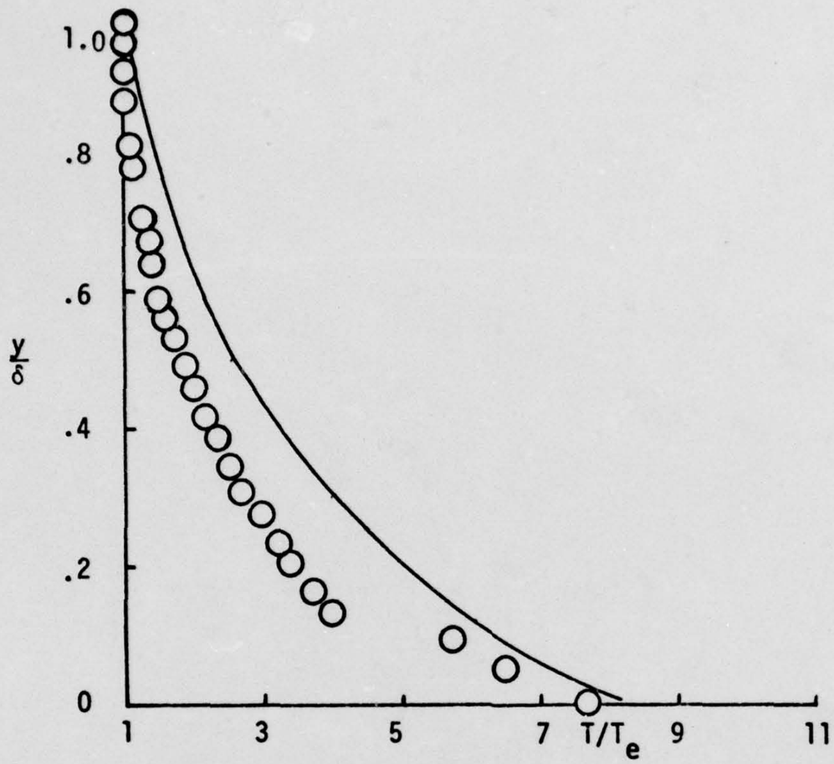

Fig. 16a. A Profile Comparison for Data Group 201 (Ref 15)

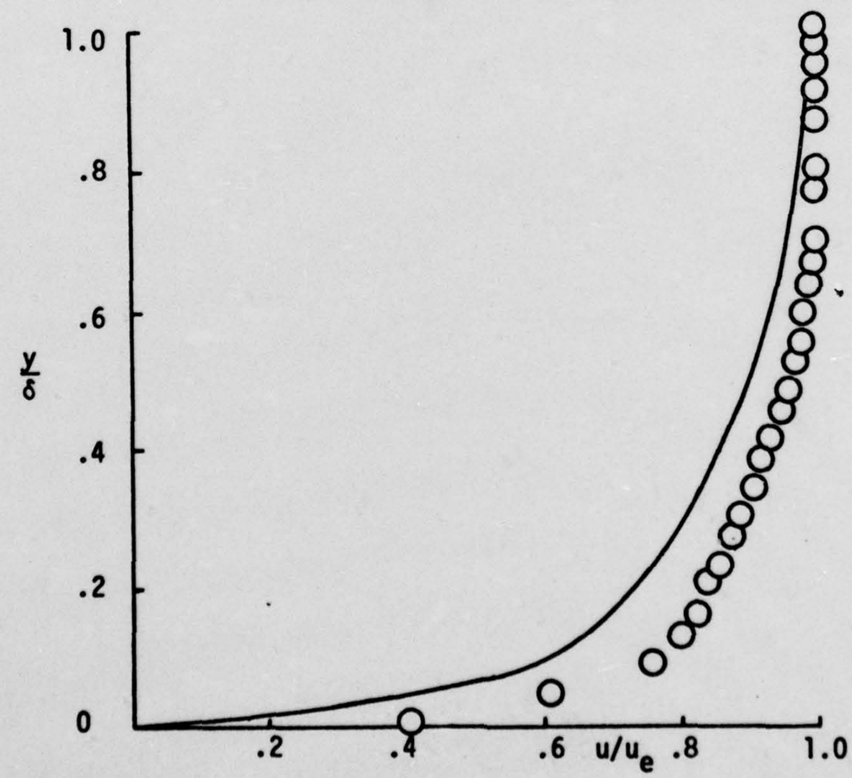

Fig. 16b. A Profile Comparison for Data Group 201 (Ref 15)

V. Summation

Originally, the computer program, Itract, incorporated a boundary condition of zero mass transfer at the surface in calculating the boundary layer. With the program modified to accept the condition of mass transfer at the surface, boundary layer flows perturbed by this mass transfer could be solved. The purpose of this study, then, was to modify the basic code and verify this modification through comparison of the numerical results with analytical expressions and with published experimental data. Data was chosen from experiments on both a flat surface and an axisymmetric cone.

From the study of flow over a flat plate four results were outstanding. First, the grid size was of fundamental importance in solving the problem. A finer mesh of nodal points yielded better results to a point where the effects of truncating higher order terms in the finite difference expressions became insignificant. Second, the cases investigated with suction were clearly more stable in computation. Further, these cases were more accurate predictors of the experimental results to the extreme of the asymptotic suction limit. Third, the results for the blowing cases were less accurate, and the error did not show regular trends insofar as a fixed error amount or a fixed percentage error. The heat transfer predictions were low. Fourth, for the case of blowing, the best results were obtained by using eddy model zero. However, for the cases with suction, eddy model one provided the best results. Overall, the modified code was verified for flow at an M_∞ much less than one over a flat plate. For both laminar and turbulent flow, the code was proven to be accurate for the case of the blowing parameter to a

strength of $1.(10)^{-3}$. For the suction case, the code was accurate to the suction asymptotic limit.

From the study of flow over an axisymmetric cone four results were noted as outstanding. First, the grid size, again, remained an important factor in the success of the numerical predictions. The finer lattice of nodes yielded better and better results. Second, the case of suction was not studied but for the case of blowing, the predictions became erratic as the blowing parameter was increased. The resulting errors did not show a systematic trend. Third, the best results for the cases of positive mass transfer occurred when eddy model one was used, unlike the results of the flat plate study. Fourth, the results of these blowing cases were shown in fig 15 to be extremely sensitive to the blowing parameter, and the precision with which the blowing rate was measured would have to be considered in completely evaluating the validity of the modified code. Overall, the modified code provided reasonably predictive results in the case of laminar and turbulent hypersonic flow over a slender cone. Specifically, for a mach number of eight the code provided reasonable results for mass transfer rates, defined as $(\rho v)_w/(\rho u)_e$, up to $3.1(10)^{-4}$. To verify the code within an acceptible limit, the precision of the measurement of the blowing rate would have to be quantified. Assuming a measurement error between $1.(10)^{-4}$ and $2.(10)^{-4}$ was possible, the code was verified for turbulent, hypersonic flow over the cone for mass transfer rates up to a strength of $3.1(10)^{-4}$.

With the limits of the code specified for the particular cases studied, factors that contributed to the obvious limits of the code for the positive mass transfer case included the following: First, at the

initiation of blowing, sharp temperature gradients in the streamwise direction resulted in numerical problems for the code. Second, with this temperature change in the streamwise direction normally considered insignificant as a boundary layer assumption, the effect of blowing may have violated a basic proposition in derivation of the boundary layer equations. Third, if the flow were separating from the solid boundary, as it seemed to do in some of the velocity profiles, another basic proposition of boundary layer theory was violated, and the imminent arithmetic mode failure of the code was to be expected. The success of this code ultimately depended on the condition that the classical boundary layer assumptions were not violated. Finally, in at least the study of the conical flow it has been found from previous study that though it was valid to use experimental data to describe the flow environment downstream of the oblique shock wave, this could have misrepresented the needed inputs of this code. Further, it has been found that the near adiabatic condition of a wall has been a most difficult problem for a finite difference scheme to compute accurately, more so than in the cold wall case as was shown in the favorable results of fig 11 (Ref 19).

Bibliography

1. Shapiro, A. H. The Dynamics and Thermodynamics of Compressible Fluid Flow. New York: Ronald Press Company, 1954.

2. Eckert, E. R. G. "Survey of Boundary Layer Heat Transfer at High Velocities and High Temperatures." WADC Technical Report 59-624, AD238 292, 10-11. Wright Patterson Air Force Base, Ohio: Wright Air Development Center (April 1960).

3. Rubesin, M. W. "An Analytical Estimation of the Effect of Transpiration Cooling on the Heat Transfer and Skin Friction Characteristics of a Compressible, Turbulent Boundary Layer." Technical Note 3341, 5-6. Langley Air Force Base, Virginia: National Advisory Committee For Aeronautics (December 1954).

4. Laganelli, A. L.; Fogaroli, R. O.; and Martellucci, A. "The Effects of Mass Transfer and Angle of Attack on Hypersonic Turbulent Boundary Layer Characteristics." Technical Report AFFDL-TR-75-35, 1-64. Wright Patterson Air Force Base, Ohio: Air Force Flight Dynamics Laboratory (April 1975).

5. Cebeci, T.; Smith, A. M. O.; and Mosinskis, G. "Calculation of Compressible Adiabatic Turbulent Boundary Layers." AIAA Journal, 8: 1975-1976 (November 1970).

6. Shang, J. S. and Hankey, W. L. Jr. Engineers, Flight Dynamics Laboratory, Wright Patterson Air Force Base, Ohio. Unpublished notes and interviews to introduce and explain thesis topics for study (April - September 1976).

7. Shang, J. S.; Hankey, W. L. Jr.; and Dwoyer, D. L. "Numerical Analysis of Eddy Viscosity Models in Supersonic Turbulent Boundary Layers." AIAA Journal, 11: 1677-1683 (December 1973).

8. Harris, J. E. "Numerical Solution of the Equations for Compressible Laminar, Transitional, and Turbulent Boundary Layers and Comparisons with Experimental Data." Technical Report NASA-TR-R-368, N71-32164, 1-29, 67-71. Hampton, Virginia: Langley Research Center (August 1971).

9. Van Driest, E. R. "Turbulent Boundary Layer in Compressible Fluids." Journal of the Aeronautical Sciences, 18: 145-150 (March 1951).

10. Shang, J. S. Engineer, Flight Dynamics Laboratory, Wright Patterson Air Force Base, Ohio. Unpublished notes documenting the derivation of the boundary layer equations for viscous flow (March - July 1976).

11. Lee, D. A. Department of Mathematics, Air Force Institute of Technology, Wright Patterson Air Force Base, Ohio. An interview concerning the application of spline theory (July 1976).

12. Schlichting, H. Boundary-Layer Theory. New York: McGraw-Hill, Inc., 1968.

13. Moffat, R. J. and Kays, W. M. "The Turbulent Boundary Layer on a Porous Plate: Experimental Heat Transfer with Uniform Blowing and Suction." International Journal of Heat and Mass Transfer, 11: 1547-1566 (October 1968).

14. Martellucci, A.; Laganelli, A.; and Hahn, J. "Hypersonic Turbulent Boundary Layer Characteristics with Mass Transfer." G. E. Document 74SD2039, SAMSO TR-74-112, 3 Volumes of Experimental Results. Philadelphia: General Electric Reentry and Environmental Systems Division (June 1974).

15. Martellucci, A.; Hahn, J.; and Laganelli, A. "Effects of Mass Addition and Angle-of-Attack on the Turbulent Boundary Layer Characteristics of a Slender Cone." G. E. Document 73SD210, SAMSO TR-73-147, 3 Volumes of Experimental Results. Philadelphia: General Electric Reentry and Environmental Systems Division (April 1973).

16. Kays, W. M. Convective Heat and Mass Transfer. New York: McGraw-Hill, Inc., 1966.

17. Sims, J. L. "Supersonic Flow Around Right Circular Cones, Tables for Zero Angle of Attack." Report Number DA-TR-11-60, AD234736. Redstone Arsenal, Alabama: Army Ballistic Missile Agency (March 1960).

18. Harms, R. J.; Schmidt, C. M.; Hanawalt, A. J.; and Schmidtt, D. A. "A Manual for Determining Aerodynamic Heating of High-Speed Aircraft." Report 7006-3352-001, AD229434. Bell Aircraft Corporation (June 1959).

19. Kyriss, C. L. Supervisor, Advanced Aerothermodynamics and Test Engineering, General Electric Company, Philadelphia, Pennsylvania. Interviews by telephone, a discussion of the experimental data from references 14 and 15 (July - November 1976).

20. Hinze, J. O. Turbulence. New York: McGraw-Hill, Inc., 1975.

21. Tennekes, H. and Lumley, J. L. A First Course in Turbulence. Cambridge: The MIT Press, 1972.

22. Klebanoff, P. "Characteristics of Turbulence in a Boundary Layer with Zero Pressure Gradient." Technical Note 3178, 1-28. Washington, D.C.: National Advisory Committee for Aeronautics (July 1954).

Appendix A

A Background and Derivation of Some Key Expressions Used in the Analytical Solution

The differential equations which described two-dimensional laminar boundary layer flow in a cartesian coordinate system were

Continuity

$$\frac{\partial \rho}{\partial t} + \frac{\partial(\rho u)}{\partial x} + \frac{\partial(\rho v)}{\partial y} = 0 \tag{38}$$

Momentum

$$\rho \frac{\partial u}{\partial t} + \rho u \frac{\partial u}{\partial x} + \rho v \frac{\partial u}{\partial y} = \frac{\partial p_x}{\partial x} + \frac{\partial \tau_{yz}}{\partial y} \tag{39}$$

$$\rho \frac{\partial v}{\partial t} + \rho u \frac{\partial v}{\partial x} + \rho v \frac{\partial v}{\partial y} = \frac{\partial p_y}{\partial y} + \frac{\partial \tau_{xy}}{\partial x}$$

Energy

$$\begin{aligned} &\rho \frac{\partial}{\partial t}(c_pT) + \rho u \frac{\partial}{\partial x}(c_pT) + \rho v \frac{\partial}{\partial y}(c_pT) \\ &- \frac{\partial p}{\partial t} - u \frac{\partial p}{\partial x} - v \frac{\partial p}{\partial y} = \frac{\partial q_x}{\partial x} + \frac{\partial q_y}{\partial y} \\ &+ (p_x+p)\frac{\partial u}{\partial x} + (p_y+p)\frac{\partial v}{\partial y} + \tau_{yx}\frac{\partial u}{\partial y} + \tau_{xy}\frac{\partial v}{\partial x} \end{aligned} \tag{40}$$

where

$$p = -1/3\,(p_x+p_y+p_z)$$

$$p_x+p = -\frac{2}{3}\mu\left(\frac{\partial u}{\partial x} + \frac{\partial v}{\partial y}\right) + 2\mu\frac{\partial u}{\partial x}$$

$$p_y+p = -\frac{2}{3}\mu\left(\frac{\partial u}{\partial x} + \frac{\partial v}{\partial y}\right) + 2\mu\frac{\partial v}{\partial y} \tag{41}$$

$$p_z + p = -\frac{2}{3}\mu\left(\frac{\partial u}{\partial x} + \frac{\partial v}{\partial y}\right)$$

$$\tau_{yx} = \tau_{xy} = \mu\left(\frac{\partial u}{\partial y} + \frac{\partial v}{\partial x}\right) \tag{41}$$

$$q_x = k\,\frac{\partial T}{\partial x} \text{ and } q_y = k\,\frac{\partial T}{\partial y}$$

From Reynolds the following definitions were made to describe a turbulent boundary layer:

$$u = \overline{u} + u',\ \rho = \overline{\rho} + \rho',\ \tau_{yx} = \overline{\tau_{yx}} + \tau_{yx}'$$
$$\rho u = \overline{\rho u} + (\rho u)',\ \rho v = \overline{\rho v} + (\rho v)',\ p_x = \overline{p_x} + p_x' \tag{42}$$

where bars indicated mean values and the primes designated instantaneous fluctuations. Finally, the definition of time averaging was necessary and was explained by the following example:

$$\overline{u} = \frac{1}{T}\int_{T-T/2}^{T+T/2} u\,dt \tag{43}$$

where T was used in this example to represent time, not temperature. With these basic definitions and assuming steady state conditions, the laminar equations could be transformed into descriptions of turbulent boundary layer flow.

To ultimately reach the form of the equations listed in Eqs (8), (9), and (10), the steps were included for the simplest case, continuity. Time averaging and substituting from the above definitions yielded:

$$\frac{\partial}{\partial x}\left(\overline{\rho u} + \overline{\rho' u'}\right) + \frac{\partial}{\partial y}\left(\overline{\rho v} + \overline{\rho' v'}\right) = 0 \tag{44}$$

It has been accepted that the $\overline{\rho'u'}$ term was strongly uncorrelated, and this term was eliminated from further consideration. Then, following two coordinate transformations the final form of Eq (8) was reached.

An assumption of this study was that flow could be considered two-dimensional. Further, a body oriented axis system was employed for both the flat plate and axisymmetric cone. Finally, a cylindrical coordinate frame was chosen to describe both of the flows. Performing the cylindrical transformation, it was found, first, that in cartesian coordinates

$$\frac{\partial(\rho u)}{\partial x} + \frac{\partial \rho\left[v \div \frac{\overline{\rho'v'}}{\rho}\right]}{\partial y} = 0 \tag{45}$$

having dropped the time averaging symbol from the mean quantities. Then, by defining

$$\rho\underline{u} \text{ as } \left[\rho u,\ 0,\ \rho\left(v + \frac{\overline{\rho'v'}}{\rho}\right)\right]$$

and employing the definition of the divergence of $\rho\underline{u}$ or $\nabla\cdot\rho\underline{u}$, continuity in a cylindrical frame was shown to be

$$\frac{\partial(r\rho u)}{\partial x} + \frac{\partial\left\{r\rho\left[v + \frac{\overline{\rho'v'}}{\rho}\right]\right\}}{\partial y} = 0 \tag{46}$$

By including an exponent with the r term to yield r^j, it was noted that by setting j equal to zero or one would yield the expressions for continuity related to the flat plate and to the cone, respectively. Then having demonstrated a transformation to cylindrical coordinates, it was reassuring to show also that a body oriented axis system x', y' could be used in the case of the conical flow as an x,y system had been used for the flat plate. Figure 17 was included as a pictorial description of this situation, with the prime symbols serving here only to differentiate direction.

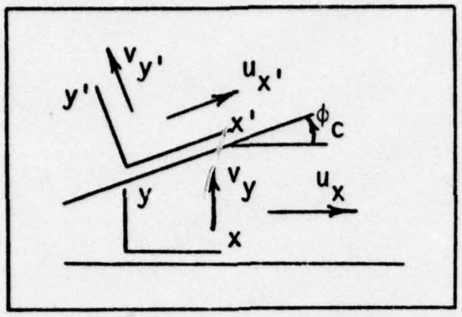

Fig. 17. Showing the Equivalence of Expressions in Rotated Coordinates

First, it was recognized that

$$
\begin{aligned}
y &= x' \sin\phi_c + y' \cos\phi_c \\
x &= x' \cos\phi_c - y' \sin\phi_c \\
y' &= y \cos\phi_c - x \sin\phi_c \\
x' &= y \sin\phi_c + x \cos\phi_c \\
v_y &= u_{x'} \sin\phi_c + v_{y'} \cos\phi_c \\
u_x &= u_{x'} \cos\phi_c - v_{y'} \sin\phi_c
\end{aligned}
\tag{47}
$$

Then, from fig 17, it was true that

$$\frac{\partial(r\rho u_x)}{\partial x} + \frac{\partial(r\rho v_y)}{\partial y} = 0 \tag{48}$$

If F were equal to $(r\rho u_x)$ and G were equal to $(r\rho v_y)$, it was demonstrated that the chain rule could be used to ultimately produce expressions for $\frac{\partial F}{\partial x}$ and $\frac{\partial F}{\partial y}$ such that the following equality was true:

$$\frac{\partial(r\rho u_x)}{\partial x} + \frac{\partial(r\rho v_y)}{\partial y} = \frac{\partial(r\rho u_{x'})}{\partial x'} + \frac{\partial(r\rho v_{y'})}{\partial y'} = 0 \tag{49}$$

Thus, through two transformations the immerging expression for continuity was

$$\frac{\partial(r^j \rho u)}{\partial x} + \frac{\partial\left[r^j \rho\left(v + \frac{\overline{\rho' v'}}{\rho}\right)\right]}{\partial y} = 0 \tag{50}$$

which matched Eq (8).

In the same manner, but with increased complexity of expression, the equations of momentum were written as follows using the equation of continuity:

$$\frac{\partial(\rho u^2)}{\partial x} + \frac{\partial(\rho u v)}{\partial y} = \frac{\partial p_x}{\partial x} + \frac{\partial \tau_{yx}}{\partial y}$$

$$\frac{\partial(\rho u v)}{\partial x} + \frac{\partial(\rho v^2)}{\partial y} = \frac{\partial p_y}{\partial y} + \frac{\partial \tau_{xy}}{\partial x} \tag{51}$$

Employing the equation of continuity, and with the substitutions of Eq (42), it was noted in the final form that $\overline{v}$ was much less than $\overline{u}$ and that Eq (51-2) became a negligible expression. Eq (51-1) was dominant by an order of magnitude analysis, and after dropping the bar symbol over mean quantities, reduced in the steady state case to

$$\rho u \frac{\partial u}{\partial x} + \rho\left(v + \frac{\overline{\rho' v'}}{\rho}\right)\frac{\partial u}{\partial y} = \frac{\partial}{\partial x}\left(p_x + \overline{(\rho u)' u'}\right) + \frac{\partial}{\partial y}\left(\tau_{yx} + \overline{(\rho v)' u'}\right) \tag{52}$$

Then, using Eqs (41) and (42), discarding negligible terms, and transforming to the cylindrical coordinates, Eq (52) reduced to

$$\rho u \frac{\partial u}{\partial x} + \rho\left(v + \frac{\overline{\rho' v'}}{\rho}\right)\frac{\partial u}{\partial y} = -\frac{dp}{dx} + \frac{1}{r^j}\frac{\partial}{\partial y}\left[r^j\left(\mu\frac{\partial u}{\partial y} + \rho\overline{u' v'}\right)\right] \tag{53}$$

which was the momentum equation in Eq (9).

Finally, and with still greater complexity, the rules of substitution of Eqs (41) and (42) along with the idea of time averaging and

coordinate transformation could have been employed with Eq (40). Then, following steps similar to those of Van Driest, the energy equation could also have been simplified to the form shown in Eq (10) (Ref 9:145-150).

Appendix B

A Program Listing

```
      PROGRAM ITRACT(INPUT,OUTPUT,TAPE5=INPUT,TAPE6=OUTPUT)
      COMMON G, PR, REY, XMINF, OMEGA, BO, TW, P10, T10, R10, VIS10, TE,
     1 PE,RE,UE,VISINF,SU,EPS,DS,DYW,SI,ERROR,TC,TA,IEDGE,IEND1,INTACT,
     2 PRT,XXK,BTRX,XLAM,VAPPRT,XINTER,SERO,ICHS(8),IPRN(9),EO(200),
     3 EN(200),EP(200),ETO(200),ETN(200),ETP(200),FO(200),FN(200),J2DA,
     4 FP(200),TH(200),TO(200),XNN(200),VN(200),VO(200),VP(200),TP(200),
     5 D1(200),D2(200),D3(200)
      DIMENSION Y(200),A1(200,3),A2(200,3),A3(200,3),B1(200,3),
     1 B2(200,3),B3(200,3),C1(200,3),C2(200,3),C3(200,3)
      COMMON/CPDATA/ CP(24),XP(24),DP(24),IPRES
      COMMON/BLWDATA/NUMDAT,XPOS(24),RHOVRAT(24),TRP,TREF,XNUE,S,SS,SO,
     6 IBLW,XLGTHMO,RVRAT
      DATA R/1716./
 1100 FORMAT(1H0,12X,3HO/L,15X,2HCP,15X,6HP/PINF)
 1101 FORMAT(1X,3(4X,E15.3))
 2208 FORMAT(1X,*PROFILE FAILED TO RELAX AT M = *,I5)
 8001  FORMAT(4E15.9)
 8002 FORMAT (5E15.9)
 8003 FORMAT (10I5)
 9002 FORMAT(1H1,47X*INTERACTING BOUNDARY LAYER SOLUTION*)
 9003 FORMAT (7H0GAMMA=F6.3,4H PR=F6.3,5H MFS=F5.3,7H REYFS=E10.4,8H TFS
     1(R)=F7.1,11H BO=TW/T10=F6.4,5H EPS=F8.5)
 9004 FORMAT(5H0P10=,E10.4,7H RHO10=,E10.4,5H T10=,E10.4,7H VIS10=,E10.4
     1,4H SI=,E10.4)
 9005 FORMAT(7H0OMEGA=,F7.4,2X,6HPRT = ,F7.4,2X,7HBTRX = ,F7.4)
 9019 FORMAT(10X,*WITH INTERMITTENCY CORRECTION*)
 9020 FORMAT(10X,*WITHOUT INTERMITTENCY CORRECTION*)
 9021 FORMAT(10X,*TWO-DIMENSIONAL BOUNDARY LAYER*)
 9022 FORMAT(10X,*AXISYMETRICAL BOUNDARY LAYER*)
C
C     INPUT INITIAL CONDITIONS
C
      READ(5,8001) G, PR, XMINF, TA
      READ(5,8002) DS, SI, OMEGA, ERROR, XXK
      READ(5,8002) BO,BTRX, PRT, XINTER, DYW
      READ(5,8003) IEDGE, INTACT, IDIFF, IEND1, MSP, J2DA , IPRES
      READ(5,8003) (ICHS(I), I = 1, 8)
      READ(5,8003) (IPRN(I), I = 1, 9)
      READ(5,*) XLGTHMO,RINFA,IBLW
      IF (IBLW) 1,2,3
    1 READ(5,*) STRT,DONE,RVRAT
      SS=STRT/XLGTHMO
      SO=DONE/XLGTHMO
      GO TO 2
    3 READ(5,*) NUMDAT,(XPOS(I),I=1,NUMDAT),(RHOVRAT(I),I=1,NUMDAT)
      SS=XPOS(1)/XLGTHMO
      SO=XPOS(NUMDAT)/XLGTHMO
    2 A=SQRT(G*R*TA)
      UINFA=XMINF*A
      XMUINFA=((2.27*TA**1.5)/(TA+198.6))*(1.E-8)
      REY=(RINFA*UINFA*XLGTHMO)/XMUINFA
      TRR=(TA+198.6)/((TA*(G-1.)*XMINF**2)+198.6)
      XLAM=.5*BTRX
      IF(IPRES.EQ.0) GO TO 20
      READ(5,8002) DPMAX
      READ(5,8002) (CP(IJ),IJ=1,IPRES)
      READ(5,8002) (XP(IJ),IJ=1,IPRES)
      WRITE(6,1100)
      XMSQ=XMINF*XMINF
      DO 10 IJ=1,IPRES
      POPINF=1.0+0.5*G*XMSQ*CP(IJ)
      WRITE(6,1101) XP(IJ),CP(IJ),POPINF
   10 CP(IJ)=POPINF
      CALL SMTHPR(BTRX,DPMAX,G,XMSQ)
C
C     COMPUTE NONDIMENSIONALIZING QUANTITIES
C
   20 Z1= 1. + (G - 1.)/2.*XMINF**2
      P10 = (1./(G*XMINF**2))*(Z1**(G/(G-1.)))
      T10 = (1./((G - 1.)*XMINF**2))*Z1
```

```
      R10 = G*P10/(T10*(G - 1.))
      TINF = T10/TA
      TW = BO*T10
      IF(OMEGA .EQ. 0.) GO TO 101
      VIS10 = T10**OMEGA
      EPS = (((G - 1.)*XMINF**2)**(OMEGA/2.))/SQRT(REY)
      VISINF = TINF**OMEGA
      GO TO 102
 101  TC=198.6/((G-1.)*XMINF**2*TA)
      VIS10 = (T10**1.5)*(1. + TC)/(T10+TC)
      EPS = ((((1.+(198.6/TA))*(((G - 1.)*XMINF**2)**1.5))/(((G - 1.)*X
     1MINF**2)+(198.6/TA)))/REY)**.5
      VISINF = (TINF**1.5)*(1. + TC)/(TINF+TC)
 102  SU=198.6
C
C     OUTPUT INITIAL CONDITIONS
C
      WRITE(6,3002)
      WRITE(6,3003) G, PR, XMINF, REY, TA, BO, EPS
      WRITE(6,3004) P10, R10, T10, VIS10, SI
      WRITE(6,3005) OMEGA,PRT,RTPX
      IF(XINTER.EQ.1.) WRITE(6,9019)
      IF(XINTER.EQ.0.) WRITE(6,9020)
      IF(J20A.EQ.0) WRITE(6,9021)
      IF(J20A.NE.0) WRITE(6,9022)
C
C     INPUT INITIAL PROFILE
C
 12   MSTART=2
C     INITIALIZE THE STREAMWISE LOCATION
      S=SI
      DS2=DS1=DS
      DX2DS=DX1DS=DXDS=0.
      SEPO=1.
C     INITIALIZE THE STREAMWISE LOCATION
      Y(1)=0.0
      DO 201 LL=2,200
      DY=XXK**(LL-2)*DYW
 201  Y(LL)=Y(LL-1)+DY
      DO 700 LL = 1, 200
      D1(LL)=D2(LL)=D3(LL)=XMN(LL)=0.
      VP(LL)=VM(LL)=VO(LL)=-Y(LL)
      FP(LL)=FO(LL)=FN(LL)=TP(LL)=TN(LL)=TO(LL)=EP(LL)=EO(LL)=EN(LL)=
     1 ETP(LL)=ETO(LL)=ETN(LL)=1.0
 700  CONTINUE
      DO 701 J = 1, 200
      DO 701 I = 1, 3
 701  A1(J,I)=A2(J,I)=A3(J,I)=B1(J,I)=B2(J,I)=B3(J,I)=C1(J,I)
     1 =C2(J,I)=C3(J,I)=0.
      PREF=G*XMINF**2
      TREF = (G - 1.)*XMINF**2
C
C     INITIALIZE COUNTERS
C
      ICOUN=MSTART
      IO=IEDGE
      IG=1
      IP=1
      INDCH=0
      ICONT1 = 1
      IIN=0
C
C  ***   BEGIN FIRST-ORDER TRIDIAGONAL MATRIX SOLUTION   ***
C
      DO 115 M=MSTART,IEND1
      IF(M.EQ.MSTART) MP=MSTART
      IF(M.EQ.IEND1) MP=M
      IF(M.EQ.(M/MSP)*MSP) MP=M
      S=S+DS2
      DX2DS = DX1DS
```

```
      DX1DS = DXDS
C
C     COMPUTE LOCAL PRESSURE AND PRESSURE GRADIENT
C
      CALL PRESSM(S,XMINF,G,PRG1,DPRG1,TETNF,XME)
C
C     COMPUTE LOCAL EDGE PROPERTIES
C
      PE = PRG1/PREF
      PP = DPRG1/PREF
      TE = TETNF/TREF
      UE = SQRT(2.*(T10 - TE))
      RE=G*PE/((G-1.0)*TE)
      TR=SU/(TETNF*TA)
      IF (OMEGA) 642,676,642
  642 XNUE=TE**OMEGA
      GOTO688
 676  XNUE=TE**1.5*(1.+198.6/(TA*TREF))/(TE+198.6/(TA*TREF))
 688  CONTINUE
C
C     COMPUTE LOCAL XI AND STEP LENGTHS
C
      DXDS=RE*UE*XNUE
      IF(J2DA.NE.0) DXDS=DXDS*S**2
      IF(M.EQ.2) DX1DS=DX2DS=DXDS
      DX2=.5*DS2*((1.+DS2/DS1)*DX1DS+DS1*DXDS/(DS1+DS2)-DS2*DS2*DX2DS/
     1 (DS1*(DS1+DS2)))
      REYNDE=RE*UE*S/XNUE
      REYEXT=REY*VISINF*REYNDE
      IF(M.EQ.2) DX1=DX2
      IF(M.EQ.2) X=DXDS*SI
      X=X+DX2
C     COMPUTE STEP LENGTH FUNCTIONS
C
      Y1=2.*(DX1+2.*DX2)/(DX1+DX2)
      IF(IDIFF .EQ. 1) Y1 = 2.
      Y2=((DX1+DX2)/DX1)*2.0
      Y3=(DX2*DX2/(DX1*(DX1+DX2)))*2.0
      Y4=(DX1+DX2)/DX1
      Y5=DX2/DX1
      TWTE = TW/TE
C
C     COMPUTE ALPHA, BETA, AND LAMBDA
C.......................................................................
      DUEDX=-PP/(RE*UE*DXDS)
      XAL=UE*UE/TE
      XBE=2.0*X*DUEDX/UE
C
 6998 LENGTH=IEDGE
C
C     ASSIGN THE MATRIX ELEMENTS FOR THE FINITE DIFFERENCE EQUATIONS
      CALL ELMATX(   M,DX2,X,XAL,XBE,TP,IDIFF,Y1,Y2,Y3,Y4,Y5,TWTE,ITCNT1,
     1          A1,A2,A3,B1,B2,B3,C1,C2,C3)
C     ASSIGN THE MATRIX ELEMENTS FOR THE FINITE DIFFERENCE EQUATIONS
C
C
C     MATRIX INVERSION, SOLVE FOR F, THETEA AND V
C
      CALL MATEQN3(FP,TP,VP,D1,D2,D3,A1,B1,C1,A2,B2,C2,A3,B3,C3,3,LENGTH
     1 ,200)
C
C     MATRIX INVERSION, SOLVE FOR F, THETEA AND V
C
      ITCNT1=ITCNT1+1
      N=IEDGE+1
      YN=YWA*XKK**(IEDGE-2)
      VN=(VP(IEDGE)/(XKK*(1.+1./XKK))-VP(IEDGE-1)*(1.-1./XKK)*XXK-
     1 VP(IEDGE-2)*XKK/(1.+1./XKK))/DY
      YN=YWA*XKK**(IEDGE-1)
      [illegible]
```

```
      DO65IO=N,KON
      DY=DYW*XXK**(N-1)+DY
      FP(IO)=TP(IO)=1.0
 65   VP(IO)=VP(IEDGE-1)+VK*DY
C     INITIATION OF SIMILAR SOLUTIONS
      IF(M.EQ.2) GO TO 8020
      GO TO 8018
 8020 DO 8019 I=1,KON
      VO(I)=VN(I)=VP(I)
      FO(I)=FN(I)=FP(I)
 8019 TO(I)=TN(I)=TP(I)
C     INITIATION OF SIMILAR SOLUTIONS
 8018 IO=IEDGE+1
C
C     U AND THETA PROFILES ITERATIONS
      TAU2=(FP(2)-FP(1))/DYW
      IF(ITCNT1.EQ.2) TAU1=10.*TAU2
      RT12=TAU1/TAU2-1.
      TAU1=TAU2
      IF(ITCNT1 .LE. 100) GO TO 7005
      WRITE(6,7008) M
      CALL EXIT
 7005 IF(ABS(RT12).GT.ERROR) GO TO 6998
C     U AND THETA PROFILES ITERATIONS
C
C
C     COMPUTE BLT, BDT(DELTA STAR) AND BMT(THETA)
 55   CO=TP(1)
      TPI=0.
      BLT=BLDT=BLMT=0.
      XNN(1)=0.
      DO 57 N=2,KON
      DY=DYW*XXK**(N-2)
      C=TP(N)
      TPI=TPI+.5*DY*(CO+C)
      CO=C
      XNN(N)=TPI*SQRT(2.*X)/(RE*UE)
      IF(J2D A.NE.0) XNN(N)=XNN(N)/S
      BLDT=BLDT+(2.-FP(N) /TP(N)-FP(N-1)/TP(N-1))*(XNN(N)-XNN(N-1))/2.
      BLMT=BLMT+(FP(N)*(1.-FP(N))/TP(N)+FP(N-1)*(1.-FP(N-1))/TP(N-1))
     1 *(XNN(N)-XNN(N-1))/2.
      IF(BLT.GT.0.) GO TO 57
      IF(FP(N).GE.0.995) BLT=XNN(N)-(FP(N)-.995)*(XNN(N)-XNN(N-1))
     1 /(FP(N)-FP(N-1))
 57   CONTINUE
      BLT=BLT*EPS
      BLDT=BLDT*EPS
      BLMT=BLMT*EPS
C     COMPUTE BLT, BDT(DELTA STAR) AND BMT(THETA)
C
C     COMPUTE THE EDDY VISCOSITY COEFFICIENT
      IF(S.LE.STRX)   GO TO 58
      CALL REYSTR (KON,TP,X,TREF,XMUE,XBE,S,ITCNT1,TRR)
C     COMPUTE THE EDDY VISCOSITY COEFFICIENT
C
 58   ITCNT1=1
C
C     ASSESMENT OF GRID PONITS IN ETA
C
      IF(INDCH) 71, 71, 732
 71   CONTINUE
      IF(M - 20) 732, 732, 72
 72   IF(ABS(FP(IEDGE-15)-FP(IEDGE-16))-0.0001) 73,73,74
 73   IF(ABS(TP(IEDGE-15) - TP(IEDGE-16)) - .0001) 732, 732, 74
 74   IEDGE=IEDGE+1
      IO=IO+1
      DY=DYW*XXK**(IEDGE-2)
      Y(IEDGE) = Y(IEDGE-1) + DY
 732  IO = IO - 1
C     ASSESMENT OF GRID PONITS IN ETA
```

```
C
C
C      COMPUTE WALL STRESS AND HEAT TRANSFER AND OUTPUT STATION
       CALL   CFSTND (IR,XNUE,Y,S,XBE,M,BLOT,BLMT,BLT,PBG1,DPBG1,REYEXT,
      1 XMI,MP)
C      COMPUTE WALL STRESS AND HEAT TRANSFER AND OUTPUT STATION
C
C
C      SHIFT PROFILES BACK ONE XI STATION
C
       NN = IQ + 5
       DO 118 N=1,NN
       FN(N)=FO(N)
       FO(N)=FP(N)
       TN(N)=TO(N)
       TO(N)=TP(N)
       VN(N)=VO(N)
       VO(N)=VP(N)
       ETN(N)=ETO(N)
       ETO(N)=ETP(N)
       EN(N)=EO(N)
       EO(N)=EP(N)
  118  CONTINUE
       DX1=DX2
       DS1=DS2
       IF(M+1-ICHS(IG)) 114,113,114
  113  DS2=2.0*DS1
       IG = IG+1
       INDCH = 1
       IF (M.EQ.IEND1) GO TO 237
       GO TO 111
  114  DS2=DS1
       INDCH = 0
       IF (M.EQ.IEND1) GO TO 237
       GO TO 111
  237  IIN = 1
  111  CALL PUNCHS      (ICOUN,IP,IG,IQ,MSTART,IIN,M,S,Y,BLT)
  115  CONTINUE
       STOP
       END
       SUBROUTINE PRESSM(S,XM,G,P,DPDX,T,YM)
       COMMON/SPDATA/ CP(24),XP(24),PP(24),IPRES
  100  FORMAT( 5X,*WARNING....CALCULATION IS OUTSIDE OF THE PRESCRIBED PR
      1ESSURE DATA, S IS LESS THAN XP(1)*)
  200  FORMAT( 5X,*WARNING....CALCULATION IS OUTSIDE OF THE PRESCRIBED PR
      1ESSURE DATA, S IS GREATER THAN XP(END)*)
  300  FORMAT(1X,5E15.9)
       IR=0
       IPM1=IPRES-1
       IF(IPRES.EQ.0) GO TO 40
       DO 20 I=1,IPRES
       IF(S.LT.XP(1)) WRITE(6,100)
       IF(S.GT.XP(IPRES)) WRITE(6,200)
       IF(S.LE.XP(1)) IR=1
       IF(IR.NE.0) GO TO 30
       IF(S.GE.XP(IPM1)) IR= IPRES
       IF(IR.NE.0) GO TO 30
       IF((S.GE.XP(I)).AND.(S.LT.XP(I+1))) IR=I
       IF(IR.EQ.0) GO TO 20
C      SEEKING THE BEST FIT
       RS=(S-XP(I))/(XP(I+1)-XP(I))
       IF(RS.GT.0.5) IR=I+1
C      SEEKING THE BEST FIT
       IF(IR.NE.0) GO TO 30
   20  CONTINUE
   30  IF(IR.GT.IPM1) IR=IPM1
       IRP=IR+1
       IRM=IR-1
       IF(IR.EQ.1) IRM=IR+2
C      COMPUTE THE CUBIC SPLINE COEFFICENTS
```

```
      X1=(XP(IPP)+XP(IPM)-2.0*XP(IP))*(XP(IPP)-XP(IPM))
      X2=(XP(IPM)-XP(IP))*(XP(IPM)-XP(IP))
      X3=(XP(IPP)-XP(IP))*(XP(IPP)-XP(IP))
      X4=XP(IPM)-XP(IPP)
      X5=XP(IPM)-XP(IP)
      X6=XP(IPP)-XP(IP)
      DETS=X5*X6*X4
      C2=(DP(IP)*X1+DP(IPP)*X2-DP(IPM)*X3)/DETS
      C3=(DP(IP)*X4-DP(IPP)*X5+DP(IPM)*X6)/DETS
C     COMPUTE THE CUBIC SPLINE COEFFICENTS
      DXP=S-XP(IP)
      DXP2=DXP**2
      DXPF=DXP/20.
      DPDX1=DP(IP)
      P=CP(IP)
      DO 10 I=1,20
      X=I*DXPF
      X2=X*X
      DPDX2=DP(IP)+C2*X+C3*X2
      P=P+0.5*(DPDX1+DPDX2)*DXPF
 10   DPDX1=DPDX2
      DPDX=DP(IP)+C2*DXP+C3*DXP2
      T=P**((G-1.0)/G)
      YM=SQRT(2.0*((2.0+(G-1.0)*XM*XM)/(2.0*T)-1.0)/(G-1.0))
      WRITE(6,300) S,P,DPDX,T,YM
      GO TO 50
 40   P=1.0
      DPDX=0.
      T=P**((G-1.0)/G)
      YM=SQRT(2.0*((2.0+(G-1.0)*XM*XM)/(2.0*T)-1.0)/(G-1.0))
 50   RETURN
      END
      SUBROUTINE SMTHPR(BTRX,DPMAX,G,XMSQ)
      COMMON/CPDATA/ CP(24),XP(24),DP(24),IPRES
 100  FORMAT(1X,*FIRST CP DATA POINT YIELDS ADVERSE PRESSURE GRADIENT TO
     1O STEEP FOR CALCULATION TO CONTINUE*)
 200  FORMAT(1H0,11X,3HS/L,15X,2HCP,11X,5HP/PINF,14X,4HDPDX)
 300  FORMAT(1X,4(4X,E15.8))
      DPTOL=DPMAX*1.01
C     COMPUTE THE TRAILING EDGE DPDX
      IPM1=IPRES-1
      IPM2=IPRES-2
      DX1=XP(IPM1)-XP(IPRES)
      DX2=XP(IPM2)-XP(IPRES)
      DX12=DX1*DX1
      DX22=DX2*DX2
      DP(IPRES)=(CP(IPM2)*DX12-CP(IPM1)*DX22-CP(IPRES)*(DX12-DX22))/
     1 (DX1*DX2*(DX1-DX2))
C     COMPUTE THE TRAILING EDGE DPDX
 10   IMAX=0
C     COMPUTE THE LEADING EDGE DPDX
      DX1=XP(2)-XP(1)
      DX2=XP(3)-XP(1)
      DX12=DX1*DX1
      DX22=DX2*DX2
      DP(1)=(CP(3)*DX12-CP(2)*DX22-CP(1)*(DX12-DX22))/(DX1*DX2*(DX1-
     1 DX2))
      IF(DP(1).GT.DPMAX) WRITE(6,100)
      IF(DP(1).GT.DPMAX) CALL EXIT
C     COMPUTE THE LEADING EDGE DPDX
      DO 20 I=2,IPM1
      IM1=I-1
      IP1=I+1
      DX1=XP(IM1)-XP(I)
      DX2=XP(IP1)-XP(I)
      DX12=DX1*DX1
      DX22=DX2*DX2
      DP(I)=(CP(IP1)*DX12-CP(IM1)*DX22-CP(I)*(DX12-DX22))/(DX1*DX2*
     1 (DX1-DX2))
 20   IF((DP(I).GT.DPTOL).AND.(XP(I).LE.BTRX)) IMAX=I
```

```
      IF(IMAX.EQ.0) GO TO 50
C     SMOOTHING THE CP DATA IN THE LEADING EDGE REGION
      IMM1=IMAX-1
      IMP1=IMAX+1
      DX1=XP(IMM1)-XP(IMAX)
      DX2=XP(IMP1)-XP(IMAX)
      DX12=DX1*DX1
      DX22=DX2*DX2
      CP(IMM1)=(CP(IMP1)*DX12-CP(IMAX)*(DX12-DX22)-DX1*DX2*(DX1-DX2)
     1 *DPMAX)/DX22
      GO TO 10
C     SMOOTHING THE CP DATA IN THE LEADING EDGE REGION
 50   WRITE(6,200)
      DO 30 I=1,IPRES
      PC=2.0*(CP(I)-1.0)/(G*XMSQ)
 30   WRITE(6,300) XP(I),PC,CP(I),DP(I)
      RETURN
      END
      SUBROUTINE CFSTNO (TR,XNUE,X,S,XBE,M,BLDT,BLMT,BLT,PBG1,DPBG1,
     1 REYEXT,XME,MP)
      COMMON G, PR, REY, XMINF, OMEGA, BO, TW, P10, T10, R10, VIS10, TE,
     1 PE,RE,UE,VISINF,SU,EPS,DS,DYW,SI,ERROR,TC,TA,IEDGE,IEND1,INTACT,
     2 PRT,XYK,BTRX,XLAM,VAPPRT,XINTER,SEPO,ICHS(8),IPRN(8),EO(200),
     3 EN(200),EP(200),ETO(200),ETN(200),ETP(200),FO(200),FN(200),J2DA,
     4 FP(200),TN(200),TO(200),XNN(200),VN(200),VO(200),VP(200),TP(200),
     5 D1(200),D2(200),D3(200)
 2000 FORMAT(1H0,10X,5HX/L =,E15.8)
 2001 FORMAT(2X,7HXME    =,E15.8,2X,7HPE     =,E15.8,2X,7HDPPINF=,E15.8,
     1 2X,7HXBE    =,E15.8,2X,7HTW/TE =,E15.8)
 2002 FORMAT(2X,7HBLT    =,E15.8,2X,7HBLMT   =,E15.8,2X,7HBLDT   =,E15.8,
     1 2X,7HREYMT =,E15.8,2X,7HREYDT =,E15.8)
 2003 FORMAT(2X,7HCFNO   =,E15.8,2X,7HCFENO =,E15.8,2X,7HSTNO   =,E15.8,
     1 2X,7HSTENO =,E15.8,2X,7HREYEXT=,E15.8)
      TWTE=TP(1)
      IF(OMEGA.EQ.0.) GO TO 855
      IF(OMEGA .EQ. 1.) GO TO 8551
      XLM1 = 1./(TWTE**(1. - OMEGA))
      GO TO 856
  855 XLM1 = (1.0+TR)*SQRT(TWTE)/(TWTE+TR)
      GO TO 856
 8551 XLM1 = 1.
  856 CONTINUE
      Y11=((2.+XXK)*(1.+XXK+XXK**2)+1.+XXK)/((1.+XXK)*(1.+XXK+XXK**2))
      Y12=(1.+XXK+XXK**2)/XXK**2
      Y13=(1.+XXK+XXK**2)/(XXK**3*(1.+XXK))
      Y14=1./(XXK**3*(1.+XXK+XXK**2))
      TAU=XLM1*RE*XNUE*UE*UE*(-Y11*FP(1)+Y12*FP(2)-Y13*FP(3)+Y14*FP(4))
     1 /(DYW*SQRT(2.*X))
      QS = XLM1*RE*XNUE*UE*TE*(Y11*TP(1)-Y12*TP(2)+Y13*TP(3)-Y14*TP(4))
     1 /(DYW*SQRT(2.*X)*PR)
      IF(J2DA.NE.0) TAU=TAU*S
      IF(J2DA.NE.0) QS=QS*S
      STNO = 0.
      IF(BO .NE. 1.) STNO = EPS*QS/((1. - BO)*(TE + .5*UE**2))
      STENO = STNO/(RE*UE)
      CFNO = 2.*EPS*TAU
      CFENO = CFNO/(RE*UE*UE)
      REYDT=REYEXT*BLDT
      REYMT=REYEXT*BLMT
C
C     SELECTION OF THE OUTPUT
      IF(M.NE.MP) GO TO 1000
C     SELECTION OF THE OUTPUT
C
C     OUTPUT STATION DATA
C
      WRITE(6,2000) S
      WRITE(6,2001) XME,PBG1,DPBG1,XBE,TWTE
      WRITE(6,2002) BLT,BLMT,BLDT,REYMT,REYDT
      WRITE(6,2003) CFNO,CFENO,STNO,STENO,REYEXT
```

```
 1000 RETURN
      END
      SUBROUTINE ELMATX(  M,DX2,X,XAL,XBE,TR,IDIFF,Y1,Y2,Y3,Y4,Y5,THTE,
     1 ITCNT1,        A1,A2,A3,B1,B2,B3,C1,C2,C3)
      COMMON G, PR, REY, XMINF, OMEGA, BO, TW, P10, T10, R10, VIS10, TE,
     1 PE,RE,UE,VISINF,SU,EPS,DS,DYW,SI,ERROR,TC,TA,IEDGE,IEND1,INTACT,
     2 PRT,XKK,BTRK,XLAM,VAPRRT,XINTER,SEPO,ICHS(8),IPRN(9),EO(200),
     3 EN(200),EP(200),ETO(200),ETN(200),ETP(200),FO(200),FN(200),J2DA,
     4 FP(200),TN(200),TO(200),XNN(200),VN(200),VO(200),VP(200),TP(200),
     5 D1(200),D2(200),D3(200)
      DIMENSION A1(200,3),A2(200,3),A3(200,3),B1(200,3),B2(200,3),
     1 B3(200,3),C1(200,3),C2(200,3),C3(200,3)
      COMMON/BLWDATA/NUMDAT,XPOS(24),RHOVRAT(24),TRR,TREF,XNUE,S,SS,SD,
     5 IBLW,YLGTHMD,RVRAT
C
C     THE INNER EDGE BOUNDARY CONDITION
C
      DO 8011 I=1,3
 8011 A1(1,I)=A2(1,I)=A3(1,I)=B1(1,I)=B2(1,I)=B3(1,I)=C1(1,I)=C2(1,I)
     1 =C3(1,I)=0.
      A1(1,1)=1.0
      B2(1,1)=1.0
      D1(1)=0.
      D2(1)=THTE
      IF(SEPO.EQ.0.) GO TO 8012
      C3(1,1)=1.0
       BCVW=0.
       IF (IBLW.LT.0.AND.S.GE.SS.AND.S.LE.SD)
     6 CALL CONBLW(BCVW,X,REY,J2DA,EPS,RE,UE)
       IF (IBLW.GT.0.AND.S.GE.SS.AND.S.LE.SD)
     6 CALL GENBLW(BCVW,X,REY,J2DA,EPS,RE,UE)
       D3(1)=BCVW
      GO TO 8013
 8012 XL=DX2/(2.0*DYW)
      A3(1,1)=DX2+X*Y1
      C3(1,1)=-2.*XL*(2.+XXK)/(1.+XXK)
      C3(1,2)=2.*XL*(1.+XXK)/XXK
      C3(1,3)=-2.*XL/(XXK*(1.+XXK))
      D3(1)=0.
C
C     THE INNER EDGE BOUNDARY CONDITION
C
C     THE FIELD POINTS EVALUATION
C
 8013 NM1=IEDGE-1
      DO 8014 N=2,NM1
      DY=XXK**(N-1)*DYW
      DYM1=DY/XXK
      XL=DX2/(2.0*DY)
      Y6=2./(1.+DYM1/DY)
      Y7=DY/DYM1
      Y8=2./((DYM1/DY)*(1.+DYM1/DY))
      Y9=2./(1.+DY/DYM1)
      Y10=1.-DY/DYM1
      SEP=1.0
      IF(FO(N).LE.0.) SEP=0.
      IF(ITCNT1 .GT. 1) GO TO 7000
      IF(IDIFF .EQ. 1) GO TO 7501
      FM1=Y4*FO(N)-Y5*FN(N)
      TM1=Y4*TO(N)-Y5*TN(N)
      VM1=Y4*VO(N)-Y5*VN(N)
      IF(SEPC.EQ.0.) VM1=VO(N)
      EM1  =(Y4*(EO(N-1)+EO(N)+EO(N+1))-Y5*(EN(N-1)+EN(N)+EN(N+1)))/3.
      ETM1  =(Y4*(ETO(N-1)+ETO(N)+ETO(N+1))-Y5*(ETN(N-1)+ETN(N)+ETN(N+1
     1 )))/3.
      GO TO 7001
 7501 FM1  = FO(N)
      TM1  = TO(N)
      VM1  = VO(N)
      EM1=(EO(N-1)+EO(N)+EO(N+1))/3.
```

```
      ETM1=(ETO(N-1)+ETO(N)+ETO(N+1))/3.
      GO TO 7001
 7000  EM1 = EP(N)
      TM1 = TP(N)
      VM1 = VP(N)
      EM1=(EP(N-1)+EP(N)+EP(N+1))/3.
      ETM1=(ETP(N-1)+ETP(N)+ETP(N+1))/3.
 7001  IF(OMEGA .EQ. 0.) GO TO 684
      IF(OMEGA .EQ. 1.) GO TO 6841
      XLM1=1./(TM1**(1.-OMEGA))
      XLPM1=(OMEGA-1.)*XLM1/TM1
      GOTO625
 6841 XLM1=1.
      XLPM1=0.
      GOTO625
  684 XLM1=((1.+TR)*SQRT(TM1)/(TM1+TR))
      XLPM1=XLM1*(TR-TM1)/(2.*TM1*(TM1+TR))
  625 IF(ITCNT1.GT.1) GO TO 626
      FY=(Y9*FO(N+1)/2.-Y10*FO(N)-Y8*FO(N-1)/2.)/DY
      TY=(Y9*TO(N+1)/2.-Y10*TO(N)-Y8*TO(N-1)/2.)/DY
      EYM1=(Y9*EO(N+1)/2.-Y10*EM1-Y8*EO(N-1)/2.)/DY
      ETYM1=(Y9*ETO(N+1)/2.-Y10*ETM1-Y8*ETO(N-1)/2.)/DY
      GO TO 627
  626 FY=(Y9*FP(N+1)/2.-Y10*FP(N)-Y8*FP(N-1)/2.)/DY
      TY=(Y9*TP(N+1)/2.-Y10*TP(N)-Y8*TP(N-1)/2.)/DY
      EYM1=(Y9*EP(N+1)/2.-Y10*EM1-Y8*EP(N-1)/2.)/DY
      ETYM1=(Y9*ETP(N+1)/2.-Y10*ETM1-Y8*ETP(N-1)/2.)/DY
  627 IF(IDIFF.EQ.1) GO TO 7502
      FM2=Y2*FO(N)-Y3*FN(N)
      TM2=Y2*TO(N)-Y3*TN(N)
      GO TO 7505
 7502 FM2 =2.*FO(N)
      TM2 =2.*TO(N)
 7505 CONTINUE
      A1(N,1)=Y8*XL*(2.*XLM1*EM1/DY-(XLM1*EYM1+EM1*XLPM1*TY-VM1))
      A1(N,2)=-(4.*XL*XLM1*EM1*Y7/DY+2.*XL*(XLM1*EYM1+EM1*XLPM1*TY-VM1)*
     1 Y10+2.*XBE*DX2*EM1*SEP+SEP*(2.*Y1*FM1-FM2)*X)
      A1(N,3)=XL*(2.*XLM1*EM1*Y6/DY+(XLM1*EYM1+EM1*XLPM1*TY-VM1)*Y9)
      B1(N,1)=-XL*EM1*XLPM1*FY*Y8
      B1(N,2)=DX2*XBE-2.*XL*EM1*XLPM1*FY*Y10
      B1(N,3)=XL*EM1*XLPM1*FY*Y9
      C1(N,1)=C1(N,3)=0.
      C1(N,2)=-DX2*FY
      A2(N,1)=-2.*XL*XAL*XLM1*EM1*FY*Y8
      A2(N,2)=-(4.*XL*XAL*XLM1*EM1*FY*Y10+SEP*X*(Y1*TM1-TM2))
      A2(N,3)=2.*XL*XAL*XLM1*EM1*FY*Y9
      B2(N,1)=XL*Y8*(2.*XLM1*ETM1/(PR*DY)-(XLM1*ETYM1+2.*XLPM1*ETM1*TY
     1 -PR*VM1)/PR)
      B2(N,2)=-(4.*XL*XLM1*ETM1*Y7/(PR*DY)+(XLM1*ETYM1+2.*XLPM1*ETM1*TY
     1 -PR*VM1)*XL*Y10*2.0/PR+SEP*X*Y1*FM1)
      B2(N,3)=XL*(2.*XLM1*ETM1*Y6/DY+(XLM1*ETYM1+2.*XLPM1*ETM1*TY-PR*
     1 VM1)*Y9)/PR
      C2(N,2)=-DX2*TY
      C2(N,1)=C2(N,3)=0.
      A3(N,1)=A3(N,3)=0.
      A3(N,2)=DX2+X*Y1
      B3(N,1)=B3(N,2)=B3(N,3)=0.
      C3(N,1)=-XL*Y8
      C3(N,2)=-2.*XL*Y10
      C3(N,3)=XL*Y9
      D1(N)=DX2*FY*(EM1*XLPM1*TY-VM1)-FM1**2*(XBE*DX2+X*Y1)*SEP
      D2(N)=DX2*(XLPM1*ETM1*TY/PR-VM1)*TY+DX2*XAL*XLM1*EM1*FY**2-X*Y1
     1 *TM1*FM1*SEP
      D3(N)=Y*FM2
 8014 CONTINUE
C
C     THE FIELD POINTS EVALUATION
C
C
C     THE OUTER EDGE BOUNDARY CONDITION
```

```
C
      DO 8015 I=1,3
 8015 A1(IEDGE,I)=A2(IEDGE,I)=A3(IEDGE,I)=B1(IEDGE,I)=B2(IEDGE,I)=B3(
     1 IEDGE,I)=C1(IEDGE,I)=C2(IEDGE,I)=C3(IEDGE,I)=0.
      A1(IEDGE,3)=1.0
      B2(IEDGE,3)=1.0
      D1(IEDGE)=1.0
      D2(IEDGE)=1.0
      IF(SEPO.EQ.0.) GO TO 8016
      XL=DX2/(2.*DYW*XXK**(IEDGE-1))
      FM2=Y2*FO(IEDGE)-Y3*FN(IEDGE)
      IF(IDIFF.EQ.1) FM2=2.*FO(IEDGE)
      A3(IEDGE,3)=DX2+X*Y1
      C3(IEDGE,1)=2.*XXK**3*XL/(1.+XXK)
      C3(IEDGE,2)=-2.*XXK*(1.+XXK)*XL
      C3(IEDGE,3)=2.*XXK*XL*(2.*XXK+1.)/(1.+XXK)
      D3(IEDGE)=X*FM2
      GO TO 8017
 8016 VM1=VO(IEDGE)
      IF(ITCNT1.GT.1) VM1=VP(IEDGE)
      C3(IEDGE,3)=1.0
      D3(IEDGE)=VM1
 8017 CONTINUE
C
C     THE OUTER EDGE BOUNDARY CONDITION
      RETURN
      END
      SUBROUTINE PRNCHS(ICOUN,IP,IG,IQ,MSTART,IIN,M,S,Y,BLT)
      COMMON G, PR, REY, XMINF, OMEGA, BD, TW, P10, T10, R10, VIS10, TE,
     1 RE,PE,UE,VISINF,SU,EPS,DS,DYW,SI,ERROR,TC,TA,IEDGE,IEND1,INTACT,
     2 PRT,XXK,BTRX,XLAM,VAPPRT,XINTER,SEPO,ICHS(3),IPRN(9),EO(200),
     3 EN(200),EP(200),ETO(200),ETN(200),ETP(200),FO(200),FN(200),J2DA,
     4 FP(200),TN(200),TO(200),XNN(200),VN(200),VO(200),VP(200),TP(200),
     5 D1(200),D2(200),D3(200)
      DIMENSION           Y(200),Z(7,16)
   25 FORMAT (1H0,45X,23HPROFILE FOR STATION S =F14.8)
   40 FORMAT(8HON=       15F8.4 )
   41 FORMAT(8H ET1=     15F8.4 )
   42 FORMAT(8H F1=      15F8.4 )
   43 FORMAT(8H T1=      15F8.4 )
   44 FORMAT(8H V1=      15F8.2 )
   46 FORMAT(8H EO=      15F8.2)
  507 FORMAT(8H Y/BLT=  15F8.4 )
  509 FORMAT(8H RO/ROE=15F8.4 )
  510 FORMAT(8H MACH=   15F8.4)
  511 FORMAT(8H PT/POP=15F8.4 )
  512 FORMAT(8H PT/PE=  15F8.4 )
  513 FORMAT(8H H/HE=   15F8.4 )
      IF(ICOUN-IPRN(IP)) 51,38,51
C
C     OUTPUT PROFILE DATA
C
   38 KONT=IQ-1
      J2=0
      WRITE(6,25) S
      DO 50 J1=1,KONT,15
      J2=J2+1
      KON=J2*15
      WRITE (6,40) (XNN(N),N=J1,KON)
      WRITE (6,41) (Y(N),N=J1,KON)
      WRITE (6,42) (FO(N), N=J1,KON)
      WRITE (6,43) (TO(N), N=J1,KON)
      WRITE (6,44) (VO(N), N=J1,KON)
      WRITE(6,46) (EO(N),N=J1,KON)
      I=J1-1
      IF(M.EQ.MSTART) GO TO 50
      DO 530 JX=1,15
      I=I+1
      Z(1,JX)=EPS*XNN(I)/BLT
      Z(2,JX)=FO(I)
```

```
C       Z(3,JX)=TO(I)
        Z(2,JX)=1./TO(I)
        RTPED=(G-1.0)*TE+TO(I)
        IF (RTPED)   777,777,778
  777   RTPED=1.
  778   Z(4,JX)=UE*Z(2,JX)/(RTPED)**.5
        RTPE=Z(4,JX)*Z(4,JX)
        IF(Z(4,JX)-1.0)504,504,505
  504   RTPE=(1.0+(((G-1.0)/2.0)*RTPE))**(G/(G-1.0))
        GOTO506
  505   RTPE=(((G+1.0)*RTPE/2.0)**(G/(G-1.0)))*(((G+1.0)/((2.0*G*RTPE)-(G-
       11.0)))**(1.0/(G-1.0)))
  506   Z(5,JX)=RTPE
        Z(6,JX) = RTPE*PE/P10
        Z(7,JX)=(TE*TO(I)/(UE*UE)+.5*FO(I)*FO(I))/(TE/(UE*UE)+.5)
  530   CONTINUE
        WRITE(6,507)   (Z(1,N),N=1,15)
        WRITE(6,509)   (Z(3,N),N=1,15)
        WRITE(6,510)   (Z(4,N),N=1,15)
        WRITE(6,511)   (Z(5,N),N=1,15)
        WRITE(6,512)   (Z(6,N),N=1,15)
        WRITE(6,513)  (Z(7,N),N=1,15)
   50   CONTINUE
        IF(IIN .EQ. 1) RETURN
        ICOUN=0
   51   ICOUN=ICOUN+1
        IF(M+1-ICHS(IG)) 3601,3600,3601
 3600   IP=IP+1
        ICOUN=IPRN(IP)
 3601   CONTINUE
        RETURN
        END
        SUBROUTINE REYSTR (KON,TR,X,TREF,XNUE,XBE,S,ITCNT1,TRR)
        COMMON G, PR, REY, XMINF, OMEGA, BO, TW, P10, T10, R10, VIS10, TE,
       1 PE,RE,UE,VISINF,SU,EPS,DS,DYW,SI,ERROR,TC,TA,IEDGE,IEND1,INTACT,
       2 PRT,XYK,RTRX,XLAM,VARPRT,XINTER,SEPO,ICHS(8),IPRN(9),EO(200),
       3 EN(200),EP(200),ETO(200),ETN(200),ETP(200),FO(200),FN(200),J2DA,
       4 FP(200),TN(200),TO(200),XNN(200),VN(200),VO(200),VP(200),TP(200),
       5 D1(200),D2(200),D3(200)
        CO=TP(1)
        DD=EP(1)=XNN(1)=TPI=BLT=0.
C       SHEAR STRESS AT THE WALL AS THE SCALING FUNCTION
        Y11=((2.+XXK)*(1.+XXK+XXK**2)+1.+XXK)/((1.+XXK)*(1.+XXK+XXK**2))
        Y12=(1.+XXK+XXK**2)/XXK**2
        Y13=(1.+XXK+XXK**2)/(XXK**3*(1.+XXK))
        Y14=1./(XXK**3*(1.+XXK+XXK**2))
        FETW=(-Y11*FP(1)+Y12*FP(2)-Y13*FP(3)+Y14*FP(4))/DYW
        FETW=ABS(FETW)
        XLM1W=((1.+TR)*SQRT(TP(1))/(TP(1)+TR))
        PI2=XLM1W*FETW
C       SHEAR STRESS AT THE WALL AS THE SCALING FUNCTION
        DO 1   N=2,KON
        DY=DYW*XXK**(N-2)
        XLM1=((1.+TR)*SQRT(TP(N))/(TP(N)+TR))
        C=TP(N)
        TPI=TPI+.5*DY*(CO+C)
        CO=C
        XNN(N)=TPI*SQRT(2.*X)/(RE*UE)
        IF(J2DA.NE.0)  XNN(N)=XNN(N)/S
        IF(BLT.GT.0.)  GO TO 2
        IF(FP(N).GE.0.995)  BLT=XNN(N)-(FP(N)-.995)*(XNN(N)-XNN(N-1))
       1 /(FP(N)-FP(N-1))
        DD=DD+((1.-FP(N))*TP(N)+(1.-FP(N-1))*TP(N-1))*DY/2.
2       PI1=SQRT(2.*X*REY/(TREF**1.5*TRR))*TPI**2/(XNUE*TP(N)**3)
        IF(J2DA.NE.0)  PI1=PI1/S
        DY=DYW*XXK**(N-1)
        DYM1=DY/XXK
        Y8=2./((DYM1/DY)*(1.+DYM1/DY))
        Y9=2./(1.+DY/DYM1)
        Y10=1.-DY/DYM1
```

```
C     BTR=XLM1*EP(N)*ABS(Y9*EP(N+1)/2.-Y10*EP(N)-Y8*EP(N-1)/2.)/DY
C
C     CEBICE-SMITH-MONSINKIS EDDY VISCOSITY MODEL
      YPLUS=SQRT(PI1*PI2)/(26.*XLM1)
      IF(YPLUS.GT.50.) YPLUS=50.
      EP(N)=.16*PI1*(1.-EXP(-YPLUS))**2*ABS(Y9*
     1 EP(N+1)/2.-Y10*EP(N)-Y8*EP(N-1)/2.)/(DY*XLM1)
C     CEBICE-SMITH-MONSINKIS EDDY VISCOSITY MODEL
C
C     TRUNCATE THE INNER REGION CALCULATION
      IF(EP(N).LE.EP(N-1)) EP(N)=EP(N-1)
C     TRUNCATE THE INNER REGION CALCULATION
C
 1    CONTINUE
      DO 3 N=1,KON
      XLM1=((1.+TR)*SQRT(TP(N))/(TP(N)+TR))
      DD1=.0168*SQRT(2.*X*REY/(TREF**1.5*TRR))*DD/(XNUE*XLM1*TP(N)**2)
      IF(J21A.NE.0) DD1=DD1/F
      IF(DD1.LE.EP(N)) EP(N)=DD1
       IF (ABS(BTRX).LE.(1.E-6)) GO TO 93
       SUSCRP=(-.412*((S-BTRX)/XLAM)**2)
       IF (SUSCRP.LT.(-674.)) GO TO 93
       EP(N)=EP(N)*(1.-EXP(SUSCRP))
 93    IF (XINTER.EQ.0.) EP(N)=1.+EP(N)
      IF(XINTER.EQ.1.) EP(N)=1.+ (1.75/(1.+5.5*(XNN(N)/B_T)**6)+1.)*
     1 EP(N) /2.75
 3    ETP(N)=1.+PR*(EP(N)-1.)/PRT
C
      RETURN
      END
      SUBROUTINE MATEQN3 (X1,X2,X3,Y1,Y2,Y3,A11,A12,A13,A21,A22,A23,
     $ A31,A32,A33,LC,LN,LQ)
C
C*********************************************************************
C
C     THIS SUBROUTINE SOLVES THE THREE SIMULTANEOUS BAND MATRIX
C     EQUATIONS
C
C     A11*X1 + A12*X2 + A13*X3 = Y1
C     A21*X1 + A22*X2 + A23*X3 = Y2
C     A31*X1 + A32*X2 + A33*X3 = Y3
C
C     FOR X1, X2, AND X3
C
C     AIJ ARE 9 BAND MATRICES OF LENGTH LQ, WORKING LENGTH LN,
C     AND WIDTH LC
C         (THESE MATRICES ARE ASSUMED TO BE CORNER ADJUSTED, I.E. THE
C           CORNER ELEMENTS ARE STORED IN (1,1) AND (LN,LC), ETC.)
C
C     XI AND YI ARE VECTORS OF LENGTH LQ AND WORKING LENGTH LN
C
C*********************************************************************
C
      DIMENSION
     $ X1(LQ),X2(LQ),X3(LQ),Y1(LQ),Y2(LQ),Y3(LQ),
     $ A11(LQ,LC),A12(LQ,LC),A13(LQ,LC),
     $ A21(LQ,LC),A22(LQ,LC),A23(LQ,LC),
     $ A31(LQ,LC),A32(LQ,LC),A33(LQ,LC)
C
C     INITIALIZATION
C     --------------
C
      LP=LN+1
      L=(LC-1)/2
      LM=LN-L-1
      IF(LC.GE.LN) L=LN
      DO 3 I=1,LN
      X1(I)=Y1(I)
      X2(I)=Y2(I)
      X3(I)=Y3(I)
```

```
3     CONTINUE
C
C     DOWNWARD GAUSSIAN ELIMINATION WITH PIVOTING
C     -------------------------------------------
C
      DO 401 K=1,LN
      IF(L.EQ.LM) L=LN
      IF(L.LT.LN) L=L+1
C
      U=ABS(A11(K,1))
      I=K
      M=1
      DO 113 J=K,L
      IF(J.EQ.K) GO TO 111
      V=ABS(A11(J,1))
      IF(V.LE.U) GO TO 111
      U=V
      M=1
      I=J
111   V=ABS(A21(J,1))
      IF(V.LE.U) GO TO 112
      U=V
      M=2
      I=J
112   V=ABS(A31(J,1))
      IF(V.LE.U) GO TO 113
      U=V
      M=3
      I=J
113   CONTINUE
      IF(I.EQ.K) GO TO 115
      IF(M.NE.1) GO TO 115
      DO 114 J=1,LC
      U=A11(K,J)
      A11(K,J)=A11(I,J)
      A11(I,J)=U
      U=A12(K,J)
      A12(K,J)=A12(I,J)
      A12(I,J)=U
      U=A13(K,J)
      A13(K,J)=A13(I,J)
      A13(I,J)=U
114   CONTINUE
      U=X1(K)
      X1(K)=X1(I)
      X1(I)=U
      GO TO 120
115   IF(M.EQ.1) GO TO 120
116   IF(M.NE.2) GO TO 118
      DO 117 J=1,LC
      U=A11(K,J)
      A11(K,J)=A21(I,J)
      A21(I,J)=U
      U=A12(K,J)
      A12(K,J)=A22(I,J)
      A22(I,J)=U
      U=A13(K,J)
      A13(K,J)=A23(I,J)
      A23(I,J)=U
117   CONTINUE
      U=X1(K)
      X1(K)=X2(I)
      X2(I)=U
      GO TO 120
118   DO 119 J=1,LC
      U=A11(K,J)
      A11(K,J)=A31(I,J)
      A31(I,J)=U
      U=A12(K,J)
      A12(K,J)=A32(I,J)
```

```
      A32(I,J)=U
      U=A13(K,J)
      A13(K,J)=A33(I,J)
      A33(I,J)=U
  119 CONTINUE
      U=X1(K)
      X1(K)=X3(I)
      X3(I)=U
  120 CONTINUE
C
      DO 128 I=K,L
      IF(I.EQ.K) GO TO 123
      U=A11(I,1)/A11(K,1)
      DO 122 J=1,LC
      IF(J.NE.1) A13(I,J-1)=A11(I,J)-A11(K,J)*U
      A11(I,J)=A12(I,J)-A12(K,J)*U
      A12(I,J)=A13(I,J)-A13(K,J)*U
  122 CONTINUE
      A13(I,LC)=0.
      X1(I)=X1(I)-X1(K)*U
  123 CONTINUE
      U=A21(I,1)/A11(K,1)
      DO 125 J=1,LC
      IF(J.NE.1) A23(I,J-1)=A21(I,J)-A11(K,J)*U
      A21(I,J)=A22(I,J)-A12(K,J)*U
      A22(I,J)=A23(I,J)-A13(K,J)*U
  125 CONTINUE
      A23(I,LC)=0.
      X2(I)=X2(I)-X1(K)*U
      U=A31(I,1)/A11(K,1)
      DO 127 J=1,LC
      IF(J.NE.1) A33(I,J-1)=A31(I,J)-A11(K,J)*U
      A31(I,J)=A32(I,J)-A12(K,J)*U
      A32(I,J)=A33(I,J)-A13(K,J)*U
  127 CONTINUE
      A33(I,LC)=0.
      X3(I)=X3(I)-X1(K)*U
  128 CONTINUE
C
      U=ABS(A21(K,1))
      I=K
      M=2
      DO 213 J=K,L
      IF(J.EQ.K) GO TO 212
      V=ABS(A11(J,1))
      IF(V.LE.U) GO TO 211
      U=V
      M=1
      I=J
  211 V=ABS(A21(J,1))
      IF(V.LE.U) GO TO 212
      U=V
      M=2
      I=J
  212 V=ABS(A31(J,1))
      IF(V.LE.U) GO TO 213
      U=V
      M=3
      I=J
  213 CONTINUE
      IF(I.EQ.K) GO TO 215
      IF(M.NE.2) GO TO 216
      DO 214 J=1,LC
      U=A21(K,J)
      A21(K,J)=A21(I,J)
      A21(I,J)=U
      U=A22(K,J)
      A22(K,J)=A22(I,J)
      A22(I,J)=U
      U=A23(K,J)
```

```
      A23(K,J)=A23(I,J)
      A23(I,J)=U
214   CONTINUE
      U=X2(K)
      X2(K)=X2(I)
      X2(I)=U
      GO TO 220
215   IF(M.NE.3) GO TO 220
216   IF(M.NE.1) GO TO 218
      DO 217 J=1,LC
      U=A21(K,J)
      A21(K,J)=A11(I,J)
      A11(I,J)=U
      U=A22(K,J)
      A22(K,J)=A12(I,J)
      A12(I,J)=U
      U=A23(K,J)
      A23(K,J)=A13(I,J)
      A13(I,J)=U
217   CONTINUE
      U=X2(K)
      X2(K)=X1(I)
      X1(I)=U
      GO TO 220
218   DO 219 J=1,LC
      U=A21(K,J)
      A21(K,J)=A31(I,J)
      A31(I,J)=U
      U=A22(K,J)
      A22(K,J)=A32(I,J)
      A32(I,J)=U
      U=A23(K,J)
      A23(K,J)=A33(I,J)
      A33(I,J)=U
219   CONTINUE
      U=X2(K)
      X2(K)=X3(I)
      X3(I)=U
220   CONTINUE
C
      DO 228 I=K,L
      IF(I.EQ.K) GO TO 223
      U=A11(I,1)/A21(K,1)
      DO 222 J=1,LC
      IF(J.NE.1) A13(I,J-1)=A11(I,J)-A21(K,J)*U
      A11(I,J)=A12(I,J)-A22(K,J)*U
      A12(I,J)=A13(I,J)-A23(K,J)*U
222   CONTINUE
      A13(I,LC)=0.
      X1(I)=X1(I)-X2(K)*U
      U=A21(I,1)/A21(K,1)
      DO 225 J=1,LC
      IF(J.NE.1) A23(I,J-1)=A21(I,J)-A21(K,J)*U
      A21(I,J)=A22(I,J)-A22(K,J)*U
      A22(I,J)=A23(I,J)-A23(K,J)*U
225   CONTINUE
      A23(I,LC)=0.
      X2(I)=X2(I)-X2(K)*U
223   CONTINUE
      U=A31(I,1)/A21(K,1)
      DO 227 J=1,LC
      IF(J.NE.1) A33(I,J-1)=A31(I,J)-A21(K,J)*U
      A31(I,J)=A32(I,J)-A22(K,J)*U
      A32(I,J)=A33(I,J)-A23(K,J)*U
227   CONTINUE
      A33(I,LC)=0.
      X3(I)=X3(I)-X2(K)*U
228   CONTINUE
C
      IF(K.EQ.LN) GO TO 401
```

```
      U=ABS(A31(K,1))
      I=K
      M=3
      JL=K+1
      DO 313 J=JL,L
      V=ABS(A11(J,1))
      IF(V.LE.U) GO TO 311
      U=V
      M=1
      I=J
  311 V=ABS(A21(J,1))
      IF(V.LE.U) GO TO 312
      U=V
      M=2
      I=J
  312 V=ABS(A31(J,1))
      IF(V.LE.U) GO TO 313
      U=V
      M=3
      I=J
  313 CONTINUE
      IF(I.EQ.K) GO TO 320
      IF(M.NE.3) GO TO 316
      DO 314 J=1,LC
      U=A31(K,J)
      A31(K,J)=A31(I,J)
      A31(I,J)=U
      U=A32(K,J)
      A32(K,J)=A32(I,J)
      A32(I,J)=U
      U=A33(K,J)
      A33(K,J)=A33(I,J)
      A33(I,J)=U
  314 CONTINUE
      U=X3(K)
      X3(K)=X3(I)
      X3(I)=U
      GO TO 320
  316 IF(M.NE.1) GO TO 318
      DO 317 J=1,LC
      U=A31(K,J)
      A31(K,J)=A11(I,J)
      A11(I,J)=U
      U=A32(K,J)
      A32(K,J)=A12(I,J)
      A12(I,J)=U
      U=A33(K,J)
      A33(K,J)=A13(I,J)
      A13(I,J)=U
  317 CONTINUE
      U=X3(K)
      X3(K)=X1(I)
      X1(I)=U
      GO TO 320
  318 DO 319 J=1,LC
      U=A31(K,J)
      A31(K,J)=A21(I,J)
      A21(I,J)=U
      U=A32(K,J)
      A32(K,J)=A22(I,J)
      A22(I,J)=U
      U=A33(K,J)
      A33(K,J)=A23(I,J)
      A23(I,J)=U
  319 CONTINUE
      U=X3(K)
      X3(K)=X2(I)
      X2(I)=U
  320 CONTINUE
C
```

AD-A034 876 AIR FORCE INST OF TECH WRIGHT-PATTERSON AFB OHIO SCH--ETC F/G 20/4
AN ANALYTICAL STUDY OF THE EFFECTS OF MASS TRANSFER ON A COMPRE--ETC(U)
DEC 76 A J BEAUREGARD

UNCLASSIFIED GA/MC/76D-3 NL

2 OF 2
AD
A034876

END
DATE
FILMED
2-77

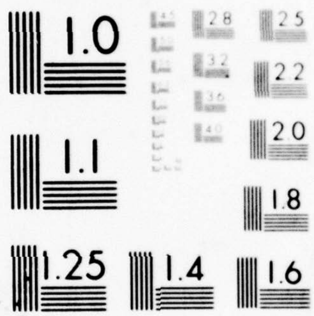

MICROCOPY RESOLUTION TEST CHART
NATIONAL BUREAU OF STANDARDS 1963

```
      IL=K+1
      DO 328 I=IL,L
      U=A11(I,1)/A31(K,1)
      DO 322 J=1,LC
      IF(J.NE.1) A13(I,J-1)=A11(I,J)-A31(K,J)*U
      A11(I,J)=A12(I,J)-A32(K,J)*U
      A12(I,J)=A13(I,J)-A33(K,J)*U
  322 CONTINUE
      A13(I,LC)=0.
      X1(I)=X1(I)-X3(K)*U
      U=A21(I,1)/A31(K,1)
      DO 325 J=1,LC
      IF(J.NE.1) A23(I,J-1)=A21(I,J)-A31(K,J)*U
      A21(I,J)=A22(I,J)-A32(K,J)*U
      A22(I,J)=A23(I,J)-A33(K,J)*U
  325 CONTINUE
      A23(I,LC)=0.
      X2(I)=X2(I)-X3(K)*U
      U=A31(I,1)/A31(K,1)
      DO 327 J=1,LC
      IF(J.NE.1) A33(I,J-1)=A31(I,J)-A31(K,J)*U
      A31(I,J)=A32(I,J)-A32(K,J)*U
      A32(I,J)=A33(I,J)-A33(K,J)*U
  327 CONTINUE
      A33(I,LC)=0.
      X3(I)=X3(I)-X3(K)*U
  328 CONTINUE
C
  401 CONTINUE
C
C     UPWARD GAUSSIAN ELIMINATION
C     ---------------------------
C
      L=1
      DO 507 K=1,LM
      I=LP-K
C
      U=X3(I)
      IF(I.EQ.LM) GO TO 502
      DO 501 J=2,L
      IJ=I+J
  501 U=U-A32(I,J-1)*X1(IJ-1)-A33(I,J-1)*X2(IJ-1)-A31(I,J)*X3(IJ-1)
      IF(L.GE.LC) U=U-A32(I,LC)*X1(I+LC)-A33(I,LC)*X2(I+LC)
  502 X3(I)=U/A31(I,1)
C
      U=X2(I)-A22(I,1)*X3(I)
      IF(I.EQ.LM) GO TO 504
      DO 503 J=2,L
      IJ=I+J
  503 U=U-A23(I,J-1)*X1(IJ-1)-A21(I,J)*X2(IJ-1)-A22(I,J)*X3(IJ-1)
      IF(L.GE.LC) U=U-A23(I,LC)*X1(I+LC)
  504 X2(I)=U/A21(I,1)
C
      U=X1(I)-A12(I,1)*X2(I)-A13(I,1)*X3(I)
      IF(I.EQ.LM) GO TO 506
      DO 505 J=2,L
      IJ=I+J
  505 U=U-A11(I,J)*X1(IJ-1)-A12(I,J)*X2(IJ-1)-A13(I,J)*X3(IJ-1)
  506 X1(I)=U/A11(I,1)
      IF(L.LT.LC) L=L+1
C
  507 CONTINUE
C
      RETURN
      END
       SUBROUTINE CONBLW(BCVW,X,REY,J204,EPS,RE,UE)
C
C      ********************************************************
C
C        CONBLW CONVERTS A CONSTANT MASS TRANSFER RATE RATIO,
```

```
C         (RHO V)W/(RHO U)*, TO A TRANSFORMED QUANTITY
C         WHICH REPRESENTS THE "V" BOUNDARY CONDITION IN
C         SUBROUTINE ELMATX.
C
C        *****************************************************
C
      COMMON/BLWDATA/NUMDAT,XPOS(24),RHOVRAT(24),TRR,TREF,XNUE,S,SS,SD,
     6 IBLW,XLGTHMD,RVRAT
      BCVWN=(SQRT(2.*X))*RVRAT
      IF (J2DA.EQ.1) GO TO 97
      BCVWD=(EPS*XNUE*RE*UE)
      GO TO 96
   97 BCVWD=(EPS*XNUE*S*RE*UE)
   96 CONTINUE
      BCVW=BCVWN/BCVWD
      RETURN
      END
      SUBROUTINE GENBLW(BCVW,X,REY,J2DA,EPS,RE,UE)
C
C        ***********************************************************
C
C         GENBLW CONVERTS A GENERAL OR VARYING MASS TRANSFER RATE
C         RATIO, (RHO V)W/(RHO U)*, TO A TRANSFORMED QUANTITY
C         WHICH REPRESENTS THE "V" BOUNDARY CONDITION IN SUB-
C         ROUTINE ELMATX.
C
C        ***********************************************************
C
      COMMON/BLWDATA/NUMDAT,XPOS(24),RHOVRAT(24),TRR,TREF,XNUE,S,SS,SD,
     6 IBLW,XLGTHMD,RVRAT
      NUMDAT1=NUMDAT-1
      DO 99 I=1,NUMDAT1
      IF (S.LE.(XPOS(I+1)/XLGTHMD).AND.S.GE.(XPOS(I)/XLGTHMD)) VRVRAT=
     6 RHOVRAT(I)+((S*XLGTHMD)-XPOS(I))*(RHOVRAT(I+1)-RHOVRAT(I))/
     6 (XPOS(I+1)-XPOS(I))
      IF (S.LE.(XPOS(I+1)/XLGTHMD).AND.S.GE.(XPOS(I)/XLGTHMD)) GO TO 98
   99 CONTINUE
   98 BCVWN=(SQRT(2.*X))*VRVRAT
      IF (J2DA.EQ.1) GO TO 95
      BCVWD=(EPS*XNUE*RE*UE)
      GO TO 94
   95 BCVWD=(EPS*XNUE*S*RE*UE)
   94 CONTINUE
      BCVW=BCVWN/BCVWD
      RETURN
      END
```

Appendix C

Four Key Subsystems Within Itract

Nondimensionalizing the Variables and Initializing the Grid

Prior to entering the computational loop the working variables were nondimensionalized or normalized. These variables were listed below along with a definition of each. The format selected was to present the coded variable on the left side of the equal sign and the real or physical definition on the right side of the equal sign. No explanation was included as to choice of normalizing factors.

$$Z1 = \frac{a_o^2}{a_\infty^2} = \frac{T_o}{T_\infty} = 1 + \frac{\gamma-1}{2} M_\infty^2$$

$$P10 = \frac{1}{\gamma M_\infty^2}\left(\frac{T_o}{T_\infty}\right)^{\frac{\gamma}{\gamma-1}} = \frac{1}{\gamma M_\infty^2}\,\frac{p_o}{p_\infty}$$

$$T10 = \frac{1}{(\gamma-1)M_\infty^2}\left(\frac{T_o}{T_\infty}\right) = \frac{T_o}{T_\infty(\gamma-1)M_\infty^2} \tag{54}$$

$$R10 = \frac{\gamma\left(\frac{1}{\gamma M_\infty^2}\,\frac{p_o}{p_\infty}\right)}{(\gamma-1)\frac{T_o}{T_\infty(\gamma-1)M_\infty^2}} = \frac{\rho_o}{\rho_\infty}$$

$$TINF = \frac{T_o/(T_\infty(\gamma-1)M_\infty^2)}{(T_o/T_\infty)} = \frac{1}{(\gamma-1)M_\infty^2}$$

$$TW = \frac{T_w}{T_\infty(\gamma-1)M_\infty^2}$$

With Eq (54) defined for all cases, some others depended on the value of ω. If ω were not equal to zero, then

$$\text{VISIO} = \frac{T_o}{T_\infty(\gamma-1)M_\infty^2} = \frac{\mu_o}{\mu_\infty}\left(\frac{1}{(\gamma-1)M_\infty^2}\right)^{\omega}$$

$$\text{EPS} = \frac{\left\{(\gamma-1)M_\infty^2\right\}^{\omega/2}}{(Re_\infty)^{1/2}} \tag{55}$$

$$\text{VISINF} = \left(\frac{1}{(\gamma-1)M_\infty^2}\right)^{\omega} = \left(\frac{T_\infty}{T_{ref}}\right)^{\omega}$$

where the reference temperature was taken as $T_\infty(\gamma-1)M_\infty^2$. However, for the case where ω was equal to zero, the quantities of Eq (55) plus one were defined as follows:

$$\text{TC} = \frac{S}{T_\infty(\gamma-1)M_\infty^2} = \frac{198.6}{T_{ref}}$$

$$\text{VISIO} = \left(\frac{T_o}{T_\infty(\gamma-1)M_\infty^2}\right)\left[\frac{1+\dfrac{S}{T_\infty(\gamma-1)M_\infty^2}}{\dfrac{T_o}{T_\infty(\gamma-1)M_\infty^2}+\dfrac{S}{T_\infty(\gamma-1)M_\infty^2}}\right]$$

$$= \left(\frac{T_o}{T_{ref}}\right)^{1.5}\left(\frac{T_{ref}+198.6}{T_o+198.6}\right) = \frac{\mu_o}{\mu_{ref}}$$

$$\text{EPS} = \left\{\frac{\dfrac{(T_\infty+198.6)\left[(\gamma-1)M_\infty^2\right]^{1.5}}{(T_\infty(\gamma-1)M_\infty^2+198.6)}}{Re_\infty}\right\}^{1/2} \tag{56}$$

$$= \left\{ \frac{\left(\frac{T_{ref}}{T_\infty}\right)^{1.5} \left[\frac{T_\infty \quad +198.6}{T_{ref}+198.6}\right]}{Re_\infty} \right\}^{1/2} = \left(\frac{\mu_{ref}/\mu_\infty}{Re_\infty}\right)^{1/2} \tag{56}$$

$$\text{VISINF} = \left(\frac{T_\infty}{T_{ref}}\right)^{1.5} \left(\frac{T_{ref} + 198.6}{T_\infty + 198.6}\right)$$

These quantities were frequently used in the grid computation and provided a summary of the nondimensionalizing techniques used throughout the code. Before beginning this computation within the grid, however, there had to be an initialization of the profile.

Initialization began by defining Y in the code as the distance measured along the η axis. Any $\Delta\eta_j$ was defined as $\left(\frac{\Delta\eta_{K+1}}{\Delta\eta_K}\right)^{j-1} \Delta\eta_1$ which yielded a fine mesh of nodal points near the surface and an adequate spacing toward the edge. Y values were assigned by successively adding all $\Delta\eta$ values from the surface, to the point in question. Then, three hypothetical successive columns of nodes were created by the following statements:

D1 = D2 = D3 = 0., from the surface to the edge of the boundary layer.

Incorporating the notation of fig 1,

$V_{i,j} = V_{i-1,j} = V_{i-2,j} = -Y_j$, for all j from the surface to the edge of the boundary layer.

In a similar manner, three successive stations of F, $\underline{\theta}$, $\overline{\epsilon}$, and $\hat{\epsilon}$ were assigned values of 1.0. Finally, all coefficients of the system of finite difference equations were set equal to 0.

This initialization provided the primer to begin the backward differencing along the ξ direction and the central differencing along

the η direction. The finite differencing system was unconditionally stable for increments of $\Delta\eta$ and $\Delta\xi$, and the iterative stepping procedure along ξ damped the error due to the grid initialization within a few steps (Ref 6).

The Finite Difference System

Coefficients of the finite difference equations were computed for the matrix equations which would be solved in a succeeding step. These equations were derived starting with the concept of a grid as in fig 1, and the stipulation that a function could be described at a point by a Taylor series expansion about another point. For Itract the approximation was made that for any functional value, F,

$$F(i,j+1) = F(i,j) + \frac{\partial F}{\partial \eta} \Delta\eta_j + \frac{\partial^2 F}{\partial \eta^2} \frac{\Delta\eta_j^2}{2!}$$
$$F(i,j-1) = F(i,j) - \frac{\partial F}{\partial \eta} \Delta\eta_{j-1} + \frac{\partial^2 F}{\partial \eta^2} \frac{\Delta\eta_{j-1}^2}{2!} \tag{57}$$

Then, for

$$Y6 = \frac{2}{\left(1 + \frac{\Delta\eta_{j-1}}{\Delta\eta_j}\right)}$$

$$Y7 = \frac{\Delta\eta_j}{\Delta\eta_{j-1}}$$

$$Y8 = \frac{2}{\frac{\Delta\eta_{j-1}}{\Delta\eta_j}\left(1 + \frac{\Delta\eta_{j-1}}{\Delta\eta_j}\right)} \tag{58}$$

$$Y9 = \frac{2}{\left(1 + \frac{\Delta\eta_j}{\Delta\eta_{j-1}}\right)}$$

$$Y10 = \left(1 - \frac{\Delta\eta_j}{\Delta\eta_{j-1}}\right) \quad (58)$$

the second and first partial derivatives of Eq (57) were expressed by central differencing as follows:

$$\frac{\partial^2 F(i,j)}{\partial\eta^2} = \frac{Y6F(i,j+1)}{\Delta\eta_j^2} - \frac{2Y7F(i,j)}{\Delta\eta_j^2} + \frac{Y8F(i,j-1)}{\Delta\eta_j^2}$$

$$\frac{\partial F(i,j)}{\partial\eta} = \frac{Y9F(i,j+1)}{2\Delta\eta_j} - \frac{Y10F(i,j)}{\Delta\eta_j} - \frac{Y8F(i,j-1)}{2\Delta\eta_j} \quad (59)$$

The same format of expression was used for $\frac{\partial V}{\partial\xi}$, $\frac{\partial\theta}{\partial\eta}$, and $\frac{\partial^2\theta}{\partial\eta^2}$. For a streamwise series of nodal points along ξ the backward differencing system was written from

$$F(i-1,j) = F(i,j) - \Delta\xi_{i-1}\frac{\partial F}{\partial\xi} + \frac{\Delta\xi^2_{i-1}}{2!}\frac{\partial^2 F}{\partial\xi^2}$$

$$F(i-2,j) = F(i,j) - (\Delta\xi_{i-2}+\Delta\xi_{i-1})\frac{\partial F}{\partial\xi} + \frac{(\Delta\xi_{i-2}+\Delta\xi_{i-1})^2}{2!}\frac{\partial^2 F}{\partial\xi^2} \quad (60)$$

Only expressions for the first derivative with respect to ξ were required and this equation was as follows:

$$\frac{\partial F(i,j)}{\partial\xi} = \left(\frac{\Delta\xi_{i-1}}{\Delta\xi_{i-2}(\Delta\xi_{i-2}+\Delta\xi_{i-1})}\right) F(i-2,j) + \left(\frac{\Delta\xi_{i-2}+\Delta\xi_{i-1}}{-\Delta\xi_{i-2}\Delta\xi_{i-1}}\right) F(i-1,j)$$

$$+ \left(\frac{\Delta\xi_{i-2}+2\Delta\xi_{i-1}}{\Delta\xi_{i-1}(\Delta\xi_{i-2}+\Delta\xi_{i-1})}\right) F(i,j) \quad (61)$$

Again the same format of expression was used for $\frac{\partial\theta}{\partial\xi}$, and all derivative forms of Eqs (20), (21), and (22) had been derived. Then, due to their recurring use, the following definitions were made for computational convenience and efficiency:

$$FM1 = \left(\frac{\Delta\xi_{i-2}+\Delta\xi_{i-1}}{\Delta\xi_{i-2}}\right) F(i-1,j) - \left(\frac{\Delta\xi_{i-1}}{\Delta\xi_{i-2}}\right) F(i-2,j)$$

$$TM1 = \left(\frac{\Delta\xi_{i-2}+\Delta\xi_{i-1}}{\Delta\xi_{i-2}}\right) T(i-1,j) - \left(\frac{\Delta\xi_{i-1}}{\Delta\xi_{i-2}}\right) T(i-2,j)$$

$$FM2 = \left(\frac{2(\Delta\xi_{i-2}+\Delta\xi_{i-1})}{\Delta\xi_{i-2}}\right) F(i-1,j) - \left(\frac{2\Delta\xi_{i-1}^2}{\Delta\xi_{i-2}(\Delta\xi_{i-2}+\Delta\xi_{i-1})}\right) f(i-2,j) \tag{62}$$

$$TM2 = \left(\frac{2(\Delta\xi_{i-2}+\Delta\xi_{i-1})}{\Delta\xi_{i-2}}\right) T(i-1,j) - \left(\frac{2\Delta\xi_{i-1}^2}{\Delta\xi_{i-2}(\Delta\xi_{i-2}+\Delta\xi_{i-1})}\right) T(i-2,j)$$

Through Taylor series expansions about F(i,j) and T(i,j) and neglecting terms with second order partial derivatives and higher, then FM1 and TM1 were actually expressions for F(i,j) and T(i,j), respectively.

Returning to Eqs (20), (21), and (22) and the construction of linearized finite difference equations, there were three types of nonlinear terms with which to be dealt. Using F and G to represent any two general function symbols the nonlinear terms were of the types: $(F)\left(\frac{\partial G}{\partial\xi}\right)$, $\left(\frac{\partial F}{\partial\eta}\right)\left(\frac{\partial G}{\partial\eta}\right)$, and (F)(G), where F could have been equal to G. Returning to the notation of the problem variables it was shown that

$$F(i,j)\ \frac{\partial F(i,j)}{\partial\xi} = FM1\left\{\left(\frac{\Delta\xi_{i-2}+2\Delta\xi_{i-1}}{\Delta\xi_{i-1}(\Delta\xi_{i-2}+\Delta\xi_{i-1})}\right) FM1 - \left(\frac{1}{2\Delta\xi_{i-1}}\right)FM2\right\} \tag{63}$$

$$\left(\frac{\partial F(i,j)}{\partial\eta}\right)^2 = 2FY\left(\frac{\partial F(i,j)}{\partial\eta}\right) - FY^2 \tag{64}$$

where FY was equal to $\frac{\partial F(i-1,j)}{\partial \eta}$, a known, and $\frac{\partial F(i,j)}{\partial \eta}$ was unknown, and that

$$F^2 = 2F(i,j)\ f(i-1,j) - F(i-1,j) \qquad (65)$$

where only F(i,j) was unknown. All terms had been represented in finite difference form, and the final step incorporated these linearized models into Eqs (20), (21), and (22) to derive the overall system of finite difference equations (Ref 8:67-71).

From this system, the coefficients of F(i,j-1), F(i,j), F(i,j+1), and T and V at these stations were collected, computed, and passed to the matrix inversion routine resulting in solutions for F, V, and $\underline{\theta}$ from the surface to the edge of the boundary layer at the current station, s_i.

<u>Subroutine Reystr</u>

This routine was called from the main program at each station, s_i, at and beyond the point of transition to turbulence. The purpose of this subroutine was to calculate an eddy viscosity for the inner and outer regions of the two-layer turbulent boundary layer model.

Computation within Reystr began with Taylor series expansions of F to the third order partial term about the first station at the wall. With values for $F_{j=1}$, $F_{j=2}$, $F_{j=3}$ and $F_{j=4}$, a four-point finite difference expression was formed for $\left.\frac{\partial F}{\partial \eta}\right|_w$, and the coefficients of the F terms at each node, one through four, were represented by Y11, Y12, Y13, and Y14 in the code. Next, a nondimensional molecular viscosity-density term was calculated for the wall with a shear stress term that followed:

$$XLM1W = \left(\frac{T_w}{T_e}\right)^{1/2} \left(\frac{T_e+198.6}{T_w+198.6}\right) = \frac{(\rho\mu)_w}{(\rho\mu)_e} \qquad (66)$$

$$PI2 = \frac{(\rho\mu)_w}{(\rho\mu)_e} \frac{\partial F}{\partial \eta}\bigg|_w \tag{67}$$

An iterative loop was begun to generate the nondimensionalized inner eddy viscosity model, $\frac{\epsilon_{inner}}{\mu}$, of Cebeci-Smith-Mosinskis for each node in the η direction for the current s_i. In the actual code and following the calculation of a number of interim quantities that did not necessarily represent any real boundary layer characteristic, three important computations were made. First, δ/L was calculated. Next, an intermediate quantity, DD, to be used later in the outer eddy model, was calculated. Finally, PI1, another intermediate quantity used in the inner model, was computed:

$$\delta/L = XNN_j - \frac{\left(\frac{u_j}{u_e} - .995\right)\left(\Delta XNN_{j-(j-1)}\right)}{\Delta\left(\frac{u}{u_e}\right)_{j-(j-1)}}$$

$$DD = \sum_{j=2}^{\substack{\text{edge of the}\\ \text{boundary layer}}} \left[\left(1 - \frac{u_j}{u_e}\right)\left(\frac{T_j}{T_e}\right) + \left(1 - \frac{u_{j-1}}{u_e}\right)\left(\frac{T_{j-1}}{T_e}\right)\right] \frac{\Delta\eta_{j-1}}{2} \tag{68}$$

$$PI1 = \left[\frac{2XRe_\infty}{[(\gamma-1)M_\infty^2]^{1.5}\left(\frac{T_\infty+198.6}{T_\infty(\gamma-1)M_\infty^2+198.6}\right)}\right] \frac{\sum_{j=2}^{edge} \frac{\Delta\eta_{j-1}}{2}\left(\frac{T_w}{T_e} + \frac{T_j}{T_e}\right)}{\frac{\mu_e}{\mu_{ref}}\left(\frac{T_j}{T_e}\right)^3 s}$$

where the s was included for the case of conical flow only. Again, a $\frac{\partial F}{\partial \eta}$ term was generated, but using only a three-point central differencing

scheme on this occasion. The final step of the loop was the actual computation of $\frac{\epsilon_{inner}}{\mu}$ at the current node j:

$$\left.\frac{\epsilon_{inner}}{\mu}\right|_j = .16(PI1)(1 - \exp(-[(PI1)(PI2)]^{1/2}/(26\,\frac{(\rho\mu)_j}{(\rho\mu)_e})))^2 \qquad (69)$$

$$\cdot \frac{\left(\frac{Y9}{2}\,F(i,j+1) - Y10\,F(i,j) - \frac{Y8}{2}\,F(i,j-1)\right)}{\Delta\eta_j \left(\frac{(\rho\mu)_j}{(\rho\mu)_e}\right)}$$

where Y8, Y9, and Y10 were coefficients obtained through Taylor series expansions of F(i,j-1) and F(i,j+1) about a point F(i,j). As the calculation of $\frac{\epsilon_{inner}}{\mu}$ progressed from the wall out into the field of flow, $\frac{\epsilon_{inner_{j+1}}}{\mu}$ retained its own computed value or that of $\frac{\epsilon_{inner_j}}{\mu}$, whichever was greater.

The outer law, $\frac{\epsilon_{outer}}{\mu}$, was computed through an iterative loop similar to that of the inner model. It culminated with the expression

$$\frac{\epsilon_{outer}}{\mu} = .0168 \left[\frac{2XRe_\infty}{[(\gamma-1)M_\infty^2]^{1.5}\left[\frac{T_\infty+198.6}{T_\infty(\gamma-1)M_\infty^2+198.6}\right]}\right]^{1/2} \frac{DD}{\left(\frac{\mu_e}{\mu_{ref}}\right)\frac{(\rho\mu)_j}{(\rho\mu)_e}\left(\frac{T_j}{T_e}\right)^2}\; s \qquad (70)$$

where the s was included only for the case of conical flow. In order that a compatible combination of computed viscosities were retained, the values of eddy viscosity from the outer law replaced those of the inner law from the point of intersection of the graphs to the edge of the boundary layer. Graphically, this was depicted in Fig 18.

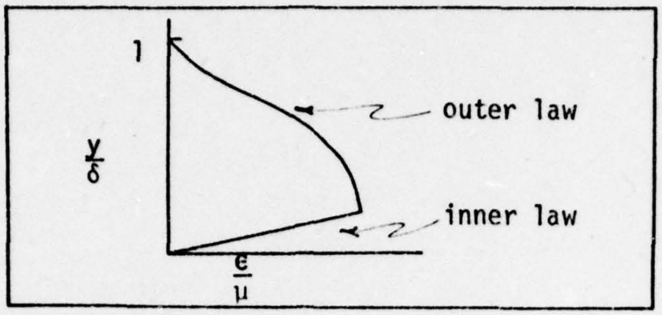

Fig. 18. Matching the Inner and Outer Eddy Viscosity Models (From Ref 8:21)

Having calculated the initial eddy values for the inner and outer viscous regions of the boundary layer, it was appropriate to subject this model to two more factors. Both were factors of degradation and were included to better describe the character of turbulent activity within the boundary layer.

Objections have been raised to the use of an eddy viscosity term, e, in place of, or in addition to the molecular viscosity, μ, of a fluid. μ is a real property of a fluid. e is only an effective description when a fluid is in motion, and it is clearly not a property of the fluid. But, with reservation, it has been used to express the behavior of turbulent stresses in terms of mean velocity gradients of a flowing fluid. It has been possible to obtain a satisfactory description of mean properties within turbulent flows by assuming this flow to behave as a Newtonian fluid, incorporating an eddy viscosity model along with μ, and including two factors of intermittency when appropriate (Ref 20:25-26). A laminar and irrotational flow became turbulent as it passed through a region of transition in which only a fraction of the time was spent in a turbulent state. During that time in laminar motion, the Reynolds stress, hence e, would have been zero. Then, to adequately describe the effects of e at

any point by the relative fraction of time that that point would be engulfed in turbulent flow (Ref 21:117). Therefore, the first multiplicative factor, called an intermittency factor, was applied to ϵ to more accurately describe the ϵ within the transition region. The intermittency or probability factor of Dhawan and Narasimha was used for this program. The factor was computed as follows (Ref 8:28-29):

$$\Gamma(s) = \left[1 - \exp \left(-.412 \left[\frac{s_{current} - s_{transition\ point}}{(.5) s_{transition\ point}} \right]^2 \right) \right] \quad (71)$$

Then, the computed $\left.\frac{\epsilon}{\mu}\right|_{original}$ was replaced by

$$\left.\frac{\epsilon}{\mu}\right|_{modified} = (\Gamma(s)) \left.\frac{\epsilon}{\mu}\right|_{original} \quad (72)$$

The second factor was then considered. It was observed by Klebanoff that in a turbulent boundary layer with a free boundary, as the free stream was approached the turbulence became intermittent. This intermittent nature was observed first at y/δ greater than .4 with less turbulent intensity as y/δ grew larger. It was thought that a good prediction of turbulent intensity probably depended on a correct weighting of the probability density for the turbulence of the free stream with that within the boundary. It was found that a good description of γ' was a Gaussian integral curve given by

$$\gamma' = \frac{1}{2} (1 - \mathrm{erf}(\xi')) \quad (73)$$

where

$$\xi' = \left(\sqrt{2}\ \frac{\sigma}{\delta}\right)^{-1} \left[\frac{y}{\delta} - .78\right] = 5\left[\frac{y}{\delta} - .78\right] \quad (74)$$

These expressions indicated that the edge of the boundary layer had a random character with a mean position at y/δ equal to .78. The edge vacillated from y/δ equal to .4 to y/δ equal to 1.2. Finally, if it were assumed that the free stream contributed little to the measured turbulent quantities of the boundary layer, an allowance could be made for the effect of intermittency by dividing by the factor γ' (Ref 22:15-18).

Cebeci used the approximate expression for Eq (73) to give a multiplicative version:

$$\gamma' = \left[1 + 5.5\left(\frac{y}{\delta}\right)^6\right]^{-1} \quad \text{(Ref 7:1679)} \tag{75}$$

which led to the coding for this second factor. If γ' were not included, then a newly defined viscosity was

$$\bar{\epsilon} = 1 + \frac{\epsilon}{\mu}\,\Gamma(s) \tag{76}$$

Including γ', Shang formed the following model:

$$\bar{\epsilon} = 1 + \left[\frac{1.75}{\left[1+5.5\left(\frac{y}{L}\Big/\frac{\delta}{L}\right)^6\right]} + 1\right]\left(\frac{\frac{\epsilon}{\mu}}{2.75}\right) \tag{77}$$

For purposes of this study Eq (76) became eddy model zero, and Eq (77) became eddy model one. Then, whether or not γ' was included, the quantity $\hat{e}$ was defined by

$$\hat{e} = 1 + \frac{Pr}{Pr_t}(\bar{e} - 1) \tag{78}$$

In a final note, the decision of whether to use eddy model zero or eddy model one depended on the original assumption that either the free stream turbulence had an effect on the ϵ of the boundary layer, or it did not. This factor, γ', was to have a definite effect on the analytical results,

and this entire subroutine was included with the program listing of Appendix B.

Subroutine Cfstno

Like Reystr this routine was called from the main program. But unlike Reystr, Cfstno performed its computation throughout the laminar, transition, and turbulent regions of flow. The purpose of this routine was to calculate a Stanton number, a measure of heat transfer; the local coefficient of friction, indicative of shear stress at the surface; and Reynolds numbers based on displacement thickness and momentum thickness.

Computation began with $\frac{(\rho\mu)_w}{(\rho\mu)_e}$, coded XLM1 in the program. The formula by which XLM1 was computed depended on the value of the exponent in the viscosity law of Sutherland, the value of this exponent being specified by the programmer. If the exponent were zero, then

$$XLM1 = \left(\frac{T_w}{T_e}\right)^{1/2} \left(\frac{T_e+198.6}{T_w+198.6}\right) \tag{79}$$

If this exponent were one, then XLM1 was one. Otherwise,

$$XLM1 = \left(\frac{T_w}{T_e}\right)^{\omega-1} \tag{80}$$

Next to be calculated were transformed quantities similar to $\dot{q}$ or heat flux and τ or shear stress. First, the same four-point finite difference scheme used in Reystr for $\left.\frac{\partial F}{\partial \eta}\right|_w$ was repeated at this point to calculate $\left.\frac{\partial F}{\partial \eta}\right|_w$ and $\left.\frac{\partial \theta}{\partial \eta}\right|_w$. Then the transformed τ, coded TAU, was computed:

$$TAU = \frac{(\rho\mu)_w}{(\rho\mu)_e} \frac{\rho_e}{\rho_\infty} \frac{\mu_e}{\mu_{ref}} \left(\frac{u_e}{u_\infty}\right)^2 \left.\frac{\partial F}{\partial \eta}\right|_w \frac{1}{(2X)^{1/2}} \tag{81}$$

or,

$$\mathrm{TAU} = \frac{(\rho\mu)_w}{\rho_\infty \mu_{ref}} \left(\frac{u_e}{u_\infty}\right)^2 (2X)^{-1/2} \left.\frac{\partial F}{\partial \eta}\right|_w \tag{81}$$

Following τ, the transformed $\dot{q}$, coded QS, was replaced by the following expression:

$$\mathrm{QS} = \frac{1}{(2X)^{1/2}Pr} \frac{(\rho\mu)_w}{(\rho\mu)_e} \frac{\rho_e}{\rho_\infty} \frac{\mu_e}{\mu_{ref}} \frac{u_e}{u_\infty} \frac{T_e}{T_\infty(\gamma-1)M_\infty^2} \left.\frac{\partial \theta}{\partial \eta}\right|_w$$

or,

$$\mathrm{QS} = \frac{(\rho\mu)_w}{\rho_\infty \mu_{ref}} \frac{u_e}{u_\infty} \frac{T_e}{T_\infty(\gamma-1)M_\infty^2} Pr^{-1} (2X)^{-1/2} \left.\frac{\partial \theta}{\partial \eta}\right|_w \tag{82}$$

For the case of the axisymmetric flow, both TAU and QS were divided by the nondimensional station, s_i. With this, preliminary calculations were completed.

A Stanton number and coefficient of friction followed next in the computation. If T_w equaled T_o, there was no heat transfer and St, coded STNO, was zero. Otherwise,

$$\mathrm{STNO} = \frac{\left[\left(\frac{\mu_{ref}}{\mu_\infty}\right)^{1/2} \left(\frac{\rho_\infty u_\infty L}{\mu_\infty}\right)^{-1/2} \frac{(\rho\mu)_w}{\rho_\infty \mu_{ref}} \frac{u_e}{u_\infty} \frac{T_e}{T_\infty(\gamma-1)M_\infty^2} Pr^{-1} (2X)^{-1/2} \left.\frac{\partial \theta}{\partial \eta}\right|_w\right]}{\left[\left(1 - \frac{T_w}{T_o}\right)\left(\frac{T_e}{T_\infty(\gamma-1)M_\infty^2} + \frac{1}{2}\left(\frac{u}{u_e}\right)^2\right)\right]} \tag{83}$$

The model from which this expression came was

$$St_e = \frac{\dot{q}}{\rho_e u_e (H_e - h_w)} \tag{84}$$

For the calculation of $c_f\big|_{\text{local station}}$, coded CFNO,

$$\mathrm{CFNO} = 2\left(\frac{\mu_{ref}}{\mu_\infty}\right)^{1/2} \left(\frac{\rho_\infty u_\infty L}{\mu_\infty}\right)^{-1/2} \frac{(\rho\mu)_w}{\rho_\infty \mu_{ref}} \left(\frac{u_e}{u_\infty}\right)^2 (2X)^{-1/2} \left.\frac{\partial F}{\partial \eta}\right|_w \tag{85}$$

With St and $c_{f_{local}}$ computed, only the transformed expressions for Re_{δ^*} and Re_θ remained. Coded as REYDT and REYMT, these quantities were computed from the following statments:

$$\text{REYDT} = \left[\frac{\rho_e u_e x_{real}}{\mu_e}\right]\left(\frac{\delta^*}{L}\right)$$

$$\text{REYMT} = \left[\frac{\rho_e u_e x_{real}}{\mu_e}\right]\left(\frac{\theta}{L}\right) \tag{86}$$

This completed calculations within this routine, and further, completed the formal description of four important subsystems within Itract. Again, this subroutine was included with the program listing of Appendix B. In this appendix consideration was given to the important concepts of the nondimensionalization of working quantities, initialization of the grid, and the generation of finite difference coefficients. Also included was a brief description of the two subroutines used in the computation of eddy viscosity, heat transfer, and skin friction. The theory presented in this appendix should provide a better understanding of the code in general, and the modification for mass transfer specifically.

Appendix D

Fortran Computer Code Key

Coded Symbol	Represented Quantity (Values included for those quantities remaining constant throughout this project)
Inputs	(in order read by computer)
G	$\gamma = 1.4$
PR	$Pr = .73$
XMINF	M_∞
TA	T_∞
DS	Stepping increment in s_i along the streamwise direction, DS = .0004
SI	Initial station, s_1, began computation within the grid, SI = .0006
OMEGA	Exponent in the viscosity law of Sutherland, OMEGA = 0
ERROR	A convergence criterion, the acceptable difference between the quantity $\left.\frac{\Delta F}{\Delta \eta}\right\rvert_w$ calculated in two successive calls of the matrix inversion routine at the same station s_i
XXK	$\frac{\Delta\eta_{j+1}}{\Delta\eta_j}$, a constant ratio from surface to the edge of the boundary layer
BO	$\frac{T_w}{T_o}$
BTRX	Station s_i at which transition from laminar to turbulent flow began
PRT	$Pr_t = .9$ (exceptions noted)
XINTER	A flagged quantity; XINTER = 0., eddy model zero was used; XINTER = 1., eddy model one was used in the computation of e
DYW	$\Delta\eta_1$, the first increment in η
IEDGE	Total number of nodal points or divisions in the η direction within the grid
INTACT	Not used in this study

IDIFF	A flagged quantity; IDIFF = 0, a three-point differencing scheme was to be used; IDIFF = 1, a two-point differencing scheme was to be used; IDIFF was set equal to 0 for this project.
IEND1	Total number of nodal points or divisions in the ξ direction within the grid
MSP	A flagged quantity; MSP = 1, program printed abbreviated data from each station computed; MSP = 5, program printed every fifth station; MSP was set equal to 1 for this project.
J2DA	A flagged quantity; J2DA = 0, designated a flat plate calculation, J2DA = 1, designated an axisymmetric cone calculation
IPRES	A flagged quantity; IPRES = 0, indicated that dp/dx was zero; IPRES = 1, indicated that dp/dx was not zero; IPRES was set equal to zero for this project.
ICHS	An array of integers which designated stations where a double step was to be taken between computations of a column of nodal points
IPRN	An array of integers which designated stations where a full profile of boundary layer data was to be printed
XLGTHMD	Length of the model, L
RINFA	ρ_∞
IBLW	A flagged quantity; IBLW = 0, no mass transfer considered; IBLW = -1, mass transferred at a constant rate; IBLW = 1, mass transfer varied along the length of the model
STRT, DONE, RVRAT	If IBLW = -1, mass transfer began at some number of feet from the leading edge or tip and continued to some other position downstream, transferring at a constant rate, $\frac{(\rho v)_w}{(\rho u)_\infty}$ for the plate or $\frac{(\rho v)_w}{(\rho u)_e}$ for the cone
NUMDAT, XPOS, RHOVRAT	If IBLW = 1, this stipulated a varying transfer rate beginning at X_{pos1} at a strength of $\left(\frac{\rho v_w}{\rho u_\infty}\right)_{pos1}$ or $\frac{(\rho v)_w}{(\rho u_e)_{pos1}}$ and continuing to $X_{pos\ final}$ at a correspondingly specified strength. Varying transfer rates were designated in between.

Outputs and Miscellaneous Working Quantities Applicable in This Study

(alphabetical)

BCVW	V(i,1), defined in Eq (29)
BLDT	δ^*/L
BLMT	θ/L
BLT	δ/L
CFNO	$c_{f_{local}}$
EO	Eddy Viscosity, either from eddy model zero or eddy model one
ETA	η
F1	u/u_e (in the output listing only)
H/HE	H/H_e (in the output listing only)
MACH	Mach number (in the output listing only)
N, XNN	y/L (listed as N in the output)
RE	ρ/ρ_e
REY	Re_∞
REYEXT	Re_x
REYDT	$Re_{\delta*}$
REYMT	Re_θ
RO/ROE	ρ/ρ_e (in the output listing only)
RVRAT(VRVRAT)	$\left.\frac{(\rho v)_w}{(\rho u)_\infty}\right\vert_{\text{current station}}$ or $\left.\frac{(\rho v)_w}{(\rho u)_e}\right\vert_{\text{current station}}$
STNO	St_e
T1	T/T_e (in the output listing only)
TRR	$(T_\infty+198.6)/(T_\infty(\gamma-1)M_\infty^2+198.6)$
TW/TE	T_w/T_e (in the output listing only)
UE	u/u_e

V1	v/u_e (in the output listing only)
X	Defined in Eq (27)
XBE	β
x/L	station s_i
XME	M_e
XNUE	$\frac{\mu_e}{\mu_{ref}}$
Y/BLT	y/δ (in the output listing only)

Appendix E

A Cubic Spline Approximation for the Description of Generally Varying Mass Transfer Rate

In modeling or mathematically describing a varying mass transfer rate it was assumed that through some means, there would be knowledge of the strength of mass transfer at a finite number of stations along the model. So, there was information of the form (x_i, f_i) for i values from 1 to n. The objective was to construct a function, f(x), such that f_i was equal to $f(x_i)$ and that f(x) was twice differentiable over $[x_1, x_n]$. This f(x) would provide the value of mass transfer for any station, s_i, along the surface of the model. Figure 19 depicted the curve to be specified.

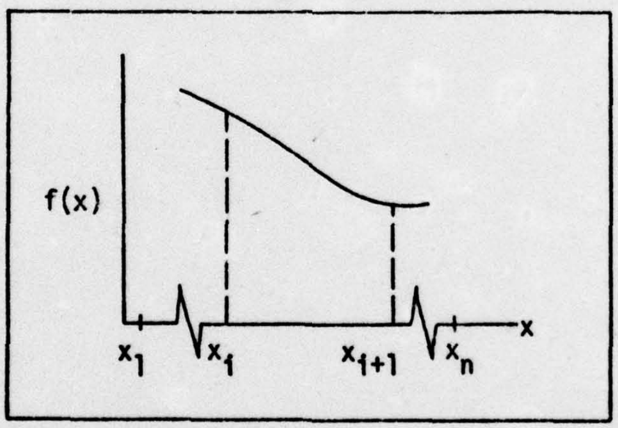

Fig. 19. Building a Cubic Polynomial Between Any x_i and x_{i+1}

The function, f(x), was specified as a different cubic polynomial in each interval, x_i to x_{i+1}. It was required that the function be continuous, together with its first two derivatives, at each junction

between two polynomials. Thus, for each $[x_i, x_{i+1}]$, an f(x) was constructed equal to $\sum_{\ell=0}^{3} C_\ell^i x^\ell$. The function was formed recursively. Supposing that f(x) had been generated to an x equal to x_i, it was necessary to choose $C_\ell^i\big|_{\ell=0 \text{ to } 3}$ such that f(x), f'(x), and f"(x) were continuous at x_i, and it was left to find f(x) over the interval $[x_i, x_{i+1}]$. This led to four linear algebraic equations with four unknowns, $C_\ell^i\big|_{\ell=0 \text{ to } 3}$. These equations were as follows:

$$
\begin{aligned}
f(x_i) &= \sum_{\ell=0}^{3} C_\ell^i \, x_i^\ell \\
f'(x_i) &= \sum_{\ell=1}^{3} C_\ell^i \, \ell x_i^{\ell-1} \\
f''(x_i) &= \sum_{\ell=2}^{3} C_\ell^i \, \ell(\ell-1) x_i^{\ell-2} \\
f_{i+1} &= \sum_{\ell=0}^{3} C_\ell^i \, x_{i+1}^\ell
\end{aligned}
\tag{87}
$$

This system was solved up to x_{i+1} at which point the process was repeated from x_{i+1} to x_{i+2} (Ref 11).

Returning to the initiation of this recursive procedure, values were known for (x_i, f_i) for i equal from 1 to n. Then, f_1' was approximated by $\frac{f_2 - f_1}{x_2 - x_1}$ and f_1'' was approximated by the expression $\frac{f_2' - f_1'}{x_2 - x_1}$. The initial conditions were then f_1, f_1', f_1'', and f_2. The four equations initially to be solved were, then, given by

$$
\begin{aligned}
C_0^1 + C_1^1 x_1 + C_2^1 x_1^2 + C_3^1 x_1^3 &= f_1 \\
C_1^1 + 2C_2^1 x_1 + 3C_3^1 x_1^2 &= f_1' \\
2C_2^1 + 6C_3^1 x_1 &= f_1'' \\
C_0^1 + C_1^1 x_2 + C_2^1 x_2^2 + C_3^1 x_2^3 &= f_2
\end{aligned}
\tag{88}
$$

Solving for C_i^1 yielded a cubic polynomial expression

$$f_1(x) = C_0^1 + C_1^1\, x + C_2^1\, x^2 + C_3^1\, x^3 \tag{89}$$

which was descriptive of an appropriate curve connecting points one and two. Then, having specified the polynomial for this first interval, the successive polynomials and their intervals were recursively computed to x_n as previously discussed, though now a polynomial expression existed for finding $f'(x)$ and $f''(x)$.

Finally, then, for any position, s', along the surface of the model, the interval s_i to s_{i+1} in which the position was contained could be found. Knowing the interval was to also know the corresponding cubic polynomial that described that increment, and hence, the value of mass transfer rate, f(s').

Appendix F

Flat Plate Heat Transfer Data

Table IV

The Combinations of Variables for the Parameter Study, the Flat Plate Case

	St_∞, Itract Prediction				
	Col 1	Col 2	Col 3	Col 4	Col 5
XXK	1.1	1.1	1.15	1.15	1.15
PRT	1.	.9	.9	.9	.9
XINTER	1.	0.	0.	0.	1.
DYW	.0005	.0005	.00025	.0005	.0005
IEDGE	120	120	120	100	100

Table V

Heat Transfer Results of the Parameter Study,

Zero Mass Transfer

$Re_x(10)^{-5}$	$St_\infty(10)^3$ Experi-mental	Itract Predictions, $St_\infty(10)^3$				
		Col 1	Col 2	Col 3	Col 4	Col 5
.455	4.13	3.45	3.59	3.63	3.63	3.57
1.36	3.08	2.81	2.97	2.99	2.99	2.94
2.27	2.79	2.46	2.60	2.63	2.63	2.58
3.18	2.59	2.29	2.44	2.46	2.46	2.42
4.09	2.44	2.19	2.33	2.35	2.35	2.31
5.00	2.36	2.11	2.24	2.27	2.27	2.23
5.91	2.29	2.05	2.18	2.20	2.20	2.17
6.82	2.22	1.99	2.12	2.15	2.15	2.11
7.73	2.13	1.95	2.08	2.10	2.10	2.07
8.64	2.10	1.92	2.04	2.06	2.06	2.03
9.55	2.07	1.88	2.01	2.03	2.03	2.00
10.5	2.07	1.85	1.97	2.00	2.00	1.97
11.4	2.02	1.83	1.95	1.97	1.97	1.94
12.3	1.91	1.80	1.92	1.95	1.95	1.92
13.2	1.93	1.78	1.90	1.92	1.92	1.89
14.1	1.90	1.76	1.88	1.90	1.90	1.87
15.0	1.90	1.75	1.86	1.88	1.88	1.86
15.9	1.87	1.73	1.84	1.87	1.87	1.84
16.8	1.88	1.71	1.83	1.85	1.85	1.82
17.7	1.83	1.70	1.81	1.83	1.84	1.81
18.6	1.80	1.68	1.80	1.82	1.82	1.79
19.5	1.85	1.67	1.78	1.81	1.81	1.78
20.5	1.81	1.66	1.77	1.79	1.79	1.77
21.4	1.82	----	----	----	----	----

(Ref 13)

Table VI

A Heat Transfer Comparison with Moffat and Kays, Mass Transfer Factor of .001

$Re_x(10)^{-5}$	$St_\infty(10)^3$ Experi-mental	Itract Prediction, $St_\infty(10)^3$		Percent Error with Eddy Model Zero
		Eddy Model One	Eddy Model Zero	
.453	3.53	3.44	3.50	.8
1.36	2.58	2.41	2.46	4.6
2.26	2.33	2.05	2.10	9.8
3.17	2.13	1.89	1.93	9.3
4.08	1.99	1.78	1.83	8.0
4.98	1.92	1.71	1.74	8.3
5.89	1.85	1.65	1.68	9.2
6.79	1.77	1.60	1.63	7.9
7.70	1.69	1.55	1.58	6.5
8.60	1.68	1.52	1.54	8.3
9.51	1.61	1.48	1.51	6.2
10.4	1.59	1.45	1.48	6.9
11.3	1.53	1.43	1.46	4.6
12.2	1.50	1.41	1.43	4.7
13.1	1.47	1.39	1.41	4.1
14.0	1.44	1.37	1.39	3.5
14.9	1.46	1.35	1.38	5.5
15.8	1.41	1.33	1.36	3.5
16.8	1.39	1.31	1.34	3.6
17.7	1.41	1.30	1.32	6.4
18.6	1.36	1.29	1.31	3.7
19.5	1.36	1.27	1.30	4.4
20.4	1.32	1.26	1.29	2.3
21.3	1.31	----	----	----

(Ref 13)

Table VII

A Heat Transfer Comparison with Moffat and Kays, Mass Transfer Factor of .00115

$Re_x(10)^{-5}$	$St_\infty(10)^3$ Experimental	Itract Prediction, $St_\infty(10)^3$ Eddy Model One	Eddy Model Zero	Percent Error with Eddy Model One
.439	4.53	3.29	3.35	27.4
1.32	3.64	3.62	3.66	.5
2.19	3.24	3.27	3.32	.9
3.07	3.10	3.10	3.15	0
3.95	2.97	2.99	3.03	.6
4.83	2.92	2.91	2.95	.3
5.70	2.78	2.85	2.88	2.5
6.58	2.83	2.79	2.83	1.4
7.46	2.66	2.75	2.78	3.3
8.34	2.67	2.71	2.74	1.5
9.21	2.61	2.67	2.71	2.2
10.1	2.56	2.64	2.68	3.0
11.0	2.58	2.62	2.65	1.5
11.8	2.57	2.59	2.63	.7
12.7	2.51	2.57	2.60	2.3
13.6	2.47	2.55	2.58	3.1
14.5	2.44	2.53	2.56	3.6
15.4	2.47	2.51	2.55	1.6
16.2	2.42	2.50	2.53	3.2
17.1	2.38	2.48	2.51	4.0
18.0	2.36	2.47	2.50	4.4
18.9	2.36	2.45	2.48	3.7
19.7	2.32	2.44	2.47	4.9
20.6	2.32	2.43	2.46	4.5

(Ref 13)

Table VIII

A Heat Transfer Comparison with Moffat and Kays at the Suction Asymptotic Limit

$Re_x(10)^{-5}$	$St_\infty(10)^3$ Experimental	Itract Prediction, $St_\infty(10)^3$ Eddy Model One	Itract Prediction, $St_\infty(10)^3$ Eddy Model Zero	Percent Error with Eddy Model One
.430	9.33	4.90	5.00	47.5
1.29	8.07	8.34	8.38	3.2
2.15	7.75	8.17	8.20	5.1
3.01	7.82	8.09	8.12	3.3
3.87	7.64	8.04	8.06	5.0
4.72	7.99	8.00	8.03	.1
5.58	7.71	7.98	8.00	3.4
6.44	7.85	7.96	7.98	1.4
7.30	7.82	7.95	7.96	1.6
8.16	7.95	7.94	7.96	.1
9.02	7.94	7.93	7.95	.1
9.88	7.91	7.93	7.94	.2
10.7	8.24	7.92	7.93	3.9
11.6	8.17	7.92	7.93	3.0
12.5	7.82	7.92	7.92	1.3
13.3	7.97	7.91	7.92	.7
14.2	7.88	7.91	7.92	.4
15.0	8.35	7.91	7.92	5.3
15.9	7.76	7.91	7.92	1.9
16.8	7.97	7.91	7.91	.8
17.6	7.75	7.91	7.91	2.0
18.5	7.75	7.91	7.91	2.0
19.3	8.08	7.91	7.91	2.1
20.2	7.85	----	----	----

(Ref 13)

Table IX

A Heat Transfer Comparison with Moffat and Kays, Mass Transfer Factor of .0019

$Re_x(10)^{-5}$	$St_\infty(10)^3$ Experimental	$St_\infty(10)^3$, Itract Predictions with Eddy Model Zero			
		Fine Mesh with % Error		Coarse Mesh with % Error	
.457	3.31	3.94	16.0	3.36	1.5
1.37	2.36	2.27	3.8	1.97	16.5
2.28	2.06	1.78	13.6	1.62	21.4
3.20	1.89	1.57	16.9	1.46	22.7
4.11	1.74	1.44	17.2	1.36	21.8
5.03	1.65	1.34	18.8	1.28	22.4
5.94	1.57	1.27	19.1	1.22	22.3
6.85	1.50	1.21	19.3	1.17	22.0
7.77	1.46	1.16	20.5	1.13	22.6
8.68	1.45	1.12	22.8	1.10	24.1
9.60	1.37	1.08	21.2	1.06	22.6
10.5	1.39	1.06	23.7	1.04	25.2
11.4	1.36	1.03	24.2	1.01	25.7
12.3	1.26	1.00	20.6	.99	21.4
13.3	1.24	Error Finish		.97	21.8
14.2	1.23			.95	22.8
15.1	1.23			.93	24.4
16.0	1.19			.92	22.7
16.9	1.20			.90	25.0
17.8	1.13			.89	21.2
18.7	1.18			.88	25.4
19.6	1.12			.87	22.3
20.6	1.09			.85	22.0
21.5	1.09			----	----

(Ref 13)

Appendix G

Cone Heat Transfer Data

Table X

A Heat Transfer Comparison with Martellucci, Laganelli, and Hahn, Data Group 132

Station, s	$St_{\infty}(10)^4$ Theoretical Fully Laminar	$St_{\infty}(10)^4$ Experi-mental	$St_{\infty}(10)^4$ Theoretical Fully Turbulent	$St_e \frac{\rho_e u_e}{\rho_\infty u_\infty}(10)^4$ Itract	Percent Error with Eddy Model One
.191	4.0	4.77	7.7	4.63	2.9
.262	3.5	3.50	7.3	3.96	11.6
.315	3.0	2.4,3.1	7.0	3.78	18.0
.399	2.8	3.93	6.8	5.33	26.3
.470	2.6	5.67	6.5	6.86	17.3
.542	2.4	5.68	6.3	7.55	24.8
.589	2.3	6.91,6.61	6.0	7.67	9.9
.607	2.2	6.18	6.0	7.70	19.7
.732	2.0	6.79,6.84 6.23,7.30	5.9	7.47	2.3
.750	2.0	7.19	5.9	7.41	3.0
.816	1.9	7.67	5.8	7.23	5.7
.958	1.8	6.31	5.6	6.89	8.4

(Ref 14)

Table XI

A Heat Transfer Comparison with Martellucci, Laganelli, and Hahn, Reference Data 150

Station, s	$St_\infty (10)^4$ Experimental	$St_e \frac{\rho_e u_e}{\rho_\infty u_\infty} (10)^4$ Itract	Percent Error with Eddy Model One
.191	2.10	2.06	1.9
.227	2.70	2.63	2.6
.263	2.14	3.76	43.
.317	3.91,4.03,3.86	5.00	19.4
.353	6.48	5.33	17.7
.400	5.31	5.42	2.0
.544	4.90	5.08	3.5
.592	4.30	4.97	13.5
.610	3.94	4.93	20.1
.645	3.80	4.87	22.0
.681	3.53	4.80	26.4
.717	2.12	4.74	55.3
.735	4.27,3.98 4.10,5.08	4.73	6.9
.819	4.19	4.62	9.3
.890	5.99	4.54	24.2
.962	4.69	4.46	4.9

(Ref 15)

Table XII

A Heat Transfer Comparison with Martellucci, Laganelli, and Hahn, Reference Data 1

Station, s	$St_{\infty}(10)^4$ Experimental	$St_e \frac{\rho_e u_e}{\rho_{\infty} u_{\infty}}(10)^4$ Itract	Percent Error with Eddy Model One
.173	3.73	3.97	6.0
.191	3.85	3.92	1.8
.227	4.58	5.03	8.9
.263	5.33	7.03	24.2
.317	8.84,7.90, 7.18,7.53	8.79	.6
.353	9.68	9.22	4.8
.400	9.12	9.30	1.9
.472	8.15	8.99	9.3
.544	7.69	8.64	11.0
.592	7.19	8.43	14.7
.610	6.89	8.36	17.6
.645	7.49	8.25	9.2
.681	7.04	8.13	13.4
.717	6.99	8.04	13.1
.735	6.94,6.84, 6.75,6.86	7.99	13.1
.753	6.84	7.94	13.9
.819	6.64	7.80	14.9
.890	6.79	7.67	11.5
.962	6.34	7.54	15.9

(Ref 15)

Table XIII

A Heat Transfer Comparison with Martellucci, Laganelli, and Hahn, Data Group 60

Station, s	$St_\infty(10)^4$ Experimental	$St_e \frac{\rho_e u_e}{\rho_\infty u_\infty}(10)^4$ Itract	Percent Error with Eddy Model One
.226	3.80	5.57	31.8
.262	3.09	4.72	34.5
.315	2.45,2.49,2.54	3.85	34.0
.399	1.99	3.77	47.2
.542	1.78	6.94	74.3
.589	1.98	7.32	73.0
.607	2.17	7.40	70.7
.648	2.46	7.48	67.1
.732	1.87	7.43	74.8
.750	1.76	7.40	76.2
.816	2.00	7.28	72.5
.958	2.31	6.84	66.2

(Ref 14)

Table XIV

A Heat Transfer Comparison with Martellucci, Laganelli, and Hahn, Data Group 203

Station, s	$St_\infty(10)^4$ Experimental	$St_e \frac{\rho_e u_e}{\rho_\infty u_\infty}(10)^4$ Itract	Percent Error with Eddy Model One
.263	$1.00(10)^{-2}$	$5.15(10)^{-1}$	48.5
.317	3.42	1.68	50.9
.353	4.72	2.16	54.2
.400	5.13	2.52	50.9
.472	3.71	2.60	29.9
.544	4.02	2.52	37.3
.592	4.15	2.44	41.2
.610	3.74	2.41	35.6
.645	4.05	2.35	42.0
.681	3.65	2.30	37.0
.735	3.99,3.88 3.98,6.41	2.24	42.3
.753	3.02	2.21	26.8
.819	3.96	2.15	45.7
.890	5.35	2.09	61.0
.962	4.33	2.02	53.3

(Ref 15)

VITA

Capt A. J. Beauregard received his undergraduate training in the engineering sciences, and upon graduation and commissioning, he entered pilot training. Following this training Capt Beauregard primarily flew the C-130 in roles of armed reconnaissance and intelligence gathering. Following these flying assignments Capt Beauregard entered the Air Force Institute of Technology in June of 1975.